

https://dspace.org/

Galvanic interactions between minerals during dissolution

Holmes, Paul Richard

1994

http://hdl.handle.net/10539/22931

Holmes, Paul Richard (1994) Galvanic interactions between minerals during dissolution, University of the Witwatersrand, Johannesburg,<http://hdl.handle.net/10539/22931>

Downloaded from a DSpace repository. https://dspace.org/

GALVANIC INTERACTIONS BETWEEN MINERALS DURING DISSOLUTION.

Paul Richard Holmes.

A dissertation submitted to the Faculty of Engineering, University of the Witwatersrand, Johannesburg, in fulfilment of the requirements for the degree of Master of Science in Engineering

Johannesburg, 1994

DECLARATION.

I declare that this dissertation is my own, unaided work. It is being submitted for the Degree of Master of Science in Engineering in the University of the Witwatersrand, Johannesburg. It has not been submitted before for any degree or examination in any other University.

6th day of December 1994

ABSTRACT.

A quantitative description of galvanic interactions between sulphide minerals based on thermodynamic and kinetic parameters has been developed. The basis for quantitative description involves conducting a voltage balance over the galvanic couple. The contributions to the voltage balance include the galvanic couple cell emf, kinetic descriptions of the anodic and cathodic half reactions, the voltage characteristics of mineral-mineral contacts and solution voltage losses. The rates of the anodic and cathodic half reactions were modelled by the Butler-Volmer equation and the diffusion equation. A potentiostat was used to vary the voltages losses across mineral-mineral contacts. The galvanic couples were constructed as rotating ring disc electrodes and hence electrolyte voltage losses were negligible. Three galvanic couples, copper-platinum, copper-pyrite and galena-pyrite, were electrochemically characterised under different conditions of ferric concentration, electrode rotation rate and temperature. The effect of illumination on the anodic dissolution of galena was investigated. The electrochemical model is in good agreement with experimentally measured galvanic currents. Galvanic interaction is a dynamic function and various models are developed which account for dynamic behaviour in galvanic cells.

ACKNOWLEDGEMENTS.

I wish to extend my gratitude to the following people and institutions:

Dr. Frank Crundwell for his assistance and encouragement.

My wife, Debbie, for her love and support.

My parents for their love and encouragement.

Prof. Mike Nicol for proof reading the manuscript.

The Council for Mineral Technology (MINTEK), the Foundation for Research and Development (FRD) and the Univ...ity of the Witwatersrand for financing this research.

CONTENTS.

	Page.
Declaration	i
Abstract	ii
Acknowledgements	iii
Contents	iv
List of figures	ix
List of tables	xiii
Nomenclature	xiv
1. Introduction.	1
1.1 Electrochemical theory.	3
1.1.1 An introduction to electrochemistry.	3
1.1.2 Thermodynamics of electrode processes.	5
1.1.3 Kinetics of electrode processes.	7
1.1.3.1 Electrochemically controlled reactions.	7
1.1.3.2 Mass transfer controlled reactions.	9
1.1.4 Electrochemical theory of leaching.	13
1.1.5 Electrochemical theory of galvanic interaction.	16
1.1.6 Electrochemical techniques.	18
1.1.6.1 Steady-state potentiostatic measurements.	18
1.1.6.2 Cyclic voltammetry.	18
1.2 Literature review	19
1.2.1 Galvanic interaction studies in corrosion.	19
1.2.2 Qualitative descriptions of galvanic interaction in sulphide mineral systems.	23
1.2.3 Quantitative descriptions of galvanic interactions in sulphide mineral systems.	26
1.3 Research objectives.	32

2. Chemistry Of The Galvanic Couples Studied. 34
2.1 Chemistry associated with the copper-platinum galvanic couple. 34
2.2 Chemistry associated with the copper-pyrite galvanic couple. 36
2.3 Chemistry associated with the galena-pyrite galvanic couple. 37

3. Development Of A Theoretical Expression For Galvanic Interaction. 41
3.1 The model basis. 41
3.2 Mathematical expressions for the anodic and cathodic overpotentials. 43
3.2.1 Mathematical expressions for electrochemically controlled reactions. 43
3.2.2 A mathematical expression for a reaction controlled by electrochemical and mass transfer processes. 45
3.2.3 A mathematical expression for a reaction controlled by mass transfer processes. 47
3.3 A mathematical expression for solution voltage losses. 47
3.4 Mathematical expressions for mineral-mineral contacts. 47
3.5 Mathematical expressions for galvanic interaction. 48

4. Experimental Techniques and Procedure. 50
4.1 Description of reagents. 50
4.2 Apparatus. 51
4.2.1 Preparation of electrodes. 51
4.2.2 The three-electrode cell. 53
4.2.3 The galvanic cell. 54
4.3 Procedure for characterising the half reactions and galvanic couple. 55
4.3.1 Procedure for characterising anodic and cathodic half reactions. 56
4.3.2 Procedure for characterising the galvanic couple. 57

5. Galvanic Interaction Between Copper and Platinum In Acidic Ferric Sulphate Solutions. 59

5.1 Electrochemical characterisation of copper dissolution. 59

5.1.1 The dependence of copper dissolution rate on sodium sulphate concentration. 59

5.1.2 The dependence of copper dissolution rate on ferric concentration. 61

5.1.3 The dependence of copper dissolution rate on electrode rotation. 61

5.1.4 The dependence of copper dissolution rate on temperature. 62

5.2 Electrochemical characterisation of ferric reduction on platinum. 64

5.2.1 The dependence of ferric reduction rate on concentration. 64

5.2.2 The dependence of ferric reduction rate on electrode rotation. 67

5.2.3 The dependence of ferric reduction rate on temperature. 68

5.3 Electrochemical characterisation of the galvanic couple formed between copper and platinum. 69

5.4 Mathematical modelling of the copper-platinum galvanic couple. 70

6. Galvanic Interaction Between Copper And Pyrite In Acidic Ferric Sulphate Solutions. 73

6.1 Electrochemical characterisation of ferric reduction on pyrite. 73

6.1.1 The dependence of ferric reduction rate on ferric concentration. 73

6.1.2 The dependence of ferric reduction rate on electrode rotation. 74

6.1.3 The dependence of ferric reduction rate on temperature. 74

6.2 Electrochemical characterisation of the galvanic couple formed between copper and pyrite. 76

6.3 Mathematical modelling of the copper-pyrite galvanic couple. 80

7. Galvanic Interaction Between Galena and Pyrite In Acidic Ferric Nitrate Solutions. 83

7.1 Electrochemical characterisation of the anodic dissolution of galena. 83

7.1.1 The dependence of galena dissolution rate on sodium nitrate

concentration. 83
7.1.2 The dependence of galena dissolution rate on ferric nitrate concentration. 85
7.1.3 The dependence of galena dissolution rate on electrode rotation. 86
7.1.4 The dependence of galena dissolution rate on temperature. 88
7.1.5 The dependence of galena dissolution rate on illumination. 89
7.2 Electrochemical characterisation of ferric reduction on pyrite. 91
7.2.1 Dependence of ferric reduction rate on concentration. 92
7.2.2 Dependence of ferric reduction rate on electrode rotation. 93
7.2.3 Dependence of ferric reduction rate on temperature. 93
7.3 Electrochemical characterisation of the galvanic couple formed between galena and pyrite. 95
7.3.1 Dependence of galvanic interaction on ferric concentration. 95
7.3.2 Dependence of galvanic interaction on rotation rate. 96
7.3.3 Dependence of galvanic interaction on temperature. 97
7.3.4 Dependence of galvanic interaction on illumination. 97
7.4 Mathematical modelling of the galena-pyrite couple. 98

8. Dynamic Aspects Of Galvanic Interaction. 100
8.1 Dependence of galvanic interaction on electrode area. 101
8.2 Dependence of galvanic interaction on solution composition. 104

9. Conclusions And Recommendations. 108

10. References. 111

Appendix A. 117
Energy Dispersive X-Ray Analysis (EDXA) of the mineral samples used in the galvanic couples.
Appendix B. 120
Computer programs for recording experimental data and solving model equations.

Appendix C. 128

Derivation of dynamic expressions for galvanic current.

LIST OF FIGURES.

Figure	page
1.1 Galvanic interaction between PbS and FeS_2.	1
1.2 Models for the electrical double layer. (A) The Helmoltz model. (B) The Gouy-Chapman model.	4
1.3 Polarisation curve, for the anodic reaction Red = Ox + e, illustrating various reaction control regimes.	11
1.4 Fluid flow to a rotating disc electrode. (A) View from below. (B) Side view. (C) Force co-ordinate system.	12
1.5 The leaching of a particle, M, by oxidant A^{++}.	14
1.6 Polarisation curves for the oxidation of M and the reduction of A^{++}.	14
1.7 The hypothetical galvanic interaction between electrode M and electrode N.	16
1.8 Polarisation curves for the reactions occurring in the galvanic couple formed between electrode M and electrode N.	17
2.1 Thermodynamic stability regimes in the Cu-H_2O system.	34
2.2 Thermodynamic stability regimes in the Fe-S-H_2O system.	36
2.3 Thermodynamic stability regimes in the Pb-S-H_2O system.	38
3.1 The processes occurring in a hypothetical galvanic couple.	41
3.2 The influence mineral-mineral contact and solution conductivity on galvanic interaction.	43
4.1 Construction of, and fluid flow to, a rotating ring disc electrode.	52
4.2 The three-electrode cell.	53
4.3 Electrical circuit configuration used to investigate the galvanic couples.	55
4.4 (A) Hypothetical current-voltage data for anodic and cathodic	

half reactions at various cell voltages. (B) Galvanic currents at corresponding cell voltages. 56

5.1 The effect of sodium sulphate concentration on the rate of copper dissolution. 60
5.2 The effect of ferric concentration on the rate of copper dissolution. 61
5.3 The effect of rotation on the rate of copper dissolution in ferric sulphate solutions. 62
5.4 The rate of ferric reduction on copper at various temperatures. 63
5.5 The effect of ferric concentration on the rate of ferric reduction on platinum. 64
5.6 The dependence of limiting current on ferric concentration. 65
5.7 Steady-state polarisation curve for the ferric/ferrous reduction reaction on platinum. 66
5.8 Determination of the ferric\ferrous reaction order. 68
5.9 The effect of temperature on the rate of ferric reduction on platinum. 69
5.10 The effect of rotation on galvanic interaction in the copper-platinum cell. 70
5.11 Graph of the model prediction of galvanic current in the copper-platinum cell. 72

6.1 Tafel plot of the effect of ferric concentration on the rate of ferric reduction on pyrite. 74
6.2 The effect of electrode rotation on ferric reduction rate at low electrode potentials. 75
6.3 The effect of temperature on ferric reduction rate at low electrode potentials. 75
6.4 Determination of the activation energy for ferric reduction on pyrite. 76
6.5 The effect of ferric concentration on galvanic current in a copper-pyrite couple. 77

6.6 The dependence of galvanic potential on ferric concentration. 77
6.7 The dependence of rest potentials on ferric concentration. 78
6.8 The hypothetical dependence of galvanic potential on polarisation curve shape. 79
6.9 The effect of temperature on galvanic current in a copper-pyrite couple. 80
6.10 Model prediction of galvanic current in the copper-pyrite couple. 81

7.1 The effect of sodium nitrate concentration on the rate of galena dissolution. 84
7.2 The effect of ferric concentration on the rate of galena dissolution. 85
7.3 The effect of rotation on the rate of galena dissolution. 86
7.4 Rest potentials of PbS in $HClO_4$ solution. 87
7.5 Polarisation curves illustrating the effect of temperature on galena dissolution rate. 88
7.6 Determination of the activation energy for galena dissolution. 89
7.7 Tafel plot of the effect of illumination on the rate of galena dissolution. 90
7.8 Stages in the dissolution of galena under illumination. 91
7.9 The effect of ferric concentration on the rate of ferric reduction on pyrite. 92
7.10 Determination of the diffusion coefficient for ferric reduction on pyrite. 93
7.11 The effect of rotation on the rate of ferric reduction on pyrite. 94
7.12 The effect of temperature on the rate of ferric reduction on pyrite. 94
7.13 The effect of rotation on galvanic current in the galena-pyrite cell. 96
7.14 The effect of illumination on the galvanic interaction between galena and pyrite. 98
7.15 Model prediction of galvanic current in the galena-pyrite couple. 99

8.1 Dynamic behaviour of the copper-pyrite and galena-pyrite couples. 100
8.2 The effect of electrode areas on galvanic interaction. 101
8.3 Galvanic current decay due to shrinking galena anode. 103
8.4 Variation in solution potential with time. 105
8.5 Decay in galvanic current due to decay in cathodic equilibrium potential. 106
8.6 Model prediction of cathodic equilibrium potential decay in the copper-platinum cell. 107

A.1 EDXA peaks associated with the pyrite disc electrode. 117
A.2 EDXA peaks associated with the galena disc electrode. 118
A.3 EDXA peaks associated with the pyrite ring electrode. 119

C.1 Galvanic couple consisting of an anodic cone and cathodic sphere. 128
C.2 Diffusion of metal ions through the anodic cone. 131

LIST OF TABLES.

Table	page
1.1 Equilibrium potentials of selected sulphide minerals.	25
5.1 Comparison of copper dissolution kinetic parameters.	60
5.2 Comparison of the current densities, in 0.3M Na_2SO_4 and 0.1M $Fe_2(SO_4)_3$ solutions, at various temperatures and at an electrode potential of 0.09 V.	63
5.3 Comparison of kinetic parameters for the Fe^{3+}/Fe^{2+} reaction.	67
5.4 Parameters used in the model equation.	71
6.1 Kinetic parameters used in the galvanic model equation for the copper-pyrite cell.	81
7.1 Comparison of kinetic parameters associated with galena dissolution.	84
7.2 The effect of ferric concentration on the galvanic interaction between galena and pyrite.	95
7.3 The effect of temperature on the magnitude of galvanic interaction in the galena-pyrite cell.	97
7.4 Kinetic parameters used in the galvanic model equation for the galena-pyrite cell.	98

NOMENCLATURE.

Symbol	Description	Units
α	charge transfer coefficient	-
a	activity of species, equ. 1.44	-
A	electrode surface area	m^2
b	stoichiometric coefficient	-
b_a	anodic Tafel slope	V/decade
b_c	cathodic Tafel slope	V/decade
C	concentration	mol/m^3
δ	diffusion film thickness	m
D	diffusion coefficient	m^2/s
E	potential versus reference electrode	V
F	Faraday's constant	C/mol
h	height of anodic cone	m
h'	irreversible acceleration coefficient, equ.1.46, 1.47, 1.48	
H_o	initial height of anodic cone	m
I	current	Amps
i	current density	$Amps/m^2$
i_l	limiting current density	$Amps/m^2$
i_o	exchange current density	$Amps/m^2$
J	flux of ionic species, eqn 1.13, 1.31, C.11, C.12	$mol/m^2.s$
k	rate constant	m/s
M	molar mass	kg/mol
η	overpotential	V
n	number of electrons	-
n_{Me++}	mols of metal ionic species	mols
n_{MeS}	mols of metal sulphide	mols
n'	reaction order	-
ϕ	potential versus reference electrode	V
ρ	density of species	kg/m^3
r	anodic cone radius	m

R	universal gas constant	J/K.mol
R_o	initial anodic cone radius	m
R'	resistance	ohms
t	time	seconds
T	temperature	K
γ	kinematic viscosity	m^2/s
v	volume of solution	m^3
V	potential difference	V
ω	electrode rotation rate	rads/s
x	galvanic interaction parameter equ. 1.32, 1.40	-
y	galvanic interaction parameter equ. 1.33, 1.41	-

Subscripts

a	anode
b	bulk solution
c	cathode
cor	corrosion
d	dissolution
diff	diffusion
e	equilibrium
f	free corrosion
g	galvanic
j	mineral contact junction
MeS	metal sulphide
Me^{++}	metal ionic species
ox	oxidation
red	reduction
s	electrode surface

Superscripts

A	anode
b	backward reaction

C	cathode
f	forward reaction
o	standard conditions

1. INTRODUCTION.

Galvanic interaction occurs when electrically conducting minerals, in contact, are placed in a media which facilitates charge transfer eg. an electrolyte. The result of galvanic interaction is that the rate of dissolution of one of the minerals is enhanced and the other is retarded.

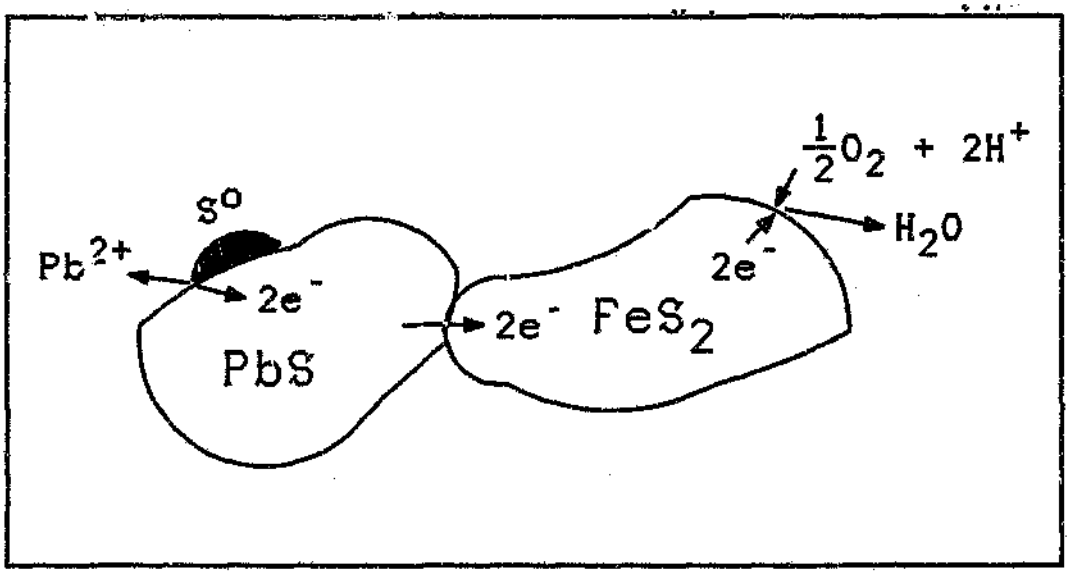


Figure 1.1 Galvanic interaction between PbS and FeS_2.

The pyrite, FeS_2, in Figure 1.1, provides a more favourable site than galena, PbS, for the reduction of dissolved oxygen. This results in an increase in the dissolution rate of galena.

It is evident therefore that galvanic interaction occurs in many minerals processing systems, especially in leaching and flotation. The importance of galvanic interaction in leaching systems was noted by Majima and Peters (1968) who stated:

" *The galvanic effect may be one of the most important electrochemical factors which*

governs the dissolution rate of sulphide minerals in hydrometallurgical systems "

Rao and Finch (1988) observed that galvanic interactions between mixtures of sulphide minerals, in the flotation pulp phase, influenced the amount of sulphide mineral floated.

Galvanic interaction is a well known phenomenon. However the exact processes and mechanisms of this effect are poorly understood in sulphide mineral systems. Research to describe galvanic interaction in sulphide mineral systems is primarily qualitative. Qualitative descriptions such as those given by Mehta and Murr (1983) have described the magnitude of the galvanic interaction in terms of the variables of the physical system eg. pulp density which effects the magnitude of mineral contact, and the particle size distribution, which determines the magnitude of the galvanic current flowing through a particle. Qualitative descriptions of galvanic interaction given by Dutrizac and MacDonald (1973) describe the magnitude of galvanic interaction in terms of the equilibrium potentials of the minerals forming the galvanic couple.

Quantitative descriptions of galvanic interaction have included thermodynamic and kinetic parameters. Pioneering work by corrosion scientists, using superposition theory, has provided a method for both monitoring and predicting the magnitude of galvanic interaction by mathematical and graphical techniques. The techniques and methodologies presented, however, have generally not been fully utilised in the description of the galvanic interaction between sulphide minerals. The quantitative descriptions of the galvanic interaction in sulphide mineral systems have either been specific or lacking in experimental verification. Previous research, in addition, highlighted the need for a dynamic description of galvanic interaction as well as the possible influence semiconducting properties of sulphide minerals may exert on galvanic interaction.

Chapter 1 consists of a review of the electrochemical theory and techniques pertinent to this research. The literature on the qualitative and quantitative descriptions of

galvanic interactions in sulphide minerals is reviewed in the latter sections of Chapter 1. The final section of the chapter describes the scope and objectives of this study. The chemistry associated with the galvanic couples characterised in this study is presented in Chapter 2. A mathematical model to describe galvanic interaction is developed in Chapter 3. In Chapter 4 the experimental techniques and procedures are discussed. The results and discussion of the study into the galvanic interaction between copper and platinum in ferric sulphate solutions are contained in Chapter 5. The galvanic interaction between copper and pyrite is analyzed and discussed in Chapter 6. The results and discussion of the galvanic interaction in a mineral system, consisting of a galena anode and a pyrite cathode, are reported in Chapter 7. Various mathematical expressions which account for dynamic behaviour during galvanic interaction are derived in Chapter 8. The conclusions and recommendations for further study are presented in Chapter 9.

1.1 Electrochemical Theory

This section reviews the electrochemical theory which is applicable to this research. Various thermodynamic and kinetic aspects of electrode processes are presented. The electrochemical techniques, cyclic voltammetry and steady-state potentiostatic measurements, are also discussed. The literature reviewed was referenced from the following sources; Atkins (1986), Pletcher (1991) and Bard and Faulkner (1980).

1.1.1 An introduction to electrochemistry.

A separation of charge occurs at the interface between two phases when the phases are brought into contact. This is due to the intermolecular forces at the phase boundaries being different to those in the interiors of the phases. If one considers a solid-solution interface the adsorption of anions or cations may occur on the surface of the electrode whilst just beneath the electrode surface an excess or deficiency of electrons is likely to occur. This charge separation is known as an

electrical double layer. The charges on each side of the interface are equal but of opposite sign.

Various models have been proposed which describe the structure of this electrical double layer. The simplest model, proposed by Helmoltz and illustrated in Figure 1.2A, describes the electrical double layer as consisting of two rigid planes of charge. The solvated ions forming the outer Helmoltz plane are held away from the surface of the electrode by their hydration spheres. The inner Helmoltz plane is formed by the charges present beneath the electrode surface. The Helmoltz model is structurally too rigid and ignores the effect of the thermal motion of ions, which cause the outer Helmoltz layer to break up and the ions to diffuse into the bulk solution.

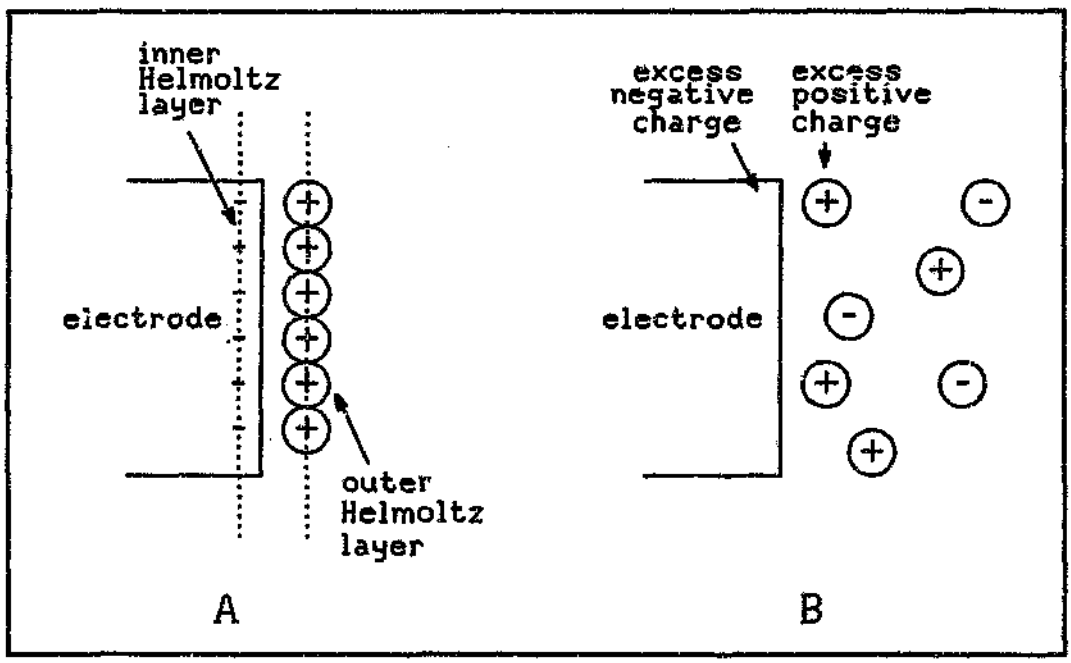


Figure 1.2 Models for the electrical double layer. (A) The Helmoltz model. (B) The Gouy-Chapman model.

The Gouy-Chapman model, illustrated in Figure 1.2B, accounts for the thermal motion of ions. The concentrations of positively and negatively charged ions at the surface of the electrode differ from the concentrations in the bulk solution. Cations

are attracted to the negatively charged electrode whilst anions are repelled from the negatively charged electrode. The Gouy-Chapman model, however, underemphasises the structure of the electrical double layer.

The Helmoltz model and Gouy-Chapman model are combined in the Stern model which proposes that the ions nearest to the electrode form the outer Helmoltz plane whilst outside this plane the ions are dispersed according to the Gouy-Chapman model.

The electrical double layer acts as a capacitor and its ability to store charge with fluctuations in potential is given by Equation 1.1.

$$C_d = \frac{\partial \sigma}{\partial E} \qquad 1.1$$

C_d is the capacitance of the double layer, σ is the charge density and E is the potential with respect to a reference electrode.

Faradaic and non-faradaic currents may flow at the surface of an electrode. A faradaic current arises when there is a transfer of charge, caused by an oxidation or reduction reaction, across the electrode-solution interface. A non-faradaic current arises when factors which affect the capacitance of the double layer, electrode area and electrode condition, are changed.

1.1.2 Thermodynamics of electrode processes.

Consider the equilibrium half reaction comprising of an oxidizing species, Ox, reducing to form the species Red.

$$Ox + ne^- \rightleftarrows Red \qquad 1.2$$

At equilibrium there is no net current since the current for the reduction reaction is equal to the current for the oxidation reaction. The equilibrium potential of the redox reaction is given by the Nernst equation.

$$E_e = E_e^\circ + \frac{RT}{nF} \ln\left[\frac{C_{Ox}}{C_{Red}}\right] \qquad 1.3$$

E_e° is the equilibrium potential of the redox reaction under standard conditions. C_{Ox} and C_{Red} are the concentrations of the Ox and Red species respectively. In cases where concentrations of species are high non-ideal behaviour can occur. In this instance the concentrations should be replaced by the activities of the species partaking in the redox reaction since the activity coefficients will not be equal to one.

The equilibrium potential E_e can only be measured by comparing it to the potential of another redox couple. The standard hydrogen electrode (SHE) is used as the reference basis for the redox couples. The reaction

$$H^+ + e^- \rightleftarrows \frac{1}{2}H_2(g) \qquad 1.4$$

has been assigned a standard equilibrium potential of 0.0 V. The standard hydrogen electrode is not a practical reference electrode for use in electrochemistry owing to the use of gaseous hydrogen. The standard calomel electrode (SCE) is generally used as a reference electrode in electrochemical studies. The standard calomel electrode has a standard equilibrium potential of 0.24 V vs SHE.

The Nernst equation has been applied in the construction of potential-pH diagrams, otherwise called Pourbaix diagrams. A Pourbaix diagram is a framework which allows one to obtain thermodynamic data for electrochemical reactions. Examples of Pourbaix diagrams which were utilised in this research are illustrated in Figures 2.1 to 2.3

For a general electrochemical reaction

$$aA + cH_2O + ne^- \rightleftarrows bB + mH^+ \qquad 1.5$$

where A is the oxidised form and B the reduced form of the species the Nernst equation can be written as

$$E_e = E_e^\circ + 0.0591\frac{m}{n}\,pH + \frac{0.0591}{n}\log\frac{C_A^a}{C_B^b} \qquad 1.6$$

where a, b and m are stoichiometric coefficients, n is the number of electrons transferred in the redox reaction and C is the concentration of species.

The Pourbaix diagram is a plot of the equilibrium potential of a redox couple versus the pH. Electrochemical reactions which are pH independent are represented as horizontal lines whilst electrochemical reactions which are pH dependant are represented by lines of non-zero slope. The Pourbaix diagram illustrates the regimes in which aqueous species are thermodynamically stable.

1.1.3 Kinetics of electrode processes.

1.1.3.1 Electrochemically controlled reactions.

An electrochemically controlled reaction is one in which the rate determining step involves the transfer of charge across the electrode-solution interface. The Butler-Volmer equation mathematically describes the relationship between the current through an electrode and the potential difference across the electrode-solution interface.

$$i = i_o\left[\exp\left(\frac{(1-\alpha)F\eta}{RT}\right) - \exp\left(\frac{-\alpha F\eta}{RT}\right)\right] \qquad 1.7$$

where : i_o is the exchange current density, α is the charge-transfer coefficient and η is the overpotential.

The exchange current density is equal to the oxidation and reduction current when the redox reaction is at equilibrium. The exchange current density is given by Equation 1.8.

$$i_o = nF(k_{ox}C_{Red})^{\alpha}(k_{red}C_{Ox})^{1-\alpha} \qquad 1.8$$

where : k_{ox} and k_{red} are the rate constants for the oxidation and reduction processes.

The departure of the electrode potential from the equilibrium electrode potential is known as the overpotential.

$$\eta = E - E_e \qquad 1.9$$

The Butler-Volmer equation is represented graphically as a plot of the current density versus the overpotential and is known as a polarisation curve. A net current, i, will result as the potential difference across the electrode-solution interface is changed. The net current varies exponentially with increases in the potential difference across the electrode-solution interface. The first exponential term in the Butler-Volmer equation is the contribution of the oxidation process to the net current whilst the second exponential is the contribution of the reduction process to the net current. There are three simplified forms of the Butler-Volmer equation:

Case I : At overpotentials less than 0.01 V the exponentials in Equation 1.7 can be approximated by $e^x = (1+x)$ to give

$$i = \frac{i_o nF\eta}{RT} \qquad 1.10$$

Case 2 : At large positive overpotentials the first exponential is much greater than the second exponential which therefore be neglected. In this instance the oxidation reaction is more significant than the reduction reaction.

$$i = i_o \exp\left(\frac{(1-\alpha)nF\eta}{RT}\right) \qquad 1.11$$

Case 3 : At large negative overpotentials the first exponential can be neglected. In this instance the reduction reaction is more significant than the oxidation reaction.

$$i = i_o \exp\left(\frac{-\alpha nF\eta}{RT}\right) \qquad 1.12$$

It is evident that a plot of ln i versus η, also known as a Tafel plot, yields the exchange current density and the charge-transfer coefficient.

1.1.3.2 Mass transfer controlled reactions.

A redox reaction may be controlled by the mass transfer of a reacting species to the surface of the electrode. There are three modes by which a reacting species can be transported namely diffusion, convection and migration.

(i) *Diffusion*

Diffusion is the transfer of species due to the existence of a concentration gradient.

The species diffuse from areas of high concentration to areas of low concentration until the concentrations are equivalent. The rate of linear diffusion, or flux, to a plane is given by Fick's first law

$$J = -D\frac{dc(x)}{dx} \qquad 1.13$$

where J is the flux of species, D is the diffusion coefficient and dc(x)/dx is the concentration gradient.

The variation of the concentration gradient over time is expressed by Fick's second law. The solution of Fick's second law, under various boundary conditions, yields the concentration profiles which are essential in the mathematical description of the electrochemical processes in which diffusion is a mode of transport.

$$\frac{\partial c(x,t)}{\partial t} = D\,\frac{\partial^2 c(x,t)}{\partial t} \qquad 1.14$$

A limiting form of Fick's first law exists when the concentration of species at the electrode surface is zero.

$$i_l = -\frac{nFDC_{Ox,b}}{\delta} \qquad 1.15$$

where : i_l is the limiting current density, $C_{Ox,b}$ is the concentration of oxidant in the bulk solution and δ is the thickness of the Nernst diffusion layer.

The limiting current density is independent of any variations in the potential difference across the electrode-solution interface. A diffusion controlled reaction is represented as a plateau, see Figure 1.3, on a polarisation curve.

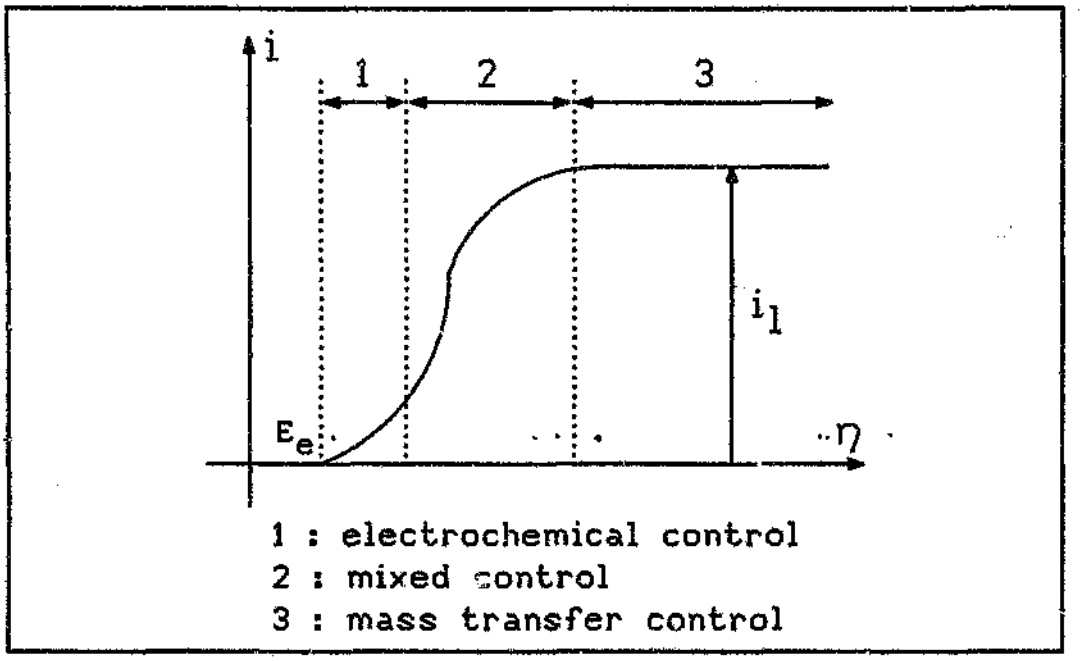


Figure 1.3 Polarisation curve, for the anodic reaction Red = Ox + e^-, illustrating various reaction control regimes.

Regime 2 is a mixed-control regime in which the electrochemical reaction is controlled by both charge-transfer and mass transfer processes. The mathematical expression for a mixed-control reaction is derived in Section 3.2.2.

(ii) *Convection*

Convection is the transfer of species by bulk movement of solution. Convection may occur due to externally applied forces, forced convection, or be a result of variations of temperature and density within the solution, natural convection. Forced convection to a circular electrode surface is achieved by rotating the electrode. The rotating electrode is termed a rotating disc electrode. The solution flow patterns to a rotating disc electrode are illustrated in Figure 1.4.

The rotation of the electrode results in a force, in the x-direction, which pulls the solution perpendicularly upwards towards the surface of the electrode. The rate of

solution movement in the x-direction decreases as the solution nears the electrode surface. As the solution approaches the electrode surface it experiences a tangential force, indicated by Θ in Figure 1.4C. The tangential velocity of the solution increases as the electrode surface is approached. Ultimately, at the electrode surface the tangential velocity of the solution is equal to the rotational velocity of the electrode. The solution, in addition, experiences a radial force which results in the solution being forced radially outwards at the electrode surface.

A mathematical description of the concentration-gradient to the surface of a rotating disc electrode was formulated by Levich (1961). The mathematical description accounts for both the diffusion of solution to the electrode surface and convective processes. Levich (1961) deduced an expression, Equation 1.16, which relates the Nernst diffusion layer thickness, δ, to the rotation rate of the electrode,

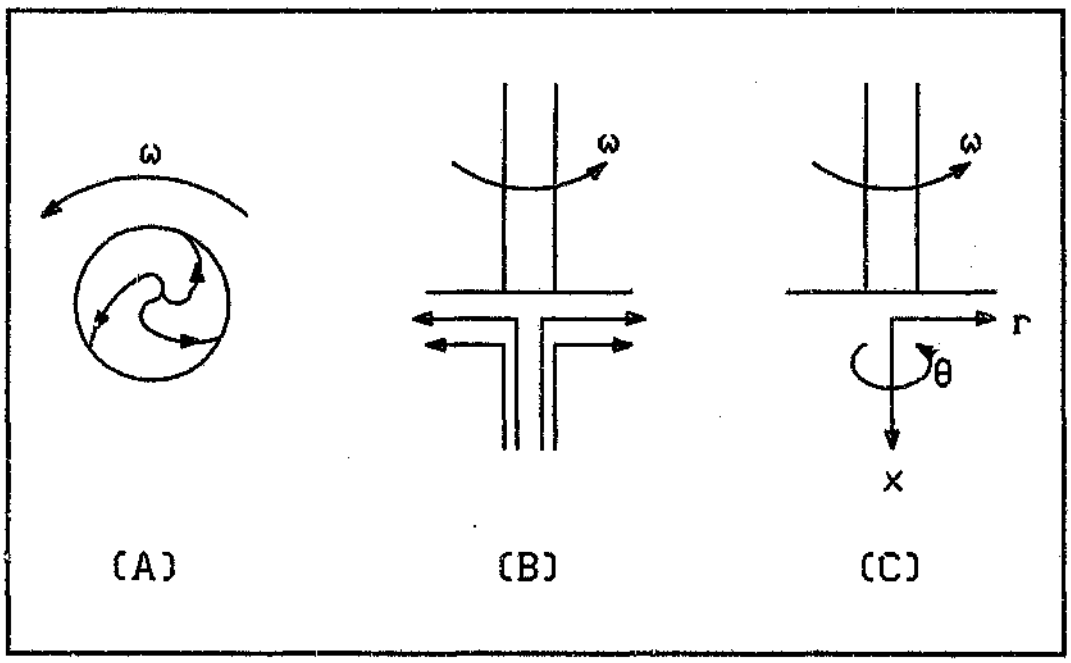


Figure 1.4 Fluid flow to a rotating disc electrode. (A) View from below. (B) Side view. (C) Force co- ordinate system. Analogous to Pletcher (1991) p.135.

$$\delta = \frac{1.61\gamma^{0.166}D^{0.33}}{\omega^{0.5}} \qquad 1.16$$

where γ is the kinematic viscosity of the solution.

The well known Levich expression is obtained from combining Equations 1.15 and 1.16.

$$i_l = 0.62\ n\ F\ D^{0.67}\ \gamma^{-0.166}\ C\ \omega^{0.5} \qquad 1.17$$

The Levich equation provides a basis for determining whether a reaction is mass transfer controlled. A plot of the limiting current density versus the square root of rotation yields a straight line for a mass transfer controlled reaction.

(iii) *Migration*

Species migrate in the presence of a potential field. A potential gradient exists between two electrodes of opposite charge and thus migration occurs in many electrochemical processes. In electrochemistry the effect of migration is usually minimised by adding high concentrations of base electrolyte to the solution. The action of the supporting electrolyte is to reduce the transport number of the migrating species.

1.1.4 Electrochemical theory of leaching.

A leaching or corrosion process consists of an oxidation and reduction reaction. The oxidation and reduction reactions occur at points on the surface of the particle and hence no net current is generated. This is illustrated in Figure 1.5. The corresponding hypothetical polarisation curves for the oxidation and reduction reactions are given in Figure 1.6.

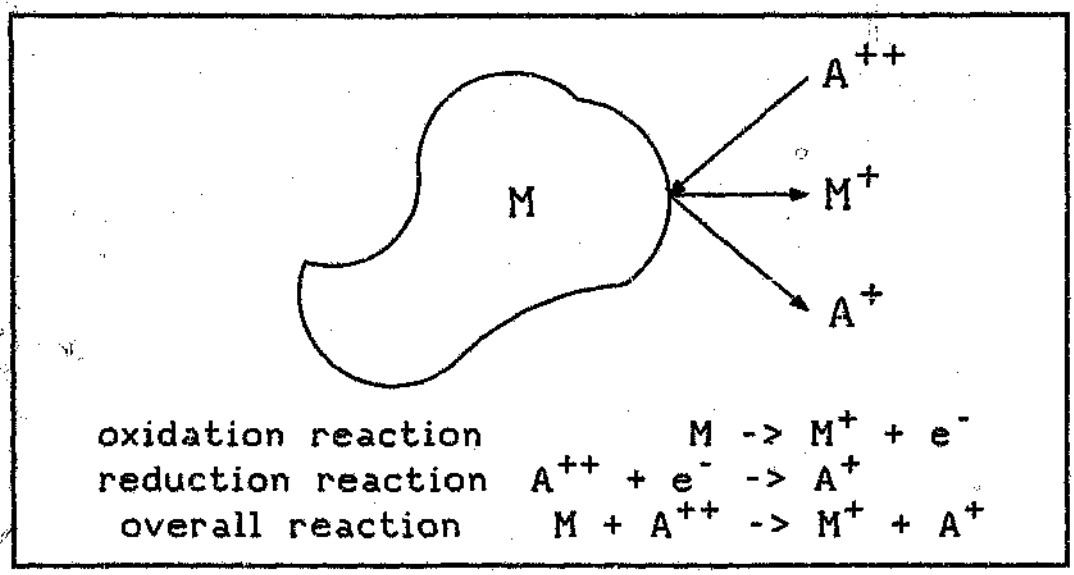


Figure 1.5 The leaching of a particle, M, by oxidant A^{++}.

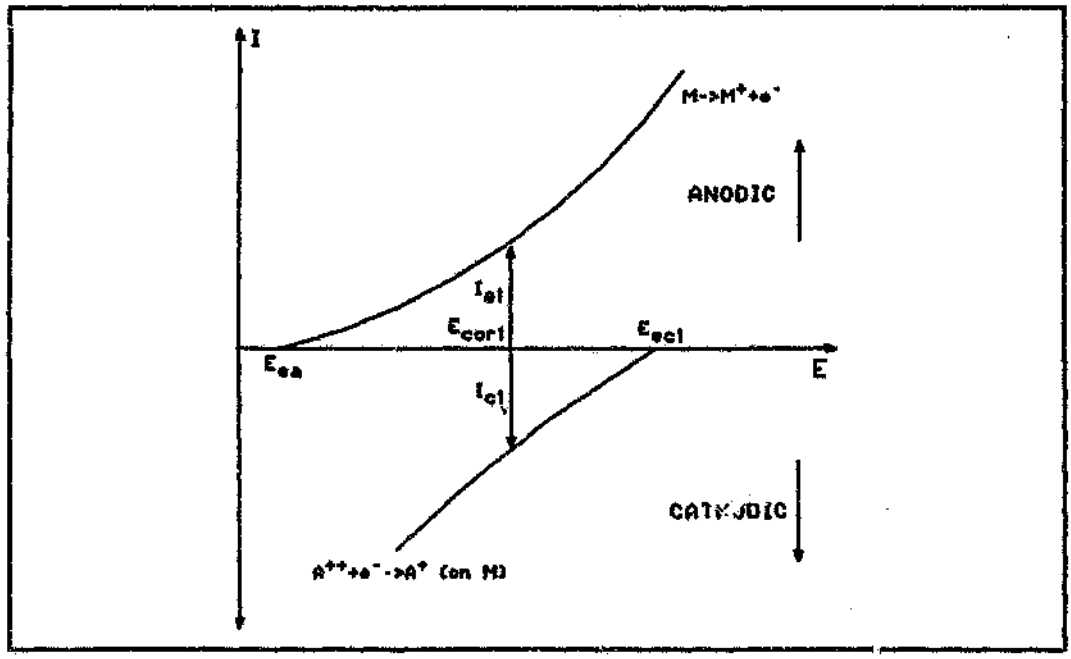


Figure 1.6 Polarisation curves for the oxidation of M and the reduction of A^{++}.

Mixed potential theory utilises the electrochemical theory of half reactions to develop rate expressions for leaching processes. An example of the derivation of a rate expression, based on mixed potential theory, is given for the oxidation of M by A^{++}. The mixed potential, or corrosion potential, E_{corl}, is reached when the oxidative current, I_{al}, is equal to the reduction current, I_{cl}. If it is assumed that the anodic part of the Butler-Volmer equation describes the oxidation of M and the cathodic part of the Butler-Volmer equation describes the reduction of A^{++} the following relationships for the anodic and cathodic reactions hold:

$$i_a = k_{ox} \exp\left[\frac{\alpha_a F E_{corl}}{RT}\right] \qquad 1.18$$

$$i_c = -k_{red} C_{A^{++}} \exp\left[\frac{-(1-\alpha_c) F E_{corl}}{RT}\right] \qquad 1.19$$

Equating 1.18 and 1.19 and rearranging

$$E_{corl} = \frac{RT}{(1+\alpha_a-\alpha_c)} \ln\left[\frac{k_{red} C_{A^{++}}}{k_{ox}}\right] \qquad 1.20$$

Substituting Equation 1.20 into Equation 1.18 one obtains an expression for the leaching rate of M by A^{++}

$$-\frac{dM}{dt} = \frac{i_a}{F} = k_{ox}^{(1-\beta)} k_{red}^{\beta} C_{A^{++}}^{\beta} \qquad 1.21$$

where β is given by

$$\beta = \frac{\alpha_a}{1 + \alpha_a - \alpha_c} \qquad 1.22$$

Li, Zhong and Wadsworth (1992) discuss the various applications of mixed potential

theory in hydrometallurgy.

1.1.5 Electrochemical theory of galvanic interaction.

Figure 1.7 illustrates the galvanic interaction which results from electrode N being brought into contact with electrode M. It is assumed that electrode N provides a more favourable site for the reduction of A^{++} which results in an increase in the rate of oxidation of electrode M. Galvanic interaction differs from leaching in that a net current, which flows through the galvanic cell, is generated. The amount of A^{++} reduced on electrode M is dependant on how favourable the reduction of A^{++} is on electrode N. If A^{++} reduction on electrode N is very favourable the amount of A^{++} reduced on electrode M, relative to the amount of A^{++} reduced on electrode N, is small.

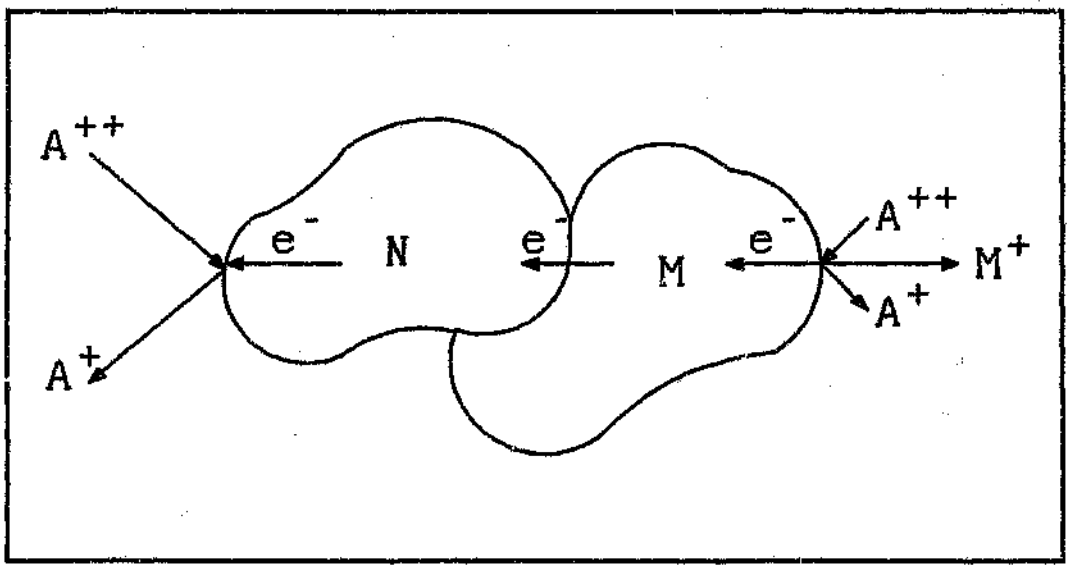


Figure 1.7 The hypothetical galvanic interaction between electrode M and electrode N.

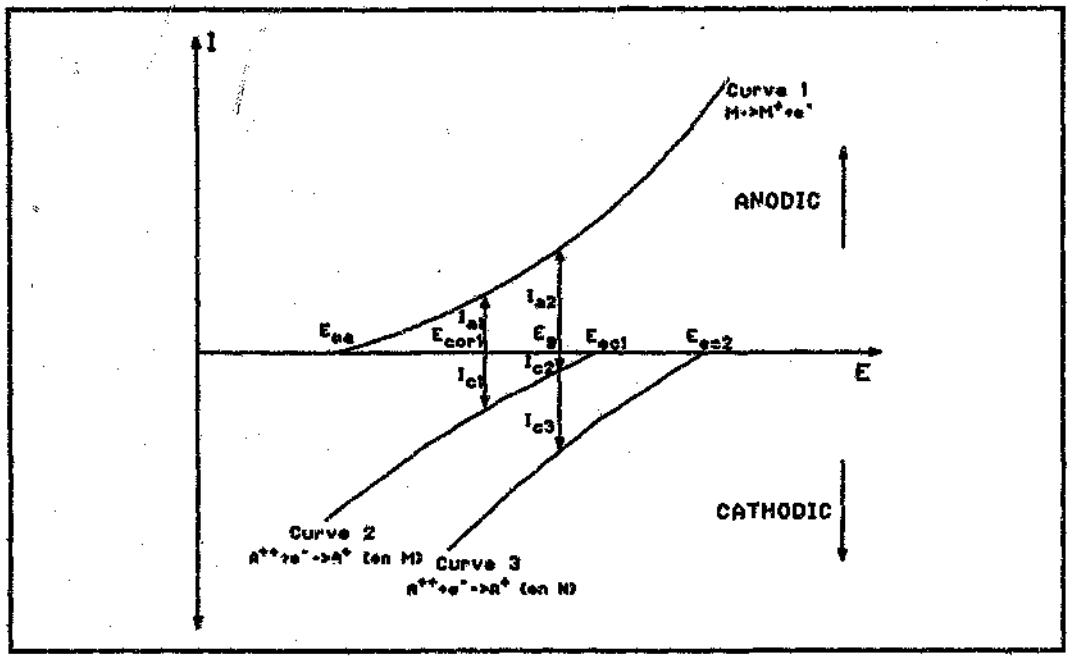


Figure 1.8 Polarisation curves for the reactions occurring in the galvanic couple formed between electrode M and electrode N.

Figure 1.8 is utilised in providing an electrochemical description of galvanic interaction based on the kinetics of the reactions occurring in the galvanic couple. The anodic oxidation of species M to M^+ is represented by curve 1, the cathodic reduction of A^{++} on electrode M is represented by curve 2 and the cathodic reduction of A^{++} on electrode N is represented by curve 3.

Electrode N when placed in electrical contact with electrode M provides a more favourable site for the reduction of species A^{++} partly due to the equilibrium potential E_{cc2} being more cathodic than E_{cc1}. The coupling of the two electrodes causes the mixed potential to shift from E_{cor1} to the galvanic potential E_g. This results in the current through the couple increasing from I_{a1} to I_{a2}. The galvanic current, I_g, is equal to the sum of the anodic currents or the sum of the cathodic currents at the galvanic potential, E_g :

$$I_g = I_{a2} = |I_{c2} + I_{c3}| \qquad 1.23$$

An increase in galvanic current will occur for any further anodic or cathodic reaction having an equilibrium potential less or greater than E_{an} and E_{cel} respectively.

1.1.6 Electrochemical techniques.

The electrochemical techniques which were used in this study are discussed in this section. Pletcher (1991) was used as a reference text.

1.1.6.1 Steady-state potentiostatic measurements.

The steady-state potentiostatic measurement technique is widely used to determine the kinetics of an oxidation or reduction reaction. The three-electrode cell, discussed in Section 4.2.2, allows the potential across the electrode-solution interface to be varied. Steady-state potentiostatic measurement consists of applying a certain potential across the electrode-solution interface and measuring the steady-state current emitted from the electrode. In most systems the steady-state current is reached in less than 60 seconds. The form of the steady-state current-potential data obtained determines the reaction control mechanism, as discussed in Section 1.1.3. The kinetic parameters for the reaction can be determined by graphical techniques, eg. a Tafel plot, or by regressing the steady-state current-potential data with the appropriate kinetic equation.

1.1.6.2 Cyclic voltammetry.

Cyclic voltammetry is widely used as an initial step, in characterising a system, to determine whether the products of an electrochemical reaction are stable or electroactive. Cyclic voltammetry involves sweeping the potential across the electrode-solution interface between lower and upper potential limits. The current and potential are recorded and the plot hereof is called a cyclic voltammogram. The

characteristic feature of a cyclic voltammogram is the presence of current peaks which are caused by non-steady-state processes. The position of the current peaks on the forward and reverse sweeps can be used to determine whether the electrochemical reaction is reversible or irreversible. In addition to this it can be determined whether an adsorbed species or phase formation are involved in the rate determining step.

The peaks generated in cyclic voltammetric studies make it difficult, although not impossible, to determine the kinetic parameters of a reaction. In this study very slow sweep rates, 1 $mV.s^{-1}$, were used to characterise the half reactions. The low sweep rates ensured that the system attained a pseudo-steady-state and hence the kinetic parameters could be readily determined.

1.2 Literature Review.

The section consists of a survey of the previous research conducted to describe galvanic interactions. Section 1.2.1 covers the research conducted by corrosion scientists whilst in Sections 1.2.2 and 1.2.3 the literature describing galvanic interactions in sulphide mineral systems is reviewed.

1.2.1 Galvanic interaction studies in corrosion.

Two methods have generally been used to experimentally measure galvanic current. The first of these is a zero impedance ammeter technique. Jones (1984) made use of a zero impedance ammeter to monitor galvanic current. In this instance the current flowing through the galvanic couple is short-circuited through an ammeter of zero impedance. This technique allows continuous recording of galvanic current.

The second method of measuring galvanic current is a weight loss measurement technique. Mansfield and Parry (1973) used a weight loss measurement technique

to monitor galvanic current in aluminium alloys. The technique involves the measurement of the mass of the corroding electrode, prior to it being placed in a corrosive environment, and comparing this with the mass of the specimen after corrosion. This difference in mass can be related to the magnitude of galvanic corrosion. A variation of this technique involves measuring the concentration of the corroding electrode in the solution at various time intervals. The concentration can be related to the galvanic current, however, discrepancies exist due to the assumption that the dissolution rate of the electrode is equivalent to the galvanic corrosion rate.

Superposition theory allows the galvanic current to be determined by mathematical or graphical techniques. Graphical solution entails superimposing all the polarisation curves on one graph and solving for the galvanic current by determining the galvanic potential at which the anodic and cathodic currents are equal. Mathematical solution requires that the relevant mathematical equations, such as the Butler-Volmer equation, are used to describe the anodic and cathodic half reactions. The equations are equated and the galvanic current is determined by eliminating the potential between these equations.

Jones (1968) observed an excellent correspondence between the galvanic currents determined by superposition theory and those measured by a zero impedance ammeter. The linear polarisation current, I, was expressed in terms of the corrosion current, I_{cor}, and the anodic and cathodic Tafel constants, b_a and b_c.

$$\frac{\eta}{I} = \frac{b_a b_c}{2.3 I_{cor}(b_a + b_c)} \qquad 1.24$$

In the study $b_a >> b_c$ and Equation 1.24 can be simplified to:

$$I_{cor} = \frac{b_c}{2.3\frac{\eta}{I}} \qquad 1.25$$

Davis, Kolts and Sridhar (1968) used superposition theory to predict the magnitude of galvanic corrosion of stainless steel in contact with a number of alloys. Polarisation curves of all the individual alloys were generated and mathematically described by the Butler-Volmer equation. It was assumed that both electrodes operate in the purely electrochemically reaction control regime. Taking into account the condition of charge neutrality on galvanic coupling as well as knowledge of Tafel constants, exchange current densities, equilibrium potentials, charge transfer coefficients and the areas of the electrodes the overall expression, Equation 1.26, was derived.

$$A_a i_{o,a}\left[\exp\left[\frac{2.3}{b_a^A}(E_g - E_{o,a})\right] - \exp\left[\frac{2.3}{b_c^A}(E_{o,a} - E_g)\right]\right] + A_c i_{o,c}\left[\exp\left[\frac{2.3}{b_a^C}(E_g - E_{o,c})\right] - \exp\left[\frac{2.3}{b_c^C}(E_{o,c} - E_g)\right]\right] = 0 \qquad 1.26$$

Equation 1.26 can be solved using a Newton Raphson technique to determine the galvanic potential E_g. Current densities at the anode and cathode are solved through the use of the Butler-Volmer equation which describes the total corrosion rate through the anode, Equation 1.27.

$$i = i_{o,a}\exp\left[\frac{2.3}{b_a^A}(E_g - E_{o,a})\right] \qquad 1.27$$

Equations 1.26 and 1.27 are not applicable to a system which exhibits active-passive behaviour. This behaviour is noticeable by the appearance of maxima and minima on the polarisation curves.

Davis *et al.* (1968) observed that the equilibrium potentials of the two alloys in a galvanic couple are not good indicators of corrosion rates. Numerical superposition of the polarisation curves yielded a good prediction of the galvanic corrosion rate. The accuracy of this method was observed to be strongly dependent on the accurate measurement of Tafel constants and exchange current densities.

Mansfield (1971) investigated the effect of anode and cathode area on the galvanic corrosion rate. Three cases were investigated.

Case 1 : At the galvanic potential, E_g, metal dissolution occurs at the anode while reduction of H^+, H_2O or O_2 occurs at the cathode. Tafel behaviour was assumed to exist at both electrodes. Equation 1.28 illustrates the relationship between the galvanic current density, i_g, and the exchange current densities, $i_{o,c}$ and $i_{o,a}$.

$$\log i_g^A = \frac{E_{o,c} - E_{o,a}}{2.3(b_a - b_c)} + 2.3\frac{b_c}{b_c + b_a}\log i_{o,c}\frac{A_c}{A_a} + 2.3\frac{b_a}{b_a + b_c}\log i_{o,a} \qquad 1.28$$

Case 2 : The galvanic couple formed between two electrodes results in the anode being slightly polarised from the corrosion potential. It was proved that the galvanic current density is not equal to the dissolution rate of the anode. Equation 1.29 illustrates the relationship between the galvanic current density, i_g, and the dissolution current density, i_d, on the anode.

$$\frac{i_d^A}{i_g^A} = 1 + \frac{i_{o,c}^A A_a}{i_{o,c}^C A_c} \qquad 1.29$$

In an extension of this work Mansfield (1973) proposed a galvanic correction factor which allows accurate predictions of dissolution rates from galvanic currents.

Case 3 : It was assumed that the cathodic processes on both electrodes are entirely diffusion controlled. Equation 1.30 illustrates the relationship between the galvanic potential, E_g, and the ratio of the cathodic and anodic areas, A^C and A^A.

$$E_g = E_{cor}^A + b_a \log\left[\frac{A^C}{A^A}\right] \qquad 1.30$$

This research highlighted the importance of electrode area in a galvanic couple. The

electrode areas of the anode and cathode determine the position of the galvanic potential.

Fangteng and Charles (1987) mathematically modelled galvanic corrosion by allowing for cathodic dissolution in addition to anodic dissolution. The rate of corrosion was controlled by the diffusion of oxygen to the surfaces of the electrodes. It was observed that the dissolution of the cathode in a galvanic couple causes a decrease in the galvanic current flowing through the couple.

It is apparent therefore that corrosion scientists have conducted extensive research to describe galvanic interactions. Practical techniques have been developed which allow ready measurement of galvanic current. In addition to this the magnitudes of galvanic interaction have been mathematically described in terms of the kinetic parameters, i.e. Tafel constants and exchange current densities, of the half reactions occurring in galvanic cells. To a large extent researchers studying galvanic interactions in sulphide minerals have neglected the techniques and theory developed by corrosion scientists even though most sulphide minerals have resistivities that are sufficiently low to allow the application of electrochemical techniques to measure electrode kinetics.

1.2.2 Qualitative descriptions of galvanic interaction in sulphide mineral systems.

Qualitative descriptions of galvanic interactions in sulphide mineral systems have been expressed in terms of the effects physical system variables have on the magnitude of galvanic interaction and in terms of the differences in the anodic and cathodic equilibrium potentials.

Mizoguchi and Habashi (1983) noted that the presence of pyrite during the leaching of sphalerite, ZnS, increased the recovery of zinc and sulphur. This was attributed to the pyrite providing a more favourable site for the cathodic reduction of dissolved oxygen.

Dutrizac, Macdonald and Ingraham (1971) studied galvanic interactions between bornite, Cu_5FeS_4, and different mixtures of sulphide minerals. Various mixtures of chalcopyrite, $CuFeS_2$, pyrite and digenite, $Cu_{1.8}S$, were sintered together with bornite to form electrodes. At 15 °C in an acidified ferric sulphate solution it was found that minor variations in the rate of bornite leaching occurred when chalcopyrite and digenite were present in the sintered sulphide electrode. The presence of pyrite greatly enhanced the rate of bornite dissolution.

Mehta and Murr (1983) conducted work on a number of galvanic couples, including chalcopyrite and sphalerite in electrical contact with pyrite. The effect that galvanic interaction had on the bacterial leaching rate of chalcopyrite and sphalerite was investigated. The effects that the particle size, the presence of bacteria and the pulp density have on the rate of leaching of the minerals in contact were described qualitatively. It was observed that as the amount of pyrite in contact with another mineral increases the leaching rate of this mineral is increased.

To explain the phenomenon of an increased leaching rate, due to galvanic coupling of two minerals, Mehta and Murr (1983) presented a series of sulphide minerals, arranged according to the equilibrium potential of the minerals with respect to the standard hydrogen electrode. The series is given in Table 1.1.

Table 1.1 Equilibrium potentials of selected sulphide minerals.

Mineral	Chemical Formula	E_e vs SHE (Volts)
Pyrite	FeS_2	0.63
Chalcopyrite	$CuFeS_2$	0.52
Chalcocite	Cu_2S	0.44
Bornite	Cu_5FeS_4	0.42
Galena	PbS	0.28
Sphalerite	ZnS	-0.24

Sulphide minerals with more positive equilibrium potentials, eg. pyrite 0.63 V vs SHE, act as cathodes in a galvanic couple whilst minerals with more negative equilibrium potentials, eg. sphalerite -0.24 V vs SHE, act as anodes. The magnitude of the difference between the cathodic and anodic equilibrium potentials was used as a measure of the magnitude of galvanic interaction. This is a simplification in that kinetic parameters are an important criterion for determining the magnitude of galvanic interaction.

Dutrizac and MacDonald (1973) investigated the effect impurities have on the dissolution rate of chalcopyrite. The presence of pyrite was observed to accelerate the dissolution rate of chalcopyrite whilst the presence of galena was observed to retard the dissolution of chalcopyrite. These observations are consistent with those proposed by the sulphide series. However, Dutrizac and MacDonald (1973) observed that the dissolution rate of chalcopyrite increased in the presence of molybdenite, MoS_2, which has an equilibrium potential of 0.11 V vs SHE. This is not consistent with the sulphide series and emphasises the need for kinetic aspects, such as reaction mechanisms and rates, to be accounted for in order to describe the magnitude of galvanic interaction accurately.

Hepel (1984) investigated the mechanisms which lead to selective leaching in sulphide mineral systems. Galvanic cell formation between electrically conducting minerals caused the suppression of leaching of some sulphides. To quantify galvanic interactions accurately it was concluded that consideration should be given to both the thermodynamics and kinetics of electrode processes.

1.2.3 Quantitative descriptions of galvanic interaction in sulphide mineral systems.

The literature reviewed in this section consists of research conducted to describe the magnitude of galvanic interaction in terms of kinetic parameters.

Lorenzen and van Deventer (1992) investigated the dissolution of gold electrodes in contact with various conducting minerals associated with gold bearing ores. The rate of gold dissolution was controlled by the diffusion of oxygen or cyanide to the surface of the gold electrode. The authors made use of the Levich equation, Equation 1.31, to predict the flux of gold, J, from the surface of the gold electrode. The Levich equation, however, predicted higher fluxes to the gold surface than those observed experimentally. This was due to the gold surface being at least partially passivated.

$$J = 0.62\, D^{0.66}\, \gamma^{-0.166}\, \omega^{0.5}\, s\, C\, M \qquad 1.31$$

where : s is the stoichiometric coefficient, C is the concentration of the diffusing species, and M is the molar mass of gold.

Nowak, Krauss and Pomianowski (1984) used a zero impedance ammeter to measure the galvanic current between a number of sulphide minerals. The researchers defined a parameter, x, as the ratio of the galvanic current, I_g, to the total current used for the anodic process on the anode, I_a^A. This parameter characterises the extent of the participation of the galvanic process on the total dissolution of the mineral.

$$x = \frac{I_g}{I_a^A} = 1 + \frac{I_c^A}{I_a^A} \qquad (x \leq 1) \qquad 1.32$$

Nowak *et al.* (1984) defined a further parameter, y, as the ratio of the anodic current produced by the galvanic couple on the anode, I_a^A, to the anodic current on the anode, $I_{a,cor}^A$, without galvanic coupling.

$$y = \frac{I_a^A}{I_{a,cor}^A} \qquad (y \geq 0) \qquad 1.33$$

The parameter y is a measure of the influence of the galvanic effect on the corrosion of a mineral. Coupling an anode to various cathodes of increasing nobility will increase the value of y and thus galvanic corrosion becomes an increasingly important factor in the corrosion of the mineral. Equations of a synonymous form are defined for the cathodic processes.

A number of models based on relationships between the equilibrium potentials of the anode and cathode and the galvanic potential are proposed.

Case 1 : The equilibrium potentials of the anode and cathode, $E_{e,a}$ and $E_{e,c}$, differ significantly from each other and once the minerals are contacted the electrode potentials differ from their equilibrium potentials by not less than 100 mV. One can therefore assume that only anodic processes occur on the anode and cathodic processes occur on the cathode. It was assumed that the anodic and cathodic reactions are electrochemically controlled and obey the Tafel law in the vicinity of the galvanic potential. The galvanic current flowing through the anode and cathode is given by Equations 1.34 and 1.35 respectively.

$$I = I_a^A = A_a i_{0,a} 10^{\frac{E}{b_a}} \qquad 1.34$$

$$I = I_c^C = A_c i_{o,c} 10^{-\frac{E_a}{b_c^C}} \qquad 1.35$$

By plotting a Tafel curve, log I versus E, one is able to determine the exchange current densities and the charge transfer coefficients for the anodic and cathodic processes.

Case 2 : The corrosion or mixed potential is near the galvanic potential. This implies that there may be anodic and cathodic processes on both the anode and the cathode. It is assumed that all reactions occurring on the anode and cathode are electrochemically controlled. The expressions for current as a function of potential for the anode and the cathode are represented by Equations 1.36 and 1.37 respectively.

$$I_a = A_a\left[i_{o,a}^A 10^{\frac{E_a}{b_a^A}} - i_{o,c}^A 10^{-\frac{E_a}{b_c^A}}\right] \qquad 1.36$$

$$I = -A_c\left[i_{o,a}^C 10^{\frac{E_a}{b_a^C}} - i_{o,c}^C 10^{-\frac{E_a}{b_c^C}}\right] \qquad 1.37$$

The net current at the equilibrium potentials for the anodic and cathodic processes are given by Equations 1.38 and 1.39 respectively.

$$I = A_a\left[i_{o,a}^A 10^{\frac{E_{a,e}}{b_a^A}} - i_{o,c}^A 10^{-\frac{E_{a,e}}{b_c^A}}\right] = 0 \qquad 1.38$$

$$I = A_c\left[i_{o,a}^C 10^{\frac{E_{a,e}}{b_a^C}} - i_{o,c}^C 10^{-\frac{E_{a,e}}{b_c^C}}\right] = 0 \qquad 1.39$$

The kinetic parameters cannot be determined directly, as in Case 1, since the number of unknown variables and equations are not equal. A correction factor was developed for the anodic and cathodic processes which contains the Tafel slopes b_a^A, b_c^A, b_a^C and b_c^C. An iterative procedure was undertaken, by guessing values of the

correction factor, to determine the Tafel slopes. The parameters x and y which characterised the anode in the galvanic couple were expressed as:

$$x = 1 - 10^{\left[(E_{a,c} - E)\left(\frac{1}{b_a^*} + \frac{1}{b_c^*}\right)\right]} \qquad 1.40$$

$$y = 10^{\left[\frac{(E_i - E_{a,c})}{b_a^*}\right]} \qquad 1.41$$

Similar expressions were developed for the cathodic processes.

The models allow one to estimate the influence of galvanic interaction in the electrochemical corrosion of minerals. The models are only applicable to reactions which are electrochemically controlled. In addition factors such as solution voltage losses and voltage losses across mineral-mineral contacts which affect the magnitude of galvanic interaction have not been considered in the model equations.

Hiskey and Wadsworth (1975) investigated the possibilities of using the galvanic interaction between copper and chalcopyrite to reduce chalcopyrite to chalcocite to facilitate ease of further processing. The anodic and cathodic reactions, Equations 1.42 and 1.43 respectively, result in a solid film of chalcocite forming on the surfaces of copper and chalcopyrite.

$$2Cu^\circ + H_2S \rightleftarrows Cu_2S + 2H^+ + 2e^- \qquad 1.42$$

$$2CuFeS_2 + 6H^+ + 2e^- \rightleftarrows Cu_2S + 2Fe^{2+} + 3H_2S \qquad 1.43$$

The galvanic conversion process was found to be chemically controlled and the authors proposed an electrochemical model to describe the galvanic interaction. The rates of the anodic and cathodic reactions were described by the Butler-Volmer equation in which anodic and cathodic processes were assumed to occur on both the anode and cathode. Hiskey and Wadsworth (1975) utilised mixed potential theory and proposed that the chalcopyrite conversion rate can be expressed by:

$$\frac{dn}{dt} = -\frac{a_H^{0.5} A_c A_a (k_a^b k_c^f - k_a^f k_c^b)}{(A_c k_c^f + A_a k_a^f)^{0.5} (A_c k_c^b + A_a k_a^b)^{0.5}} \qquad 1.44$$

where : a_H is the hydrogen ion activity, k_a^f and k_a^b are the rate constants for the forward and backward anodic reaction, k_c^f and k_c^b are the rate constants for the forward and backward cathodic reaction.

Variations in the surface areas of the copper and chalcopyrite were observed to affect the kinetics of the system. A surface reaction model, Equation 1.45, was used to account for variations in surface areas.

$$\left[1 - \left(1 - \frac{\alpha}{\phi}\right)^{\frac{1}{3}}\right] = \frac{k_1}{r_o} t \qquad 1.45$$

where : r_o is the initial radius of the reacting particle, α is the fraction of chalcopyrite converted, x is the ratio of the moles of copper to the moles of chalcopyrite and k_1 is the linear rate constant.

The model equations were found to correlate well with experimental data. The research highlighted the necessity for a dynamic description of galvanic interaction.

Hepel, Hepel and Pomianowski (1984) studied the effect the resistance of the mineral-mineral contact has on the operation of a galvanic cell. It was observed that non-linear current-voltage characteristics existed at the mineral-mineral contacts of the galena-chalcopyrite and chalcopyrite-pyrite galvanic cells. It was concluded that the voltage loss across the mineral-mineral contacts may be of sufficient magnitude to affect the operation of the galvanic cell.

Hepel *et al.* (1984) presented a mathematical model which includes a term for the current-voltage characteristics of the mineral-mineral contacts. The mathematical model, Equation 1.46, relates the overall cell current to the diffusion overpotential, electroactivation overpotential and the ohmic overpotential at the mineral-mineral

contact. An acceleration coefficient, h', for the cathode and anode has been defined which characterises the increase in dissolution rate due to the galvanic effect.

$$I_{cell}R' = E_{e,cell} + b_c^C \log(h_c') - b_a^A \log(h_a') - V_j - b_c^C \sum_i \eta_{c,i} \log\left(1 - \frac{i_{cell}}{i_{diff,i}}\right) + b_a^A \sum_j \eta_{a,j} \log\left(1 - \frac{i_{cell}}{i_{diff,j}}\right) \quad 1.46$$

By making assumptions about the processes occurring in the galvanic cell the mathematical model can be simplified.

1) Diffusion is negligible.

$$I_{cell}R' = E_{e,cell} - V_j + b_c^C \log(h_c') - b_a^A \log(h_a') \quad 1.47$$

2) An ohmic relationship describes the current-voltage characteristics of the mineral-mineral contact.

$$I_{cell} = (R'+R_j')^{-1}\left(E_{e,cell} + b_c^C \log(h_c') - b_a^A \log(h_a')\right) \quad 1.48$$

Although the authors experimentally confirmed the presence of non-linear current-voltage characteristics at mineral-mineral contacts they failed to verify the overall mathematical model by experiment.

1.3 Research Objectives.

In general the magnitude of the galvanic interaction between sulphide minerals has been described qualitatively in terms of the difference between the cathodic and anodic equilibrium potentials, (Dutrizac and Macdonald (1973); Mehta and Murr (1983)). In some quantitative descriptions of galvanic interaction, where kinetic parameters are accounted for, the description has been based on the electrode reactions being electrochemically controlled, (Hiskey and Wadsworth (1975); Nowak *et al.* (1984)). Hepel *et al.* (1984) included the effect of mass transfer processes in their mathematical model but failed to verify the model by experiment. Hepel *et al.* (1984) further noted the importance of the current-voltage characteristics of the mineral-mineral contact on the operation of a galvanic cell. With this in mind the objectives of this study can be summarised as follows:

i) Provide a general model basis for describing galvanic interaction.

ii) Investigate the kinetics of the electrode reactions in the galvanic couple and include the kinetic parameters in the model.

iii) Investigate the presence of the voltage drop across the mineral-mineral contact and include this in the model.

iv) Verify the model proposal by experiment by investigating a number of galvanic couples.

v) Conduct a preliminary study into possible dynamic factors which affect the magnitude of galvanic current.

Factors which are not accounted for in this study are summarised below:

i) Active-passive behaviour of electrode reactions are not considered.

ii) Semiconductor equations are not considered when describing current-voltage characteristics at sulphide mineral electrode-solution interfaces.

iii) Rectifying properties at mineral-mineral contacts are not considered.

iv) The research is confined to the study of two electrodes in galvanic contact. The galvanic cells which were studied are copper-platinum, copper-pyrite and galena-pyrite.

2. CHEMISTRY OF THE GALVANIC COUPLES STUDIED.

The chemistry of the galvanic couples investigated in this research is reviewed in this chapter. In particular the Pourbaix diagrams and rate determining reactions applicable to each galvanic couple are discussed.

2.1 Chemistry Associated With The Copper-Platinum Galvanic Couple.

The galvanic couple consisting of the anodic dissolution of copper and the ferric reduction to ferrous ions on a platinum cathode was studied. The Pourbaix diagram, Figure 2.1, illustrates the thermodynamic stability regimes of the copper-water system.

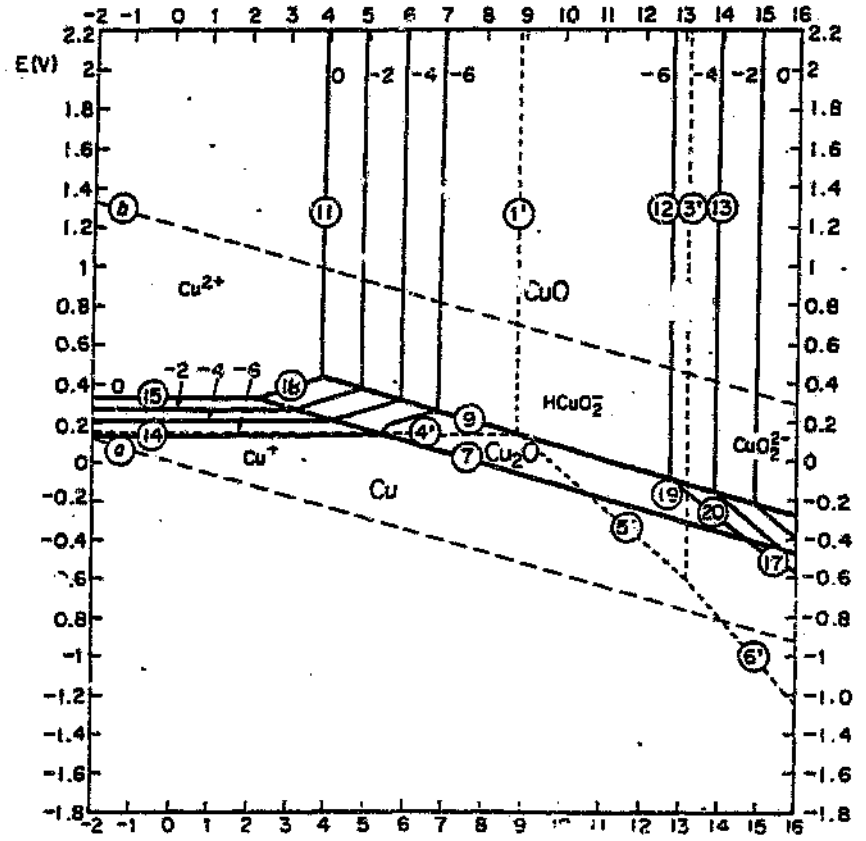


Figure 2.1 Thermodynamic stability regimes in the Cu-H_2O system. Bertocci and Turner (1974)

Copper dissolution, under standard conditions, occurs at potentials greater than 0.34 V vs SHE. The ferric reduction to ferrous occurs at potentials less than 0.77 V vs SHE. The theoretical cell e[illegible]ne copper-platinum galvanic couple is therefore 0.43 V.

An acidic ferric sulphate solution was employed to study this couple due to the complex behaviour observed during the dissolution of copper in chloride solutions, Lee, Nobe and Pearlstein (1985). In addition to this at higher pH values it becomes thermodynamically possible for ferric ions to form solid compounds such as goethite and jarosite.

The anodic oxidation of copper consists of two steps. In the first step copper is oxidised to cuprous ions. In the second step cuprous ions are oxidised to cupric ions. Mattsson and Bockris (1959) determined that the oxidation of cuprous to cupric ions is the rate controlling reaction.

$$Cu(s) \rightarrow Cu^{+} + e^{-} \qquad 2.1$$

$$Cu^{+} \rightarrow Cu^{2+} + e^{-} \qquad 2.2$$

The cathodic reduction of ferric ions to ferrous ions is a simple one electron transfer reaction. Bochmann and Vielstich (1988) observed that the reaction rate is dependent on the electrode material.

$$Fe^{3+} + e^{-} \rightarrow Fe^{2+} \qquad 2.3$$

Owing to the oxidative nature of ferric ions there was a reduction of ferric on the copper anode. The reduction reaction may take the form of a direct reduction, Equation 2.3, or a direct leaching reaction:

$$Cu + 2Fe^{3+} \rightarrow Cu^{2+} + 2Fe^{2+} \qquad 2.4$$

2.2 Chemistry Associated With The Copper-Pyrite Galvanic Couple.

The Pourbaix diagram for the iron-sulphur-water system is given in Figure 2.2. The copper-pyrite couple was studied in acidic ferric sulphate solution. Pyrite is situated in a regime of ferrous ion stability. This implies that it is thermodynamically possible for ferric ions to reduce to ferrous ions on the pyrite surface.

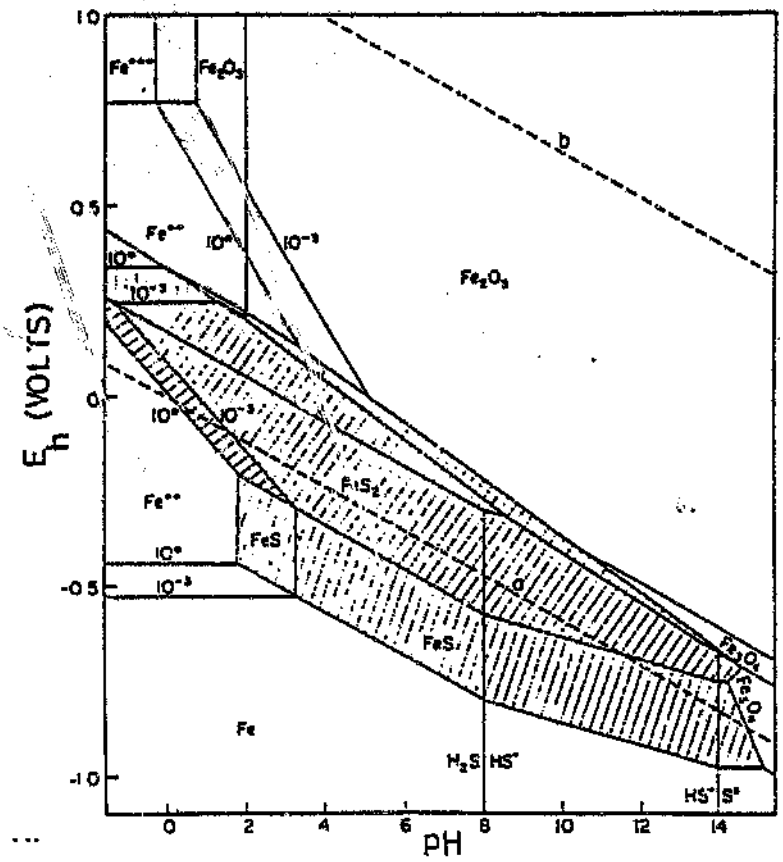


Figure 2.2 Thermodynamic stability regimes in the Fe-S-H_2O system. Peters (1976)

The electrochemistry and reaction mechanisms of the anodic dissolution of copper are discussed in Section 2.1.

The mechanism of the ferric reduction reaction on a mineral is dependent on the conductance type of the sulphide mineral. Naturally occurring pyrite exhibits both n and p-type conductance. An n-type pyrite conductor has electrons in its conduction band as majority charge carriers and the ferric reduction reaction is synonymous with that represented by Equation 2.3. A p-type pyrite electrode has holes in its valence band as the majority charge carriers and the ferric reduction reaction is given by Equation 2.5. Crundwell (1988) provides a comprehensive treatment of the semiconducting characteristics of sulphide minerals.

$$Fe^{3+} \rightarrow Fe^{2+} + h^{+} \qquad 2.5$$

The standard equilibrium potential of pyrite, 0.63 V vs SHE, is lower than the standard equilibrium potential, 0.77 V vs SHE, of the ferric reduction to ferrous reaction. This may result in leaching of the pyrite cathode. Thomas and Whalley (1958) propose that the leaching of pyrite by ferric ions at high temperatures is given by Equation 2.6.

$$FeS_2 + 7Fe_2(SO_4)_3 + 8H_2O \rightarrow 15FeSO_4 + 8H_2SO_4 \qquad 2.6$$

2.3 Chemistry Associated With The Galena-Pyrite Galvanic Couple.

The Pourbaix diagram for the lead-sulphur-water system is illustrated in Figure 2.3. The standard equilibrium potential of galena is 0.28 V vs SHE, and that of ferric reduction is 0.77 V vs SHE. The theoretical cell emf for the galena-pyrite couple is 0.49 V. It is evident, on Figure 2.3, that at solution potentials greater than approximately 0.30 V vs SHE and pH's between 0 and 2, galena dissolution in sulphate media leads to the formation of lead sulphate. Owing to the insolubility of lead sulphate the galena-pyrite couple was characterised in acidic ferric nitrate solutions.

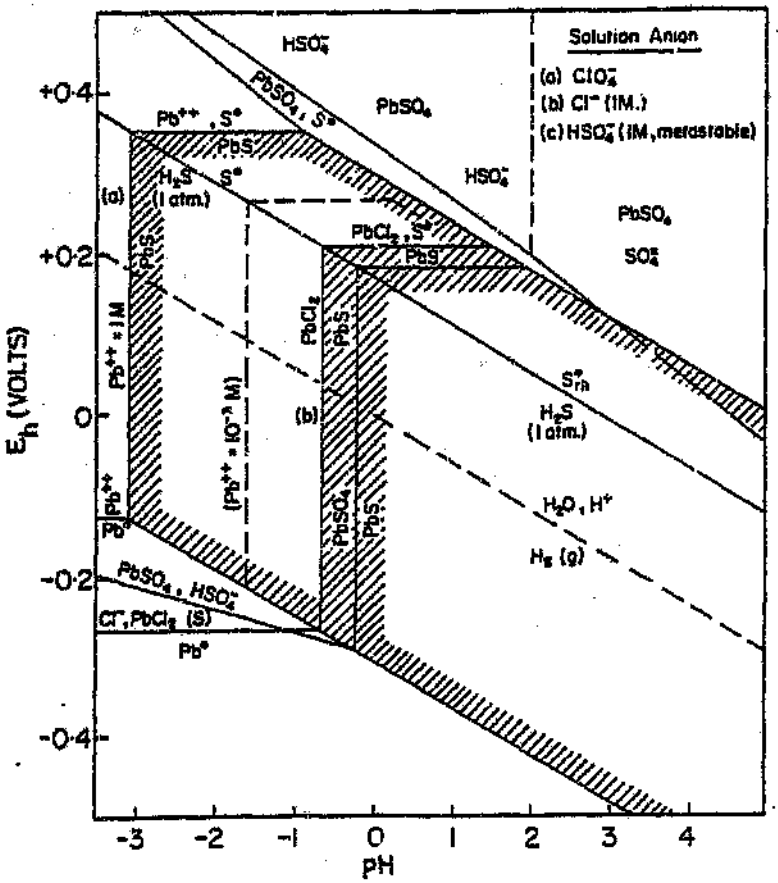


Figure 2.3 Thermodynamic stability regimes in the Pb-S-H_2O system. Peters (1976).

The anodic dissolution of galena results in the formation of plumbous ions, Pb^{2+}, and a solid sulphur film. Lead rich galena displays n-type conductance whilst sulphur rich galena displays p-type conductance. The anodic dissolution of n-type galena is expected to follow the reaction presented by Equation 2.7 whilst p-type galena dissolves according to Equation 2.8.

$$PbS \rightarrow Pb^{2+} + S^{\circ} + 2e^{-} \qquad 2.7$$

$$PbS + 2h^{+} \rightarrow Pb^{2+} + S^{\circ} \qquad 2.8$$

Paul *et al.* (1977) proposed that the dissolution of galena is a dual process involving a sulphide intermediate:

$$PbS \rightleftharpoons Pb^{2+} + S^{-} + e^{-} \qquad 2.9$$

$$S^{-} \rightarrow S^{\circ} + e^{-} \qquad 2.10$$

Paul *et al.* (1977) noted that as the sulphur film thickens it becomes more difficult for plumbous ions to diffuse through the pores and channels in the sulphur film. This causes a high concentration of plumbous ions at the electrode surface where, in order to maintain the charge balance, a low concentration of protons are required to develop. This results in an increase in pH where it is thermodynamically possible for the sulphur film to oxidise to thiosulphate by Equation 2.11.

$$2S^{\circ} + 3H_2O \rightarrow S_2O_3^{2-} + 6H^{+} + 4e^{-} \qquad 2.11$$

Paramguru, Bose and Sircar (1979) proposed a sequence of four reactions which result in the overall dissolution reaction given by Equation 2.7. The reaction sequence involves the coverage of the galena surface by a layer of water, adsorption of plumbous ion forming complexes and finally charge transfer processes involving these complexes. The rate determining reaction is:

$$(PbS.H_2O.xPb^{2+})_{ad} \rightarrow (PbS.H_2O.xPb^{2+})_{ad}^{+} + e^{-} \qquad 2.12$$

Owing to the oxidative nature of ferric ions there was a reduction of ferric ions on the galena surface. The reduction reaction may take the form of a direct reduction of ferric ions, Equation 2.3, or leaching of the galena anode as given by Equation 2.13.

$$PbS + 2Fe^{3+} \rightarrow Pb^{2+} + 2Fe^{2+} + S^{\circ} \qquad 2.13$$

The mechanisms of the ferric reduction to ferrous reaction on pyrite are discussed in Section 2.2.

3. DEVELOPMENT OF A THEORETICAL EXPRESSION FOR GALVANIC INTERACTION.

A general mathematical model which describes galvanic interaction between two electrodes is developed in this chapter. The mathematical model basis is presented and discussed in Section 3.1. The various current-voltage relationships required in the mathematical model are presented in Sections 3.2 to 3.4. The overall galvanic model is presented in Section 3.5.

3.1 The Model Basis.

The basis of the electrochemical model of galvanic current is found in Kirchoff's Voltage Law. The law states that the sum of the voltage gains is equal to the sum of the voltage losses in an electrical circuit.

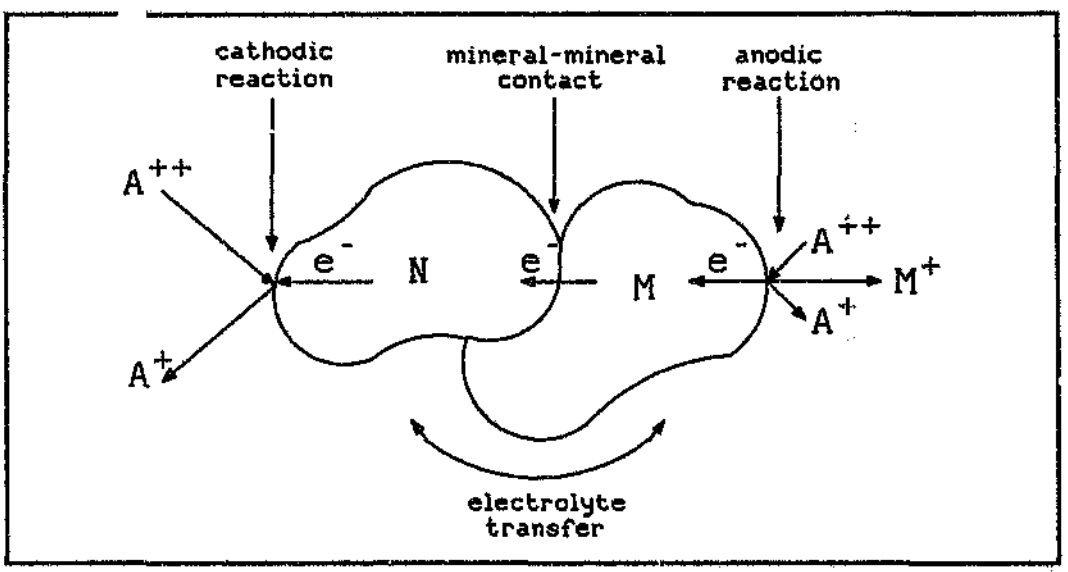


Figure 3.1 The processes occurring in a hypothetical galvanic couple.

Considering a typical galvanic couple, Figure 3.1, the following four factors, which affect the magnitude of the galvanic interaction, can be identified:

(i) The magnitude of the difference between the cathodic and anodic equilibrium potentials. This is the thermodynamic parameter commonly referred to as the cell emf.

(ii) The rates of the anodic and cathodic reactions in the galvanic couple. The reaction rate may be dependent on electrochemical and/or mass transfer processes.

(iii) The nature of the electrical contact between the two electrodes in a galvanic couple may be negligible, ohmic or rectifying.

(iv) The conductivity of the solution determines how readily ionic species, produced at one electrode and required for reaction at the other electrode, are transferred through the solution.

The effect of mineral-mineral contact and solution voltage losses is explained, in electrochemical terms, with reference to Figure 3.2.

The galvanic current I_g, at the galvanic potential E_g, occurs when the voltage drops across the electrical contact and solution are negligible. The existence of voltage drops across the electrical contact and solution causes the electrode potentials of the anode and cathode to shift from E_g to E_a and E_c respectively. This results in a decrease in the galvanic current, from I_g to I_s, flowing through the couple. As the voltage losses across the contact and solution increase the electrode potentials E_a and E_c shift towards the anodic and cathodic equilibrium potentials, E_{ea} and E_{ec}, respectively. This results in a further decrease in galvanic current.

It is evident, in Figure 3.2, that the difference between the cathodic equilibrium potential, E_{ec}, and the anodic equilibrium potential, E_{ea}, is equal to the sum of the absolute values of the electrode overpotentials, the solution conductivity and the electrical contact between the two electrodes.

(i) The magnitude of the difference between the cathodic and anodic equilibrium potentials. This is the thermodynamic parameter commonly referred to as the cell emf.

(ii) The rates of the anodic and cathodic reactions in the galvanic couple. The reaction rate may be dependent on electrochemical and/or mass transfer processes.

(iii) The nature of the electrical contact between the two electrodes in a galvanic couple may be negligible, ohmic or rectifying.

(iv) The conductivity of the solution determines how readily ionic species, produced at one electrode and required for reaction at the other electrode, are transferred through the solution.

The effect of mineral-mineral contact and solution voltage losses are explained, in electrochemical terms, with reference to Figure 3.2.

The galvanic current I_g, at the galvanic potential E_g, occurs when the voltage drops across the electrical contact and solution are negligible. The existence of voltage drops across the electrical contact and solution causes the electrode potentials of the anode and cathode to shift from E_g to E_a and E_c respectively. This results in a decrease in the galvanic current, from I_g to I_a, flowing through the couple. As the voltage losses across the contact and solution increase the electrode potentials E_a and E_c shift towards the anodic and cathodic equilibrium potentials, E_{ea} and E_{ec}, respectively. This results in a further decrease in galvanic current.

It is evident, in Figure 3.2, that the difference between the cathodic equilibrium potential, E_{ec}, and the anodic equilibrium potential, E_{ea}, is equal to the sum of the absolute values of the electrode overpotentials, the solution conductivity and the electrical contact between the two electrodes.

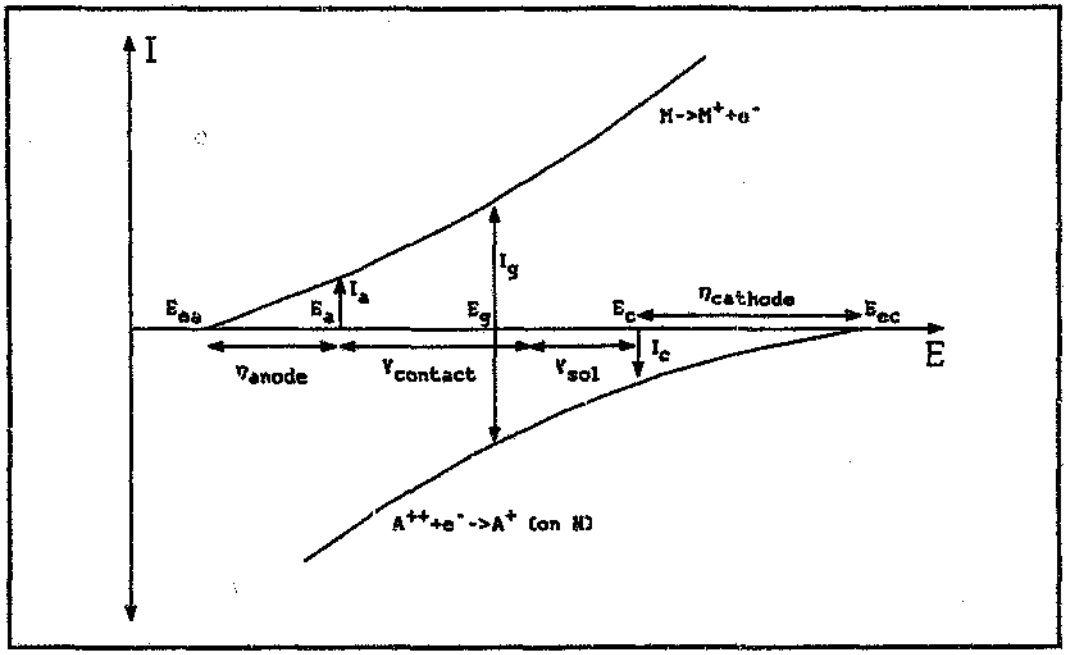


Figure 3.2 The influence of mineral-mineral contact and solution conductivity on galvanic interaction.

$$E_{ec} - E_{ea} = \text{Cell Emf} = |\eta_c| + |\eta_a| + |V_{solution}| + |V_{contact}| \qquad 3.1$$

Each of the voltages on the right hand side of Equation 3.1 can be related to the galvanic current flowing through the couple. The relationships describing the anodic and cathodic overpotentials in terms of galvanic current are presented in Sections 3.2.1 to 3.2.3. The relationships relating the voltage losses across the mineral-mineral contact and the solution are presented in Sections 3.3 and 3.4 respectively.

3.2 Mathematical Expressions For The Anodic And Cathodic Overpotentials.

3.2.1 Mathematical expressions for electrochemically controlled reactions.

A reaction which is limited by a transfer of charge at the electrode surface is

described by the Butler-Volmer equation, Equation 1.7. The Butler-Volmer equation is rearranged to express the overpotential in terms of current. The anodic dissolution of copper and galena are electrochemically controlled processes. This was confirmed by Mattsson and Bockris (1959) and Johnson *et al.* (1978) respectively. The equations below are presented in terms of anodic dissolution.

Case 1 : The half reaction is electrochemically controlled with only anodic reactions occurring on the anode:

$$\eta_a = \frac{RT}{\alpha_a F} \ln\left(\frac{I}{i_{o,a}A_a}\right) \qquad 3.2$$

Case 2 : The half reaction is electrochemically controlled with anodic and cathodic processes occurring on the anode. This situation is encountered in this research where in addition to the anodic dissolution of copper and galena there is ferric reduction on both the electrodes.

$$i = i_{o,a}\exp\left(\frac{\alpha_a F}{RT}\eta_a\right) - i'_{o,c}\exp\left(-\frac{\alpha'_c F}{RT}\eta'_c\right) \qquad 3.3$$

Equation 3.3 cannot be rearranged to express the overpotential in terms of current. It is assumed that the rate of the cathodic reaction on the anode is small in comparison with the rate of the anodic reaction. The difference between the two exponentials can then be approximated by a single exponential expression of the form given by Equation 3.4.

$$\eta'_a = \frac{RT}{\alpha'_a F} \ln\left(\frac{I}{i'_{o,a}A_a}\right) \qquad 3.4$$

The overpotential and kinetic parameters are not unique to one half reaction and for this reason the parameters are expressed with a raised dash. The anodic current, I, is equal to the galvanic current, I_g, when the copper and galena anodes are coupled to the platinum and pyrite cathodes.

3.2.2 A mathematical expression for a reaction controlled by electrochemical and mass transfer processes.

A reaction which is limited by mass transfer and electrochemical processes is termed a mixed-controlled reaction. Ferric reduction to ferrous ions is a mixed-control reaction, see Chapters 5, 6 and 7. The mixed-control equation is therefore derived for the ferric reduction to ferrous reaction.

There are three basic processes which take place when ferric ions are reduced at an electrode.

i) Diffusion of ferric ions to the surface of the electrode.
ii) The charge transfer reaction.
iii) Diffusion of ferrous ions from the electrode surface into the bulk solution.

At steady-state the rate of ferric diffusion to the electrode surface and the rate of ferrous diffusion from the electrode surface are equal. For the purposes of this work the mixed control equation is derived for the diffusion of ferric ions to the surface of the electrode.

It is assumed that near the electrode surface diffusion is the only mode of mass transport whilst in the bulk solution convection is the dominant mode of mass transfer. The diffusion of ferric ions to the surface of the electrode is described, at steady-state, by the diffusion equation,

$$i = \frac{FD}{\delta}([Fe^{3+}]_s - [Fe^{3+}]_b) \qquad 3.5$$

where $[Fe^{3+}]_s$ is the concentration of ferric at the electrode surface and $[Fe^{3+}]_b$ is the concentration of ferric in the bulk solution.

The maximum amount of current, or limiting current, occurs when the concentration of ferric at the surface of the electrode is zero.

$$i_{l,c} = -\frac{FD}{\delta}[Fe^{3+}]_b \qquad 3.6$$

Equations 3.5 and 3.6 can rearranged and expressed by equation 3.7.

$$\frac{[Fe^{3+}]_s}{[Fe^{3+}]_b} = 1 - \frac{i}{i_{l,c}} \qquad 3.7$$

The cathodic charge-transfer reaction is described by the Butler-Volmer equation where it is assumed that no anodic processes occur on the surface of the cathode.

$$i = k_c[Fe^{3+}]_s \exp\left(\frac{\alpha_c F}{RT}\eta_c\right) \qquad 3.8$$

Substituting Equation 3.7 into 3.8 one obtains the following relationship between the cathodic overpotential and current.

$$\eta_c = \frac{RT}{\alpha_c F} \ln\left(\frac{i_{l,c} - \frac{I}{A_c}}{i_{l,c}\left(\frac{I}{A_c i_{o,c}} + 1\right)}\right) \qquad 3.9$$

In this study Equation 3.9 applies to the reduction of ferric ions on an inert platinum electrode. However ferric ions will leach the pyrite electrode and therefore anodic and cathodic processes occur on the pyrite cathode. The Butler-Volmer equation describing the charge transfer, in this instance, is similar to that presented by Equation 3.3. If it is assumed that the anodic processes on the cathode are small relative to the cathodic processes the equation can similarly be expressed in terms of a single overpotential. The mixed-control equation describing ferric reduction to ferrous on a pyrite cathode is given by Equation 3.10.

$$\eta'_c = \frac{RT}{\alpha'_c F} \ln\left(\frac{i'_{l,c} - \frac{I}{A_c}}{i'_{l,c}\left(\frac{I}{A_c i'_{o,c}} + 1\right)}\right) \qquad 3.10$$

3.2.3 A mathematical expression for a reaction controlled by mass transfer processes.

An electrochemical reaction which is purely controlled by the diffusion of ionic species is described by, Equation 1.15, which is a limiting form of Fick's first law. In this study none of the reactions were purely controlled by diffusion.

3.3 A Mathematical Expression For Solution Voltage Losses.

A voltage loss may be incurred in a galvanic couple due to the motion of ions through the solution. Ions may be transferred by diffusion, convection or migration and the magnitudes of these mass transfer processes are dependent on a number of parameters related to the solution. These parameters are thoroughly treated by Atkins (1986 pp. 663-683). In this study the reacting species were transferred rapidly to the electrode surfaces by using a rotating ring disc electrode. This ensured that solution voltage losses were negligible. An ohmic relationship, Equation 3.11, is in many instances a sufficient mathematical description of solution voltage losses.

$$V_{solution} = IR'_{solution} \qquad 3.11$$

3.4 Mathematical Expressions For Mineral-Mineral Contacts.

In corrosion studies the electrical contact between metal electrodes is such that no potential drop occurs across the contact. In the case of sulphide minerals an ohmic or rectifying relationship may exist at the mineral-mineral contact. Hepel, Hepel and Pomianowski (1984) concluded that the magnitude and extent of the ohmic and rectifying relationships is strongly dependent on the semiconducting nature of the minerals. A rectifying property, or *pn*-junction, may arise when a n-type mineral is placed in contact with a p-type mineral. The electrochemical reactions at the surface

of the electrode may polarise the *pn*-junction in a negative direction and consequently the galvanic current flowing through the couple is strongly diminished. Shuey (1975) provides mathematical expressions for the rectifying properties at mineral-mineral contacts. In this study the voltage loss across the mineral-mineral contact was controlled by a potentiostat, this is discussed in Section 4.3.

3.5 Mathematical Expressions For Galvanic Interaction.

The various mathematical expressions presented through Sections 3.2 to 3.4 are substituted into the model basis, Equation 3.1, to yield the overall mathematical expressions for galvanic interaction. The mathematical expressions for galvanic interaction presented here are steady-state models. Non-steady-state mathematical expressions for galvanic interaction are derived in Chapter 8.

Model 1 : Anodic and cathodic processes occur on the anode whilst only cathodic processes occur on the cathode. The anodic reaction is electrochemically controlled whilst the cathodic reaction is mixed controlled. An ohmic relationship exists across the electrode-electrode contact. Solution voltage losses are negligible.

$$E_{oc} - E_{ea} = \frac{RT}{\alpha_c F} \ln\left(\frac{i_{l,c} - \frac{I_g}{A_c}}{i_{l,c}\left(\frac{I_g}{A_c i_{o,c}} + 1\right)}\right) + \frac{RT}{\alpha'_a F} \ln\left(\frac{I_g}{i'_{o,a} A_a}\right) + I_g R'_{contact} \qquad 3.12$$

In this study Equation 3.12 mathematically describes the galvanic interaction between copper and platinum in acidic ferric sulphate solution.

Model 2 : Anodic and cathodic processes occur on both the anode and cathode. The anodic reaction on the anode is electrochemically controlled. The cathodic reaction on the cathode is mixed controlled. An ohmic relationship exists across the electrode-electrode contact. Solution voltage losses are negligible.

of the electrode may polarise the *pn*-junction in a negative direction and consequently the galvanic current flowing through the couple is strongly diminished. Shuey (1975) provides mathematical expressions for the rectifying properties at mineral-mineral contacts. In this study the voltage loss across the mineral-mineral contact was controlled by a potentiostat, this is discussed in Section 4.3.

3.5 Mathematical Expressions For Galvanic Interaction.

The various mathematical expressions presented through Sections 3.2 to 3.4 are substituted into the model basis, Equation 3.1, to yield the overall mathematical expressions for galvanic interaction. The mathematical expressions for galvanic interaction presented here are steady-state models. Non-steady-state mathematical expressions for galvanic interaction are derived in Chapter 8.

Model 1 : Anodic and cathodic processes occur on the anode whilst only cathodic processes occur on the cathode. The anodic reaction is electrochemically controlled whilst the cathodic reaction is mixed controlled. An ohmic relationship exists across the electrode-electrode contact. Solution voltage losses are negligible.

$$E_{oc} - E_{oa} = \frac{RT}{\alpha_c F} \ln\left(\frac{i_{1,c} - \frac{I_g}{A_c}}{i_{1,c}\left(\frac{I_g}{A_c i_{o,c}} + 1\right)}\right) + \frac{RT}{\alpha'_a F} \ln\left(\frac{I_g}{i'_{o,a} A_a}\right) + I_g R'_{contact} \qquad 3.12$$

In this study Equation 3.12 mathematically describes the galvanic interaction between copper and platinum in acidic ferric sulphate solution.

Model 2 : Anodic and cathodic processes occur on both the anode and cathode. The anodic reaction on the anode is electrochemically controlled. The cathodic reaction on the cathode is mixed controlled. An ohmic relationship exists across the electrode-electrode contact. Solution voltage losses are negligible.

$$E_{ec} - E_{sa} = \frac{RT}{\alpha'_c F} \ln\left(\frac{i'_{l,c} - \frac{I_g}{A_c}}{i'_{l,c}\left(\frac{I_g}{A_c i'_{o,c}} + 1\right)}\right) + \frac{RT}{\alpha'_a F} \ln\left(\frac{I_g}{i'_{o,a} A_a}\right) + I_g R'_{contact} \qquad 3.13$$

Equation 3.13 describes the galvanic interaction occurring in the copper-pyrite and galena-pyrite couples.

The cathodic rest potential, the anodic rest potential and the voltage loss across the mineral-mineral contact, in Equations 3.12 and 3.13, are determined by experimental measurement. Pseudo-steady-state potentiostatic experiments can be used to generate the polarisation data for the anodic and cathodic reactions. The polarisation data can then be regressed on, with the appropriate kinetic equation (Section 3.2), to determine the kinetic parameters of the anodic and cathodic reactions. The galvanic current is therefore the only unknown parameter and can be readily computed by utilising a Regula Falsi iteration technique.

4. EXPERIMENTAL TECHNIQUES AND PROCEDURE.

The descriptions of the reagents and apparatus are contained in the initial sections of this chapter. The final sections of this chapter describe the procedures followed when characterising the half reactions and galvanic cell.

4.1 Description Of Reagents.

The copper and platinum which were used in the copper-platinum galvanic couple were pure. The pyrite used in the copper-pyrite galvanic couple had a polycrystalline structure and was obtained from Navajun, Spain. The galena and pyrite used in the galena-pyrite couple were obtained from single crystals emanating from the Black Mountain, South Africa and Navajun, Spain respectively.

The types of conduction that the mineral samples exhibited were determined by a thermoelectric effect measurement and energy dispersive x-ray analysis (EDXA). The thermoelectric measurement involved placing the two probes of a voltmeter on opposite sides of the surface of the mineral electrode. A soldering iron was placed adjacent to one of the multimeter probes, thus heating one side of the mineral, and the variation in the voltage output monitored. The direction, positive or negative, in which the voltage increases determines which type of conductance the mineral electrode exhibits. Both pyrite electrodes and galena were observed to behave as n-type conductors. Springer (1970) adopted a thermoelectric approach to determine the type of conductivity pyrite specimens exhibit.

Further confirmation of n-type conduction was obtained from energy dispersive x-ray analysis measurements. The technique is used to determine the quantities of species present in solid samples. A qualitative study was undertaken to determine relative amounts of species present in the pyrite and galena electrodes. The results of the investigation are reported in Appendix A. The results indicate that galena is rich in lead and the pyrite electrodes are rich in iron which implies n-type

4. EXPERIMENTAL TECHNIQUES AND PROCEDURE.

The descriptions of the reagents and apparatus are contained in the initial sections of this chapter. The final sections of this chapter describe the procedures followed when characterising the half reactions and galvanic cell.

4.1 Description Of Reagents.

The copper and platinum which were used in the copper-platinum galvanic couple were pure. The pyrite used in the copper-pyrite galvanic couple had a polycrystalline structure and was obtained from Navajun, Spain. The galena and pyrite used in the galena-pyrite couple were obtained from single crystals emanating from the Black Mountain, South Africa and Navajun, Spain respectively.

The types of conduction that the mineral samples exhibited were determined by a thermoelectric effect measurement and energy dispersive x-ray analysis (EDXA). The thermoelectric measurement involved placing the two probes of a voltmeter on opposite sides of the surface of the mineral electrode. A soldering iron was placed adjacent to one of the multimeter probes, thus heating one side of the mineral, and the variation in the voltage output monitored. The direction, positive or negative, in which the voltage increases determines which type of conductance the mineral electrode exhibits. Both pyrite electrodes and galena were observed to behave as n-type conductors. Springer (1970) adopted a thermoelectric approach to determine the type of conductivity pyrite specimens exhibit.

Further confirmation of n-type conduction was obtained from energy dispersive x-ray analysis measurements. The technique is used to determine the quantities of species present in solid samples. A qualitative study was undertaken to determine relative amounts of species present in the pyrite and galena electrodes. The results of the investigation are reported in Appendix A. The results indicate that galena is rich in lead and the pyrite electrodes are rich in iron which implies n-type

conduction. Shuey (1975) provides a comprehensive discussion on the types of conductance various minerals exhibit.

Analytical grade ferric sulphate, ferric nitrate, sodium sulphate and sodium nitrate crystals were used in the experimental investigation. Sulphuric acid (98%) and nitric acid (55%) were used to obtain the desired pH in each experiment. Doubly distilled water was used to prepare all solutions.

4.2 Apparatus.

4.2.1 Preparation of electrodes.

To electrochemically characterise the half reactions occurring at each individual electrode the species under investigation were constructed as rotating disc electrodes. Rotating disc electrodes are advantageous in that the surface area is known and the fluid flow to the electrode can be controlled. In addition to this the hydrodynamics of fluid flow to rotating disc electrodes, see Section 1.1.3.2 (ii), have been described in mathematical terms.

To characterise the electrochemistry of the galvanic couples each couple was constructed as a rotating ring disc electrode. Pletcher (1991 pp. 145-147) describes phenomenon associated with rotating ring disc electrodes. Figure 4.1 illustrates the construction of the rotating ring disc electrodes used in this study.

Due to the rotation of the ring disc electrode species are transported rapidly to the electrode surface and therefore solution voltage losses are minimised. The copper-platinum galvanic couple comprised of a ring of copper of surface area 0.28 cm^2 surrounding a platinum disc of surface area 0.12 cm^2. The platinum electrode made contact directly with the shaft of the electrode whilst wire was soldered to the copper ring and contact made externally. The copper ring and platinum disc were mounted

in a PVC casing by using araldite resin.

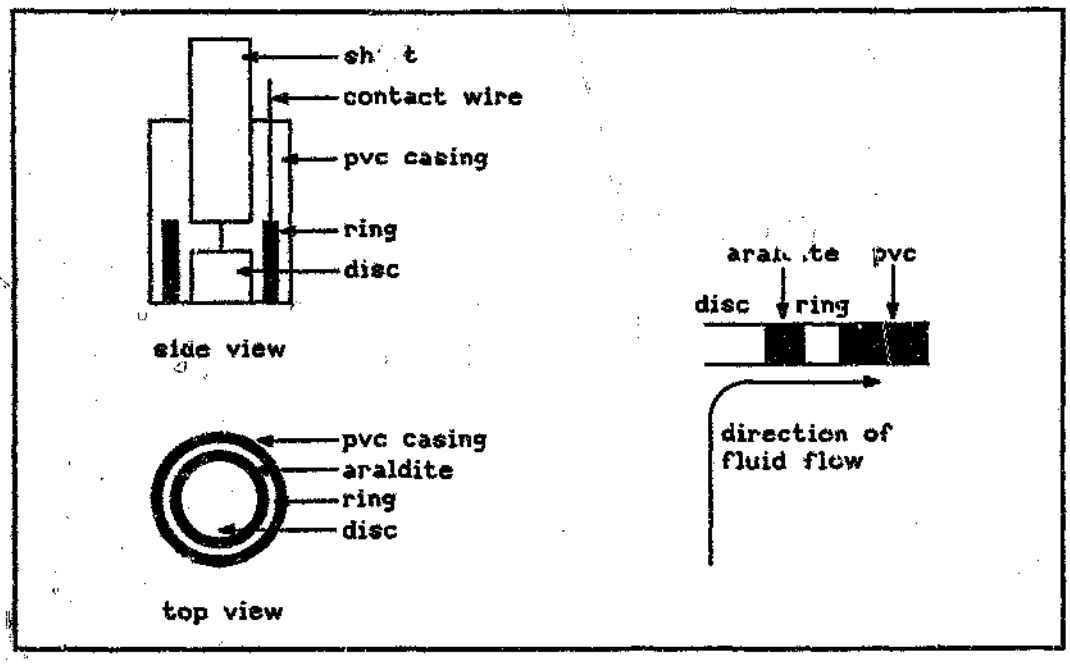


Figure 4.1 Construction of, and fluid flow to, a rotating ring disc electrode.

The rotating ring disc electrode in which mineral specimens were present were constructed in a different manner due to the brittle nature of the minerals. The mineral crystals were mounted in araldite resin to impart support to the mineral during drilling. A 10 mm core drill, having a diamond-nickel impregnated tip, was used to drill discs of mineral. The copper ring surrounding the pyrite disc was obtained from pure copper tubing and had a surface area of 0.34 cm^2. In the case of the galena-pyrite couple a galena disc was coupled with a pyrite ring. The pyrite ring was obtained by initially drilling out a 19 mm core of pyrite from a crystal. This core was then remounted in araldite resin and a 13 mm internal diameter drill bit was used to drill out a further core thus leaving a pyrite ring with surface area 1.1 cm^2. The galena disc, of surface area 0.76 cm^2, and pyrite ring were mounted in a PVC casing using araldite resin. The electrical contact on minerals was made by placing a brass strip to the back of the minerals and contacting it with a silver impregnated glue. A contact wire was soldered to the brass plate.

4.2.2 The three-electrode cell.

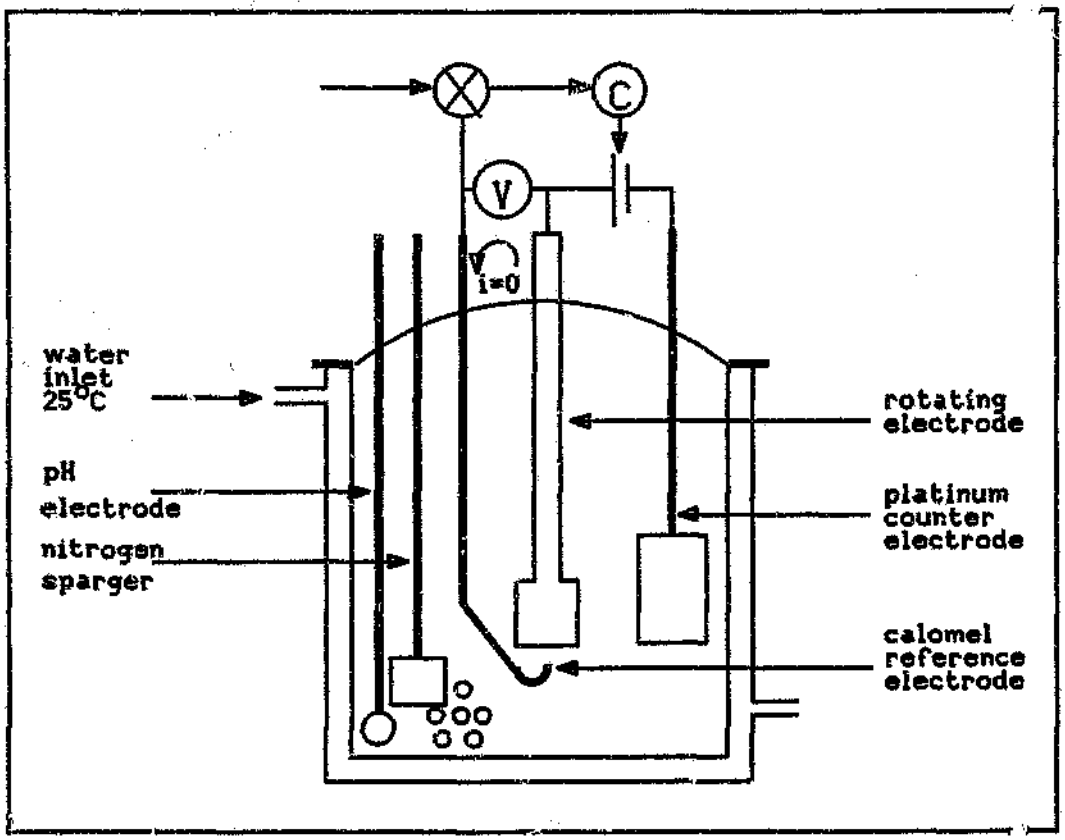


Figure 4.2 The three-electrode cell.

The three-electrode cell is used to characterise the electrochemical kinetics of the anodic and cathodic half reactions. The cell consists of a central rotating working electrode on which the half reaction of interest occurs. A platinum electrode is used as a counter electrode to complete the electrical circuit and thus, under steady-state conditions, ensure charge neutrality. A Schott-Gerade calomel electrode was used as a reference electrode.

The electrochemical cell has a jacket into which water, at the desired temperature, was fed from a Thermomix 1460 Braun temperature control bath. The rotation of the working electrode was controlled by a Pine AS2RE speed control assembly.

The external circuit configuration allows a voltage to be applied across the electrode-solution interface of the working electrode and the current through this interface to be measured. The half reactions were characterised by cyclic voltammetry. However, slow scan rates of 1 $mV.s^{-1}$ were applied in order that the half reactions were characterised under pseudo-steady-state conditions.

The voltage and corresponding current data were recorded by a 3421A Hewlett Packard Data Acquisition Control Unit. The software for recording the voltage and current outputs can be viewed in Appendix B. The control unit did not allow voltage inputs to be read simultaneously and a linear interpolation technique was employed to adjust current values to the corresponding voltage reading. The current-voltage, or polarisation, data was regressed upon, to determine the kinetic parameters, by using FIT regression software.

4.2.3 The galvanic cell.

A CV27 BAS potentiostat, acting as a zero impedance ammeter, was used to measure galvanic current. The electrochemical cell and equipment discussed in Section 4.2.2 was used to study the galvanic couples. The platinum counter electrode was replaced with the cathode in the rotating ring electrode. Software to monitor the action of the galvanic couple is listed in Appendix B. The external circuit configuration was different however and this is illustrated in Figure 4.3.

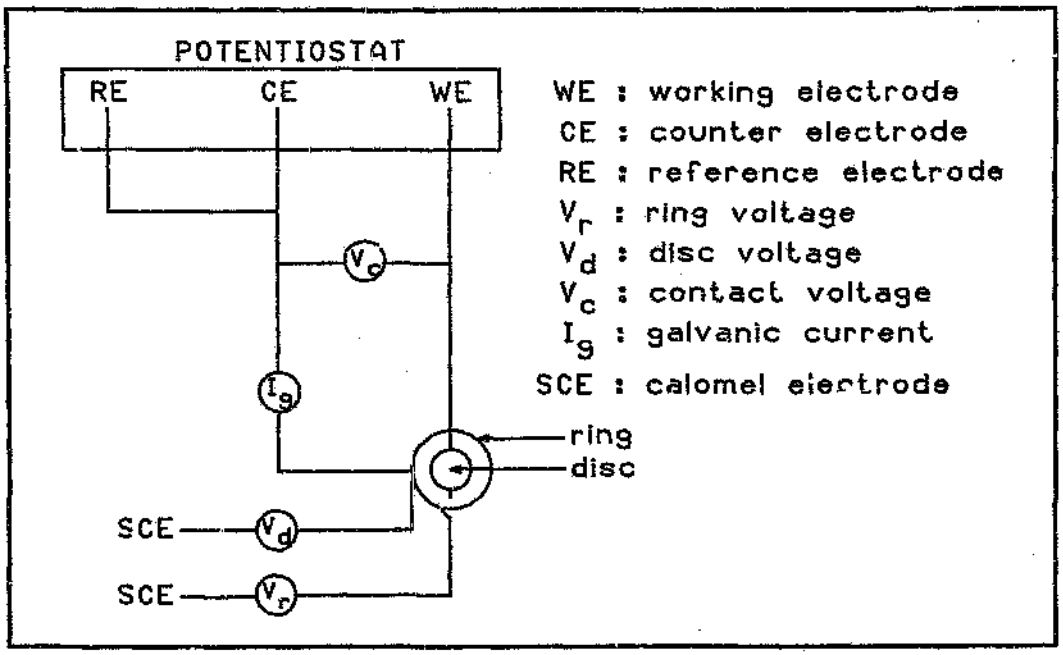


Figure 4.3 Electrical circuit configuration used to investigate the galvanic couples.

The potentiostat was used to apply voltages, V_c, across the minerals. The voltages across the electrode-solution interfaces, with respect to a saturated calomel reference electrode, for both the ring, V_r, and disc, V_d, electrodes were relayed together with the applied voltage and galvanic current to the Hewlett Packard Data Acquisition Control Unit. The software required to record the voltages and current is listed in Appendix B.

4.3 Procedure For Characterising The Half Reactions And Galvanic Couple.

Figure 4.4 illustrates the overall result of conducting the three-electrode cell and galvanic cell experiments. The hypothetical polarisation data for the anodic and cathodic half reactions is represented by Figure 4.4A. This data is regressed upon to determine the kinetic parameters of the half reactions. These kinetic parameters are then used in the overall galvanic model equation to predict galvanic current. The galvanic current in the galvanic cell experiments was measured at various cell voltages i.e. voltage drops across the mineral-mineral contact. The increases in cell

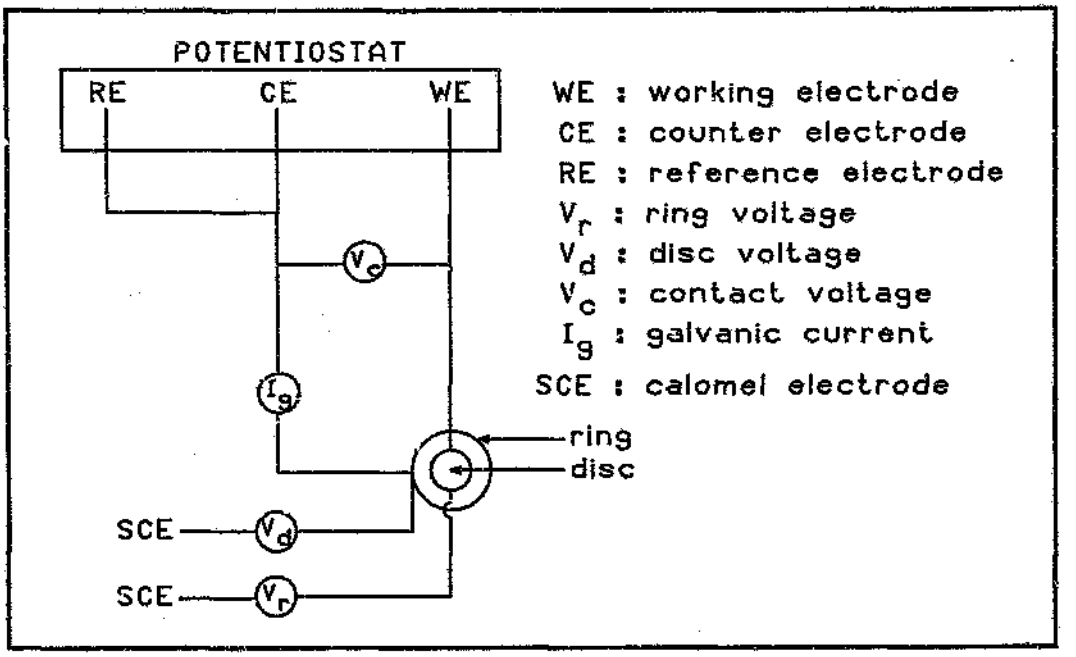


Figure 4.3 Electrical circuit configuration used to investigate the galvanic couples.

The potentiostat was used to apply voltages, V_c, across the minerals. The voltages across the electrode-solution interfaces, with respect to a saturated calomel reference electrode, for both the ring, V_r, and disc, V_d, electrodes were relayed together with the applied voltage and galvanic current to the Hewlett Packard Data Acquisition Control Unit. The software required to record the voltages and current is listed in Appendix B.

4.3 Procedure For Characterising The Half Reactions And Galvanic Couple.

Figure 4.4 illustrates the overall result of conducting the three-electrode cell and galvanic cell experiments. The hypothetical polarisation data for the anodic and cathodic half reactions is represented by Figure 4.4A. This data is regressed upon to determine the kinetic parameters of the half reactions. These kinetic parameters are then used in the overall galvanic model equation to predict galvanic current. The galvanic current in the galvanic cell experiments was measured at various cell voltages i.e. voltage drops across the mineral-mineral contact. The increases in cell

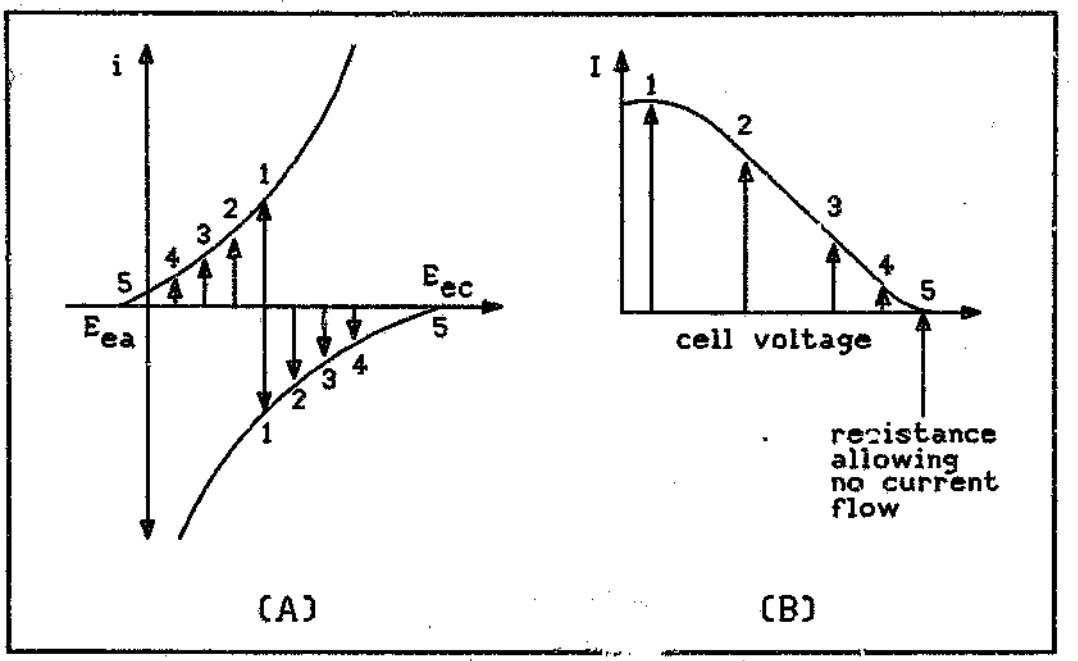


Figure 4.4 (A) Hypothetical current-voltage data for anodic and cathodic half reactions at various cell voltages. (B) Galvanic currents at corresponding cell voltages.

voltages are represented by points 1 to 5 on Figure 4.4B. At these various cell voltages the electrode potential of the anode and cathode were measured. This allows one to determine the current predicted by the half reaction responses, i.e. points 1 to 5 on Figure 4.4A correspond to points 1 to 5 on Figure 4.4B. A comparison of the galvanic currents measured in the galvanic cell experiments with the galvanic currents predicted by the half reaction responses can thus be made. This is more commonly known as graphical superposition theory. Since the kinetic parameters are obtained from the polarisation data the validity of the galvanic model equation is dependent on how well superposition theory predicts galvanic current.

4.3.1 Procedure for characterising anodic and cathodic half reactions.

Prior to each experiment the electrodes underwent a number of treatments. The electrodes were prepared by polishing with a 600 and 1200 grade water paper. The electrodes were then rinsed in distilled water and washed in acetone to remove any

species which remained on the electrode surfaces after polishing. The electrodes were further washed and polished with a 5 micron alumina polishing compound. The polishing compound was removed by distilled water before the electrodes were studied.

Solutions were prepared by placing the required amount of ferric sulphate or ferric nitrate, obtained from 1 M standard solutions, in a 250 ml volumetric flask. The required amount of sulphuric acid or nitric acid was placed in the flask. The solution was made up to 250 ml by adding doubly distilled water. The hydrogen ion concentration in all solutions was 0.5 M.

The solution was placed in the electrochemical cell where heated water in the cell jacket heated the solution to the desired temperature. The rotation rate of the electrode was adjusted to the desired value. The calomel reference electrode was placed in a Luggin capillary filled with saturated sodium sulphate, for the study of the copper-platinum and copper-pyrite couples, or saturated sodium nitrate, for the study of the galena-pyrite couple. Nitrogen was sparged into all solutions for approximately ten minutes to remove any dissolved oxygen. The oxygen present in the nitrogen from the gas cylinder was removed by passing the gas mixture through a scrubber consisting of a bed of copper pellets, which oxidised in the presence of oxygen, immersed in sulphuric acid.

The half reactions were characterised by initially recording the rest potential. The potentiostat was then switched to sweep the voltage across the electrode-solution interface and the data acquisition software was initialised.

4.3.2 Procedure for characterising the galvanic couple.

The electrodes and solutions for the galvanic cell experiments were prepared in the same manner as those discussed in Section 4.3.1. The operation of the galvanic cell was initiated by setting the cell voltage to zero. The galvanic program on the data

acquisition control unit was then started. Five readings of galvanic current, cell voltage, the potential across the ring and the potential across the disc were recorded, at short intervals, before the potentiostat was manually adjusted to apply a further cell voltage. This technique was applied to ensure that the galvanic currents did not decay to any large degree and hence corresponded to the currents produced by the half reactions in the three-electrode cell experiments.

5. GALVANIC INTERACTION BETWEEN COPPER AND PLATINUM IN ACIDIC FERRIC SULPHATE SOLUTIONS.

The electrochemical characteristics of copper dissolution and ferric reduction on platinum are analyzed and discussed in the initial sections of this chapter. Various aspects of the galvanic interaction are discussed together with the model prediction of galvanic current in the latter sections of the chapter. The purpose of this work was to establish the validity of the proposed galvanic model equation. Since the chemistry associated with sulphide minerals is complex the validity of the galvanic model was tested by examining a galvanic couple which consisted of two metallic conductors and simple chemistry.

5.1 Electrochemical Characterisation Of Copper Dissolution.

Anodic dissolution of copper occurs at potentials greater than -0.05 V vs SCE. The reduction of ferric ions on platinum occurred at potentials less than 0.55 V vs SCE. It is evident therefore that ferric ions reduce at the copper electrode as well as the platinum electrode. The anodic dissolution of copper was studied in sodium sulphate and ferric sulphate solutions. The reasons for this were two fold. Firstly the amount of ferric reduced at the copper anode could be determined by substraction of the polarisation curves obtained at the same total sulphate concentration. Secondly the study in which the solution consisted of only sodium sulphate allowed a comparison of the kinetic parameters obtained in this research with those of other researchers.

5.1.1 The dependence of copper dissolution rate on sodium sulphate concentration.

Figure 5.1 illustrates that the rate of copper dissolution remains unchanged with increasing concentrations of sodium sulphate. The reproducibility of the polarisation curves was observed to be within 6%.

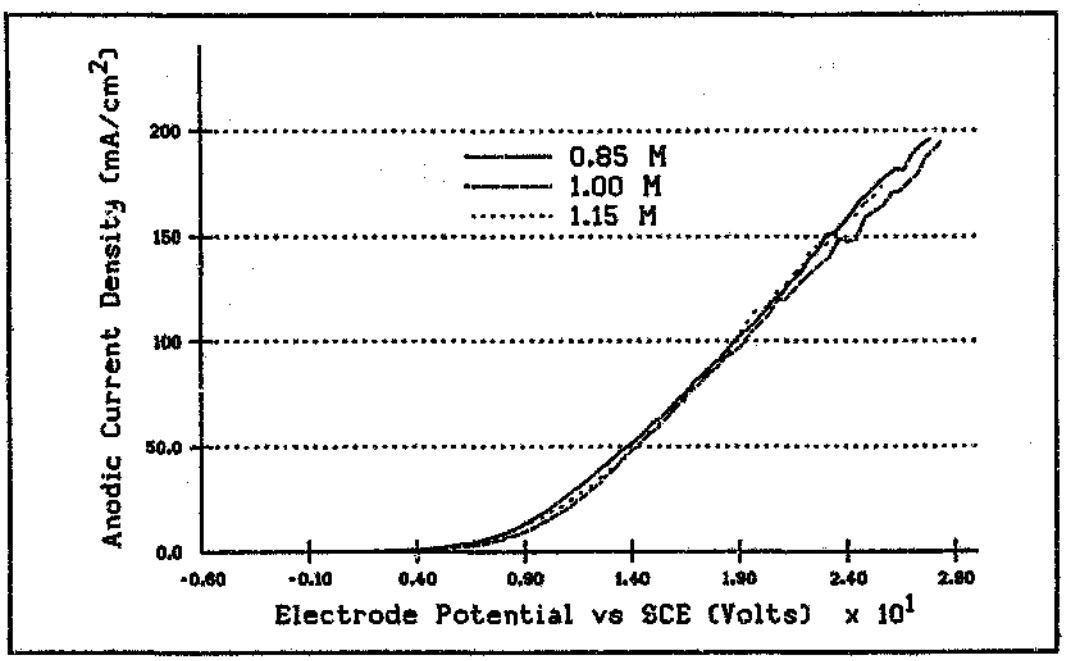


Figure 5.1 The effect of sodium sulphate concentration on the rate of copper dissolution. Conditions : 0.5M H^+, 2003rpm, 298K.

Table 5.1 illustrates that the charge-transfer coefficient, for copper dissolution, determined in this study compares favourably with that obtained by Mattsson and Bockris (1959). The charge-transfer coefficient has a value greater than one and this presents further evidence to suggest that copper dissolution occurs as a dual step mechanism, as discussed in Section 2.1. The exchange current density for copper dissolution cannot be compared to the exchange current densities of other researchers due to the use of a different solution in this study.

Table 5.1 Comparison of copper dissolution kinetic parameters.

Authors	Solution	α_a
Mattsson *et al.* (1959)	0.022N $CuSO_4$, 1N H_2SO_4	1.28-1.44
This Research	0.45M Na_2SO_4 0.25M H_2SO_4	1.35

5.1.2 The dependence of copper dissolution rate on ferric concentration.

As is illustrated in Figure 5.2, the rate of copper dissolution decreases slightly with increases in ferric ion concentration. It was observed that at higher electrode potentials the rate of copper dissolution in ferric solutions is slightly greater than the rate of copper dissolution in sulphate solutions. This could be a result of error in experimental measurement or some catalytic influence of ferric ions on the copper electrode.

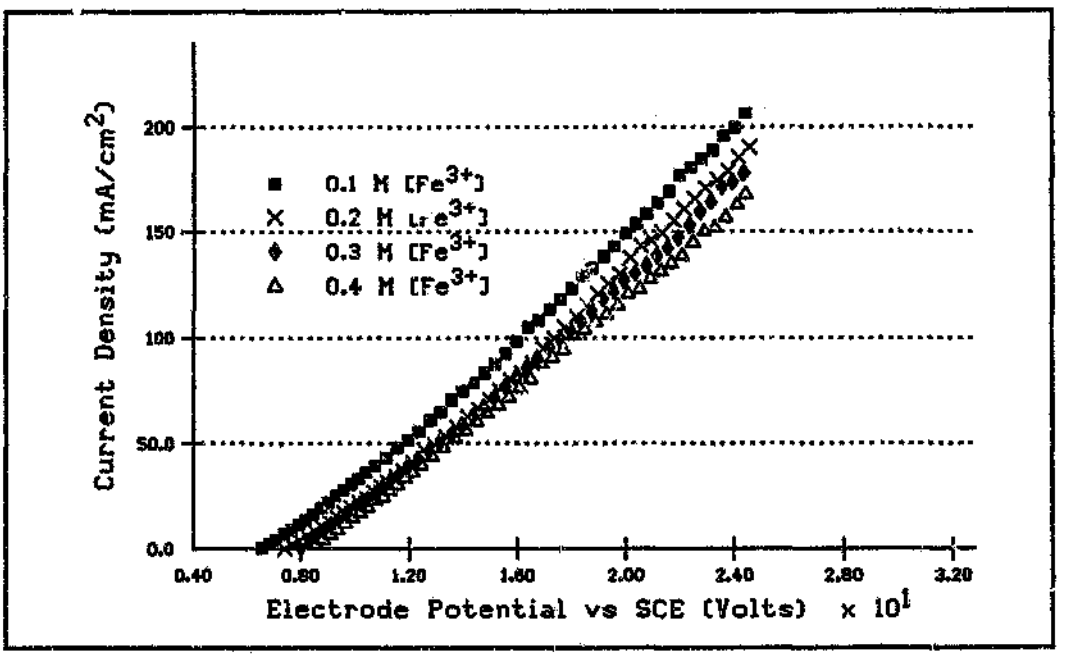


Figure 5.2 The effect of ferric concentration on the rate of copper dissolution. Conditions : 298K, 2003rpm, 0.5M H^+, scan rate 1mV/s.

5.1.3 The dependence of copper dissolution rate on electrode rotation.

In sodium sulphate solutions the rate of copper dissolution does not vary with an increase in rotation rate. This further serves as confirmation that copper dissolution is an electrochemically controlled process. The presence of ferric ions causes the overall rate of the anodic process to be weakly dependent on rotation rate as is

illustrated in Figure 5.3. As the electrode rotation rate is increased the copper dissolution increases. This can probably be attributed to the catalytic effect of ferric ions oxidizing the cuprous ion intermediate.

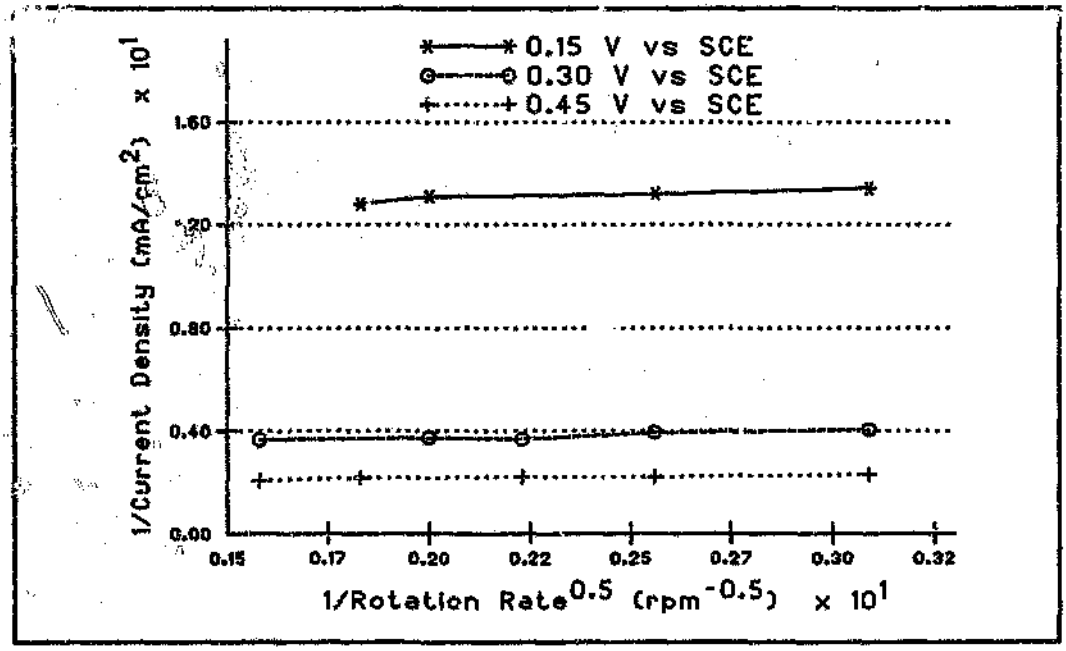


Figure 5.3 The effect of rotation on the rate of copper dissolution in ferric sulphate solutions. Conditions : T° = 298K, 0.1M $Fe_2(SO_4)_3$, 0.5M H^+.

5.1.4 The dependence of copper dissolution rate on temperature.

An increase in temperature results in an increase in the rate of copper dissolution in both ferric and sodium sulphate solutions. The current densities at the copper electrode, at various temperatures, are listed in Table 5.2.

The dependence of ferric reduction rate on temperature, at the copper anode, is illustrated in Figure 5.4. The rate of ferric reduction on copper increases with increasing temperature. The reduction of ferric ions on copper decreases rapidly with increasing electrode potential. At electrode potentials of 0.13 V vs SCE the reduction of ferric ions is almost negligible.

Table 5.2 Comparison of the current densities, in 0.3M Na_2SO_4 and 0.1M $Fe_2(SO_4)_3$ solutions, at various temperatures and at an electrode potential of 0.09 V vs SCE. 2003 rpm, scan rate 1mV/s.

Temperature K	i_a ($mA.cm^{-2}$) sodium sulphate	i_a ($mA.cm^{-2}$) ferric sulphate
298	23.0	19.5
308	28.5	25.1
318	33.8	33.1
328	45.3	39.8

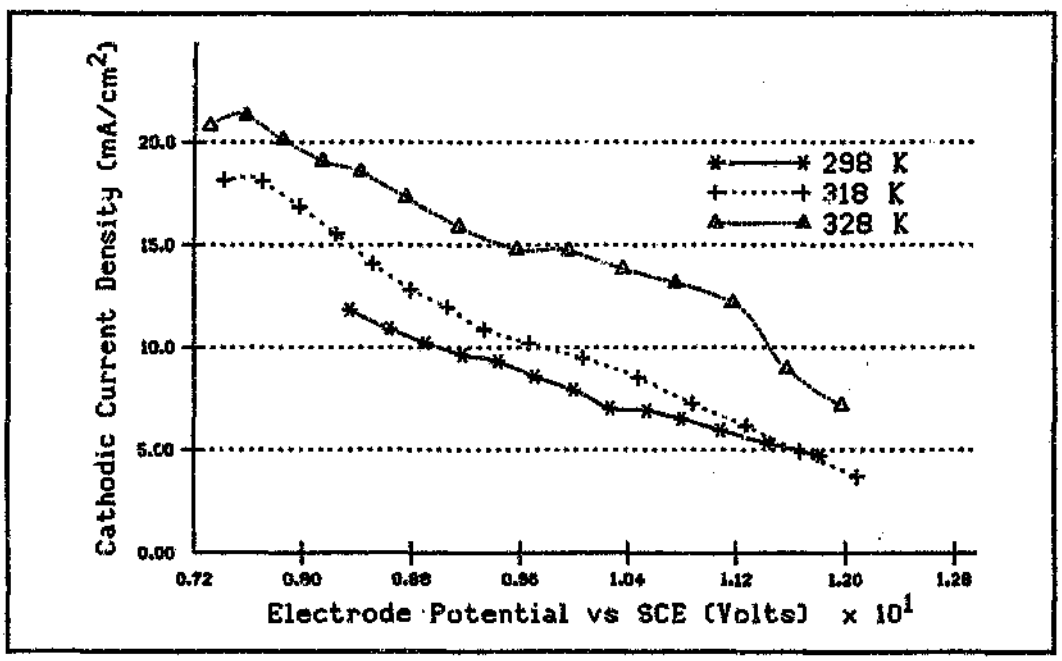


Figure 5.4 The rate of ferric reduction on copper at various temperatures. Conditions : 0.1M $Fe_2(SO_4)_3$, 2003rpm, 0.5M H^+.

5.2 Electrochemical Characterisation Of Ferric Reduction On Platinum.

5.2.1 The dependence of ferric reduction rate on concentration.

Figure 5.5 illustrates that as the ferric ion concentration is increased the rate of ferric reduction increases.

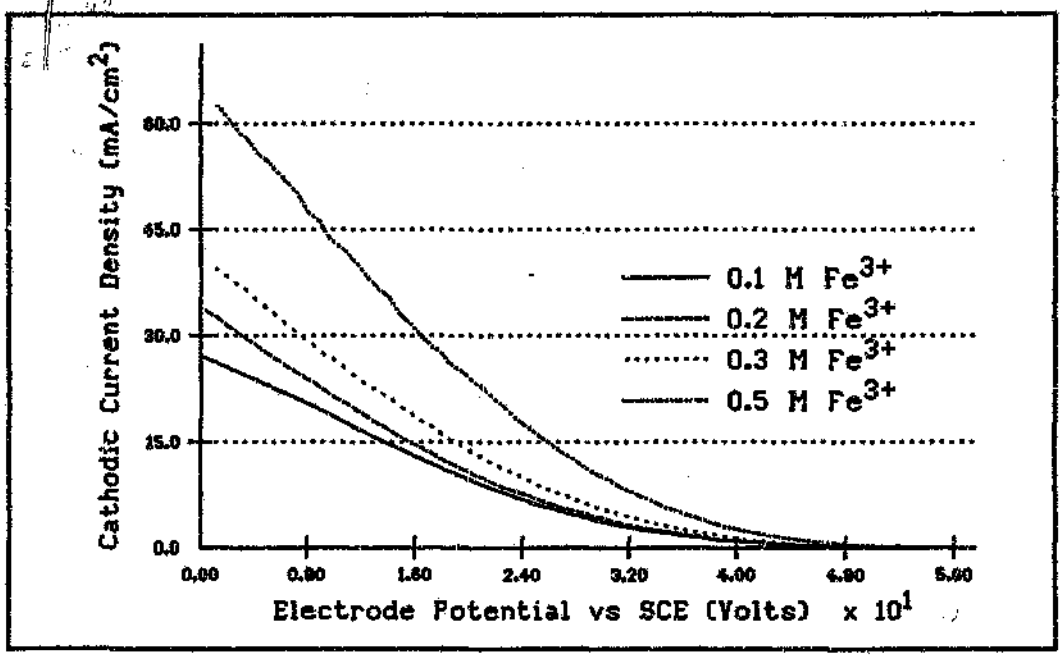


Figure 5.5 The effect of ferric concentration on the rate of ferric reduction on platinum. Conditions : 2003rpm, 298K, 0.5M H^+, scan rate 1mV/s.

Figure 5.6 illustrates the relationship between the limiting current density and the concentration of ferric ions in solution. Figure 5.6, in addition, illustrates the comparison between the limiting currents determined by regression on pseudo-steady-state polarisation data and those given by the Levich equation using steady state data.

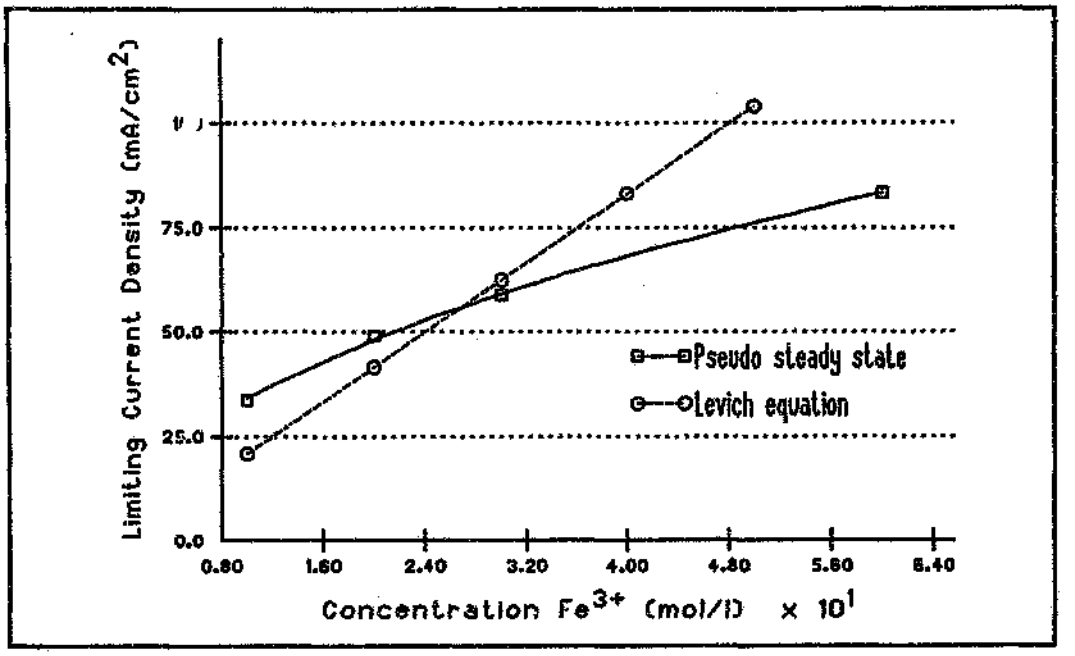


Figure 5.6 The dependence of limiting current on ferric concentration. Conditions : 2003 rpm, 298K, 0.5M H^+, scan rate 1mV/s.

Equation 5.1 depicts the theoretical mathematical relationship which should exist between the limiting current density and ferric concentration. The relationship suggests that the diffusion coefficient is a constant which can be determined from the slope of the limiting current density versus ferric concentration graph. The value of the slope, for the pseudo-steady-state data in Figure 5.6, at different ferric concentrations suggests that the diffusion coefficient decreases as the concentration of ferric increases.

$$i_l = \frac{nFD_{Fe^{3+}}[Fe^{3+}]}{\delta} \qquad 5.1$$

Madsen (1981) who measured ferric diffusion coefficients by using derivative chrono-amperometry also observed variations in the ferric diffusion coefficient with changes in concentration. Madsen (1981) proposed an empirical relationship, Equation 5.2, in which the ferric diffusion coefficient is related to the total sulphate concentration in the solution.

$$D_{Fe^{3+}} = 10^{-6}(18.33 - 7.65[SO_4^{2-}] + 56.2[SO_4^{2-}]^{\frac{1}{2}} - 63.87[SO_4^{2-}]^{\frac{1}{3}}) \quad 5.2$$

The slow sweep rates used to characterise the kinetics of ferric reduction on platinum result in a pseudo-steady-state current. Previous research has characterised the ferric reaction at steady-state, (Bochmann and Vielstich (1988) and Angell and Dickinson (1972)). The overall result is that the kinetic parameters, listed in Table 5.3, determined by regression differ from those obtained by other researchers. A steady-state potentiostatic experiment, the results of which are illustrated in Figure 5.7, was conducted in order that the kinetic parameters obtained in this study could be compared with those of other researchers.

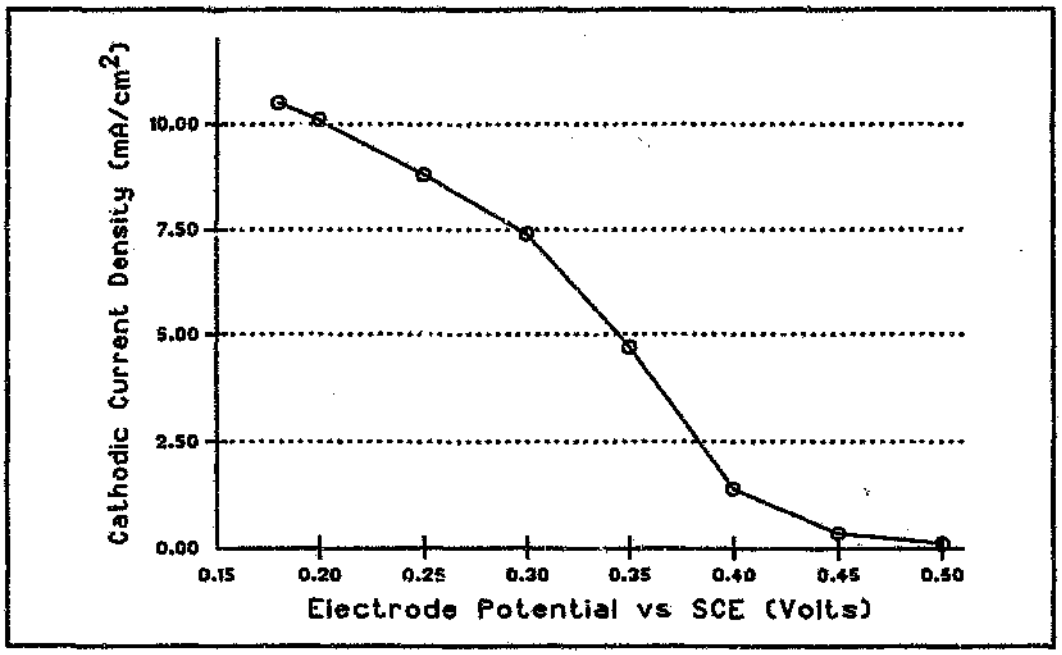


Figure 5.7 Steady-state polarisation curve for the ferric/ferrous reduction reaction on platinum. Conditions : 0.2M Fe^{3+}, 0.5M H^+, 200 rpm, T° = 298K.

The kinetic parameters obtained from the steady-state potentiostatic experiment compare very favourably with those of other researchers. The value of the diffusion coefficient obtained from the pseudo-steady-state experiment is two orders of magnitude greater than the corresponding value determined by steady-state measurements.

Table 5.3 Comparison of kinetic parameters for the Fe^{3+}/Fe^{2+} reaction.

Researchers	D_{Fe}^{3+} $cm^2.s^{-1}$	α_{Fe}^{3+}
Madsen (1981)	$5.68x10^{-6}$	-
Angell *et al.* (1972)	$5.50x10^{-6}$	0.5
This Work (steady state)	$1.39x10^{-6}$	0.6
This Work (unsteady state)	$1.75x10^{-4}$	0.25

The diffusion coefficient for ferric reduction in a 0.2 M Fe^{3+} solution was determined using the Levich equation. A Brooksfield viscometer was used to determine the kinematic viscosity, $1.24x10^{-2}$ $cm^2.s^{-1}$, of a 0.2 M Fe^{3+} solution. A comparison of the exchange current densities cannot be made due to the use of a different solution in this study.

5.2.2 The dependence of ferric reduction rate on electrode rotation.

Angell and Dickinson (1972) investigated the effect that rotation rate has on the kinetics of the ferrous/ferric reaction in order to determine the order of reaction. They propose an equation in which the relationship between current and rotation rate, at constant overpotential, is dependent on the order of reaction. For current densities less than the limiting current density a plot of the reciprocal of current versus the reciprocal of the square root of the rotation rate will yield a straight line if the reaction is first order. Figure 5.8 suggests that the reduction of ferric ion to ferrous ion is a first order process. Figure 5.8 further confirms that at low electrode

potentials the ferric reduction reaction is dependent on rotation rate and is hence controlled by electrochemical and mass transfer processes.

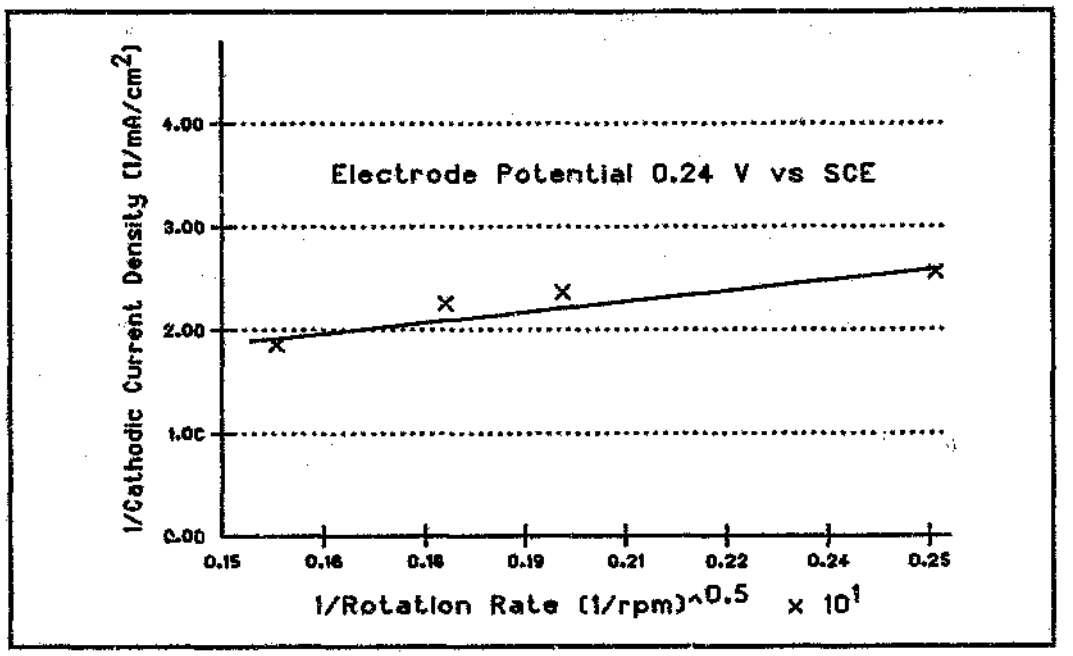


Figure 5.8 Determination of the ferric/ferrous reaction order. Conditions : 0.2M Fe^{3+}, 0.5M H^{+}, 298K.

5.2.3 The dependence of ferric reduction rate on temperature.

Figure 5.9 illustrates the increase in ferric reduction rate with increasing temperature. As temperature is increased the ferric reduction remains electrochemically controlled for higher cathodic overpotentials. This is apparent on comparison of the shapes of the 298 K and 328 K polarisation curves at an electrode potential of 0.16 V vs SCE. The apparent activation energy for ferric reduction on platinum, at an electrode potential of 0.35 V vs SCE, is approximately 27 $kJ.mol^{-1}$.

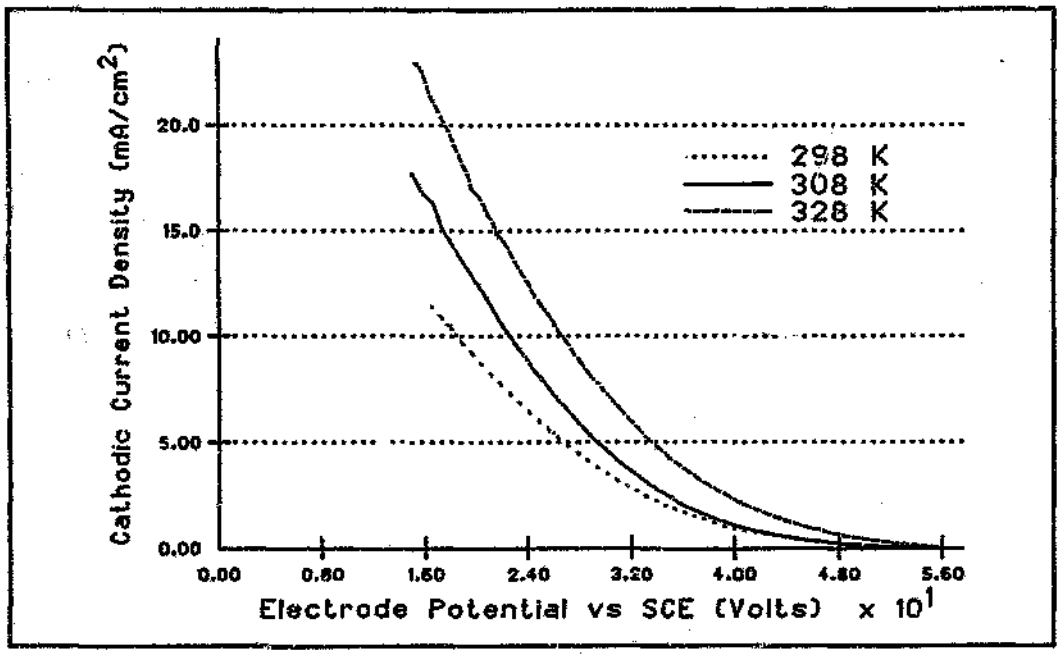


Figure 5.9 The effect of temperature on the rate of ferric reduction on platinum. Conditions : 2003rpm, 0.2M Fe^{3+}, 0.5M H^+, scan rate 1mV/s.

5.3 Electrochemical Characterisation Of The Galvanic Couple Formed Between Copper And Platinum.

The galvanic cell experiments were conducted under the same experimental conditions as the electrochemical characterisations of the half reactions and therefore effects observed in the polarisation studies translate directly to effects observed in the galvanic cell experiments. Increases in ferric concentration and temperature increased the amount of galvanic current flowing through the couple. The effect of electrode rotation is illustrated in Figure 5.10.

Increases in electrode rotation rate increase the quantity of galvanic current flowing through the couple. At low cell voltages the effect of rotation rate is more apparent than at higher cell voltages. This is due to the fact that the galvanic potential, at zero cell voltage, occurs at an electrode potential of 0.12 V vs SCE. This corresponds to a regime in which the ferric reduction reaction is a function of rotation rate. At

large cell voltages the effect tends to disappear. This is due to the electrode potential being near the rest potential and hence the ferric reduction reaction is electrochemically controlled and thus independent of electrode rotation rate.

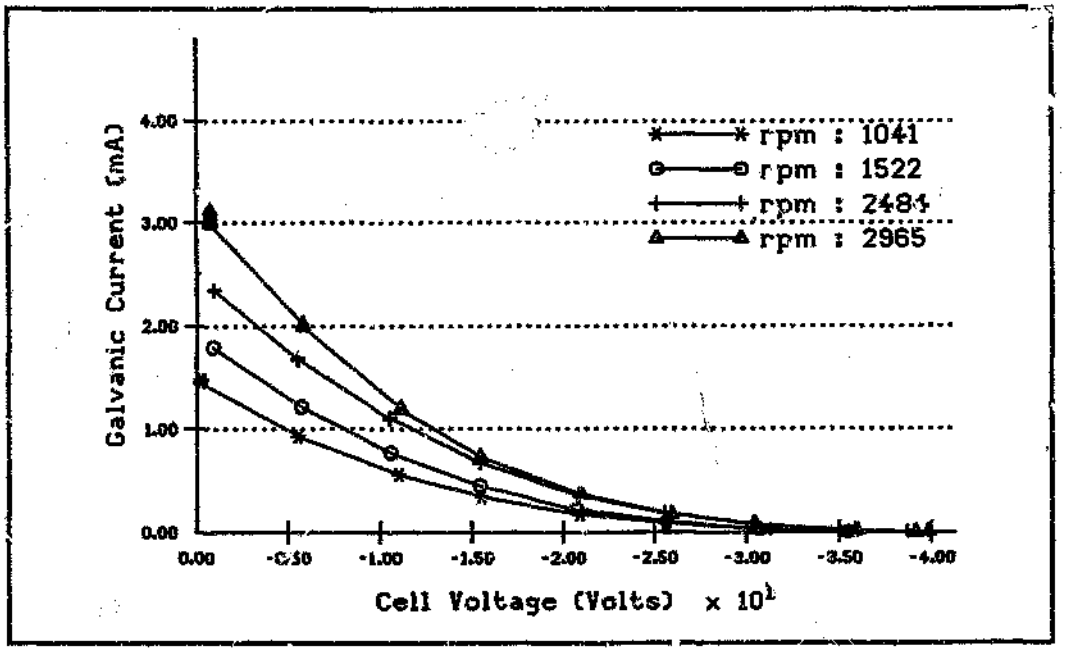


Figure 5.10 The effect of rotation on the galvanic interaction in the copper-platinum cell. Conditions : 0.2M Fe^{3+}, 0.5M H^{+}, 298K.

5.4 Mathematical Modelling Of The Copper-Platinum Galvanic Couple.

The parameters, determined by regression and experimental measurement, which were used in the galvanic model, Equation 3.12, are listed in Table 5.4. The anodic parameters were determined by fitting Equation 3.4 to the relevant copper dissolution pseudo-steady-state polarisation data. The galvanic cell experiments were conducted in a manner which ensured that the half reactions did not reach steady-state, refer to Section 4.3.2, since this would result in solution composition variations which cause a decay in galvanic current. The various dynamic factors which effect the magnitude of galvanic interaction, such as solution composition variations, are discussed in Chapter 8. The limiting current density, exchange

current density and charge-transfer coefficient for the ferric reduction reaction were determined by regressing the ferric reduction pseudo-steady-state polarisation data with Equation 3.9. The large limiting current density, and therefore diffusion coefficient, and low charge-transfer coefficient are a result of the pseudo-steady-state measurements. The model equation was solved readily using the Regula Falsi iteration program, Appendix B.

Table 5.4 Parameters used in the model equation. Conditions : 0.1 M Fe^{3+}, 0.5 M H^+, 2003 rpm, 298 K.

Parameters	Anodic	Cathodic
E_o (V)	0.065	0.54
i_o ($A.m^{-2}$)	65	2.8
α	1.1	0.28
i_l ($A.m^{-2}$)	-	337

Figure 5.11 illustrates the excellent correspondence between the experimentally measured galvanic currents and those predicted by the galvanic model equation.

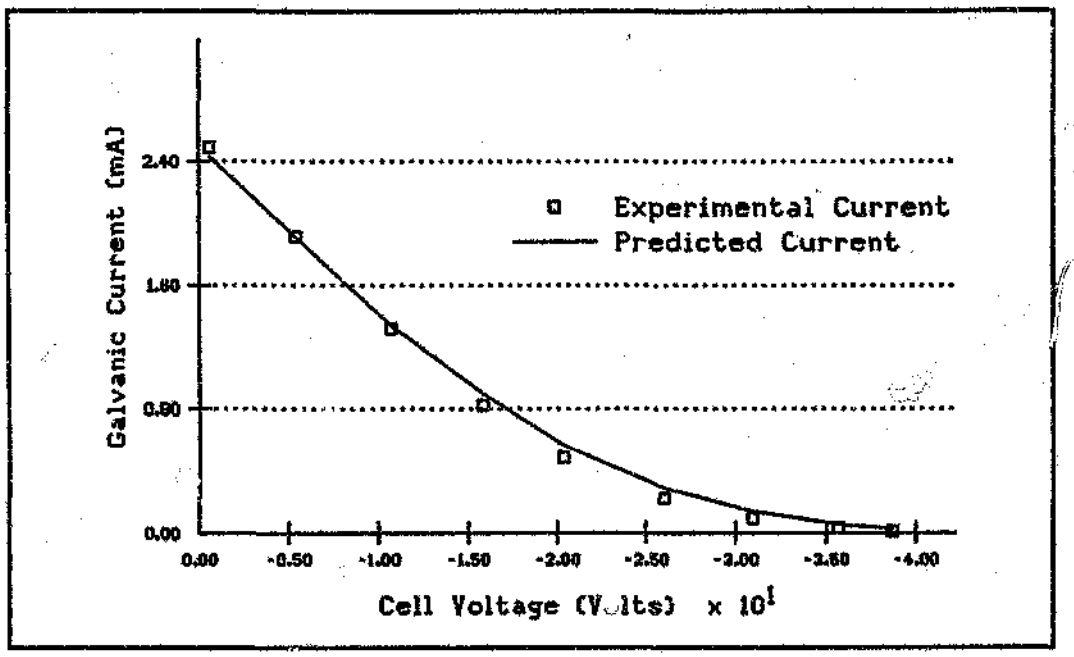


Figure 5.11 Graph of the model prediction of galvanic current in the copper-platinum cell. Conditions : 0.1M Fe^{3+}, 0.5M H^{+}, 2003rpm, 298K.

6. GALVANIC INTERACTION BETWEEN COPPER AND PYRITE IN ACIDIC FERRIC SULPHATE SOLUTIONS.

This chapter discusses the electrochemical aspects of the galvanic couple formed between copper and pyrite. One of the objectives of this chapter was to determine the validity of the galvanic model with a galvanic couple consisting of one mineral species. The work was conducted under the same experimental conditions as the work in Chapter 5, however, the platinum cathode was replaced by a pyrite cathode. The electrochemical characterisation of copper dissolution in ferric sulphate solutions is discussed in Section 5.1. This chapter analyses and discusses the kinetic aspects of ferric reduction on pyrite as well as the factors which affect the magnitude of the galvanic interaction between the copper and pyrite couple. The chapter culminates in an analysis of the model prediction of galvanic current.

6.1 Electrochemical Characterisation Of Ferric Reduction On Pyrite.

6.1.1 The dependence of ferric reduction rate on ferric concentration.

Figure 6.1 illustrates the increase in ferric reduction on pyrite as the ferric concentration is increased. The Tafel slopes of approximately 120 mV.decade^{-1} suggest that ferric reduction on pyrite is a first order process. The slight deviation from the 120 mV.decade^{-1} Tafel slope can probably be attributed to the characterisation of the ferric reduction reaction under pseudo-steady-state conditions.

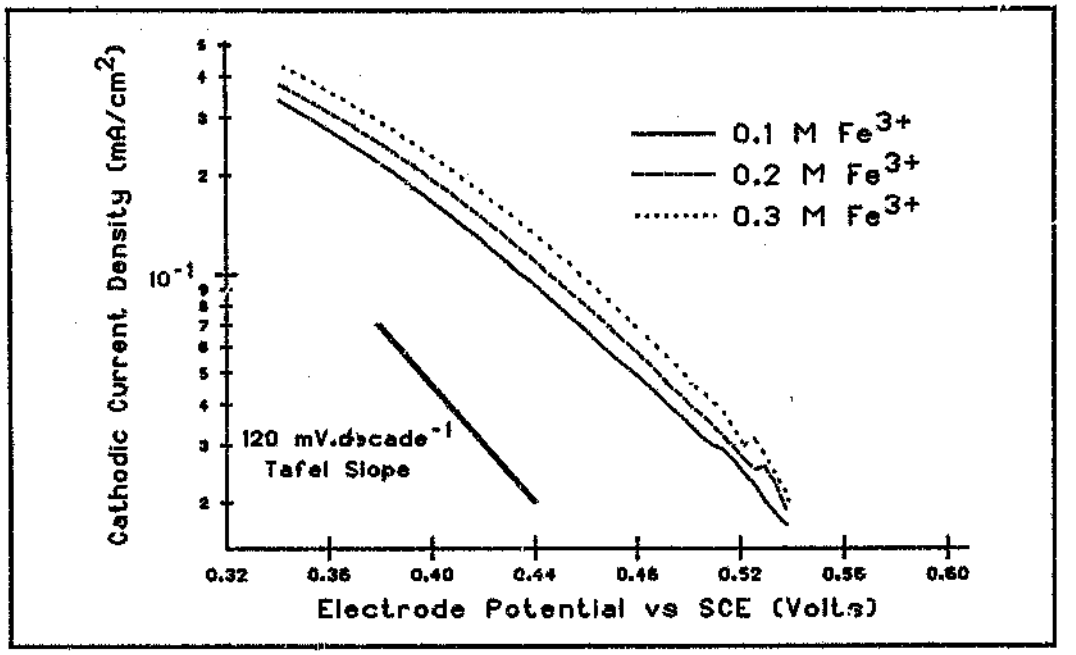


Figure 6.1 Tafel plot of the effect of ferric concentration on the rate of ferric reduction on pyrite. Conditions : 2003rpm, 298K, 0.5M H^+, scan rate 1mV/s.

6.1.2 The dependence of ferric reduction rate on electrode rotation.

Figure 6.2 illustrates the increase in the rate of ferric reduction associated with increases in electrode rotation rate. The graph is plotted at low electrode potentials, where ferric reduction is partly controlled by mass transfer processes.

6.1.3 The dependence of ferric reduction rate on temperature.

Increasing temperature increases the reduction rate of ferric ions on pyrite as is illustrated on Figure 6.3. At temperatures above 308 K the effect of increasing temperature becomes less pronounced. This suggests that the reduction of ferric on pyrite is controlled by a mechanism that is a weak function of temperature at elevated temperatures.

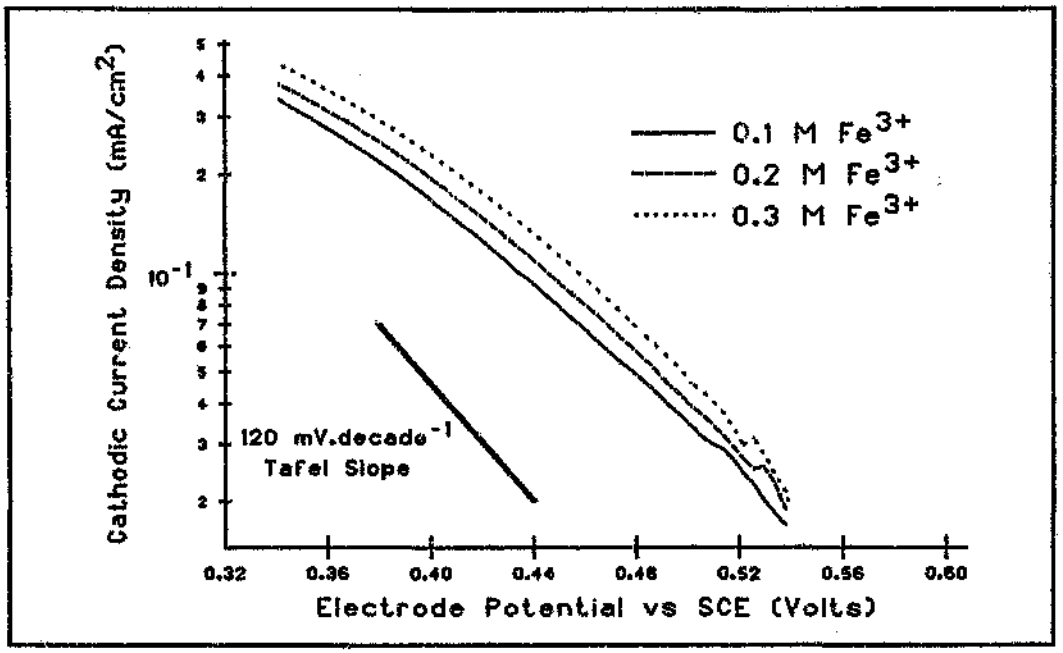


Figure 6.1 Tafel plot of the effect of ferric concentration on the rate of ferric reduction on pyrite. Conditions : 2003rpm, 298K, 0.5M H^+, scan rate 1mV/s.

6.1.2 The dependence of ferric reduction rate on electrode rotation.

Figure 6.2 illustrates the increase in the rate of ferric reduction associated with increases in electrode rotation rate. The graph is plotted at low electrode potentials, where ferric reduction is partly controlled by mass transfer processes.

6.1.3 The dependence of ferric reduction rate on temperature.

Increasing temperature increases the reduction rate of ferric ions on pyrite as is illustrated on Figure 6.3. At temperatures above 308 K the effect of increasing temperature becomes less pronounced. This suggests that the reduction of ferric on pyrite is controlled by a mechanism that is a weak function of temperature at elevated temperatures.

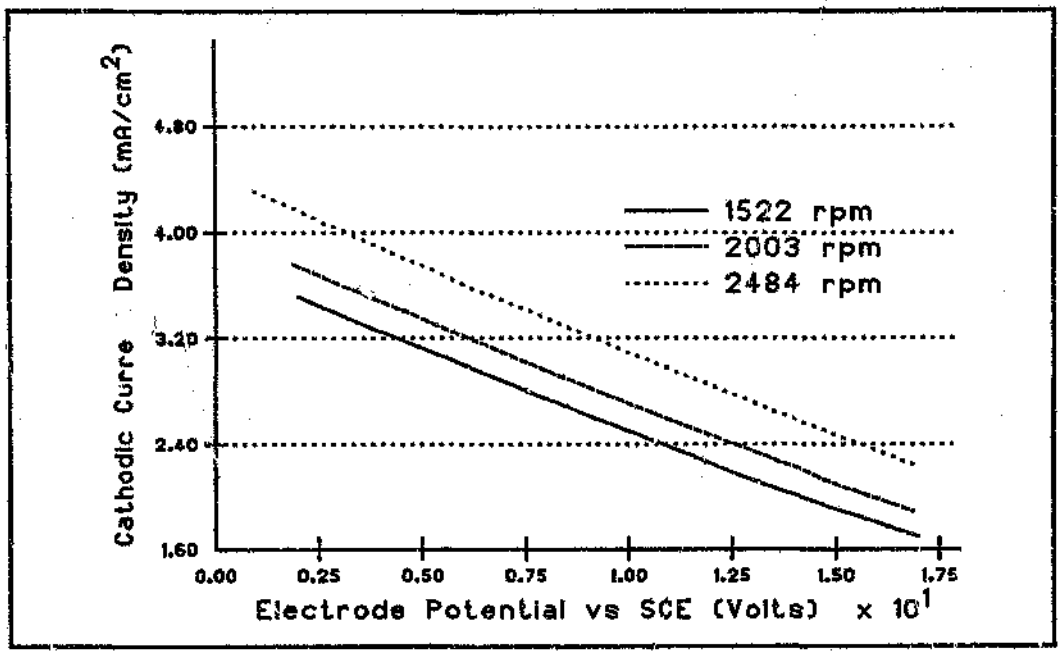


Figure 6.2 The effect of electrode rotation on ferric reduction rate at low electrode potentials. Conditions : 0.2M Fe^{3+}, 0.5M H^{+}, 298K, scan rate 1mV/s.

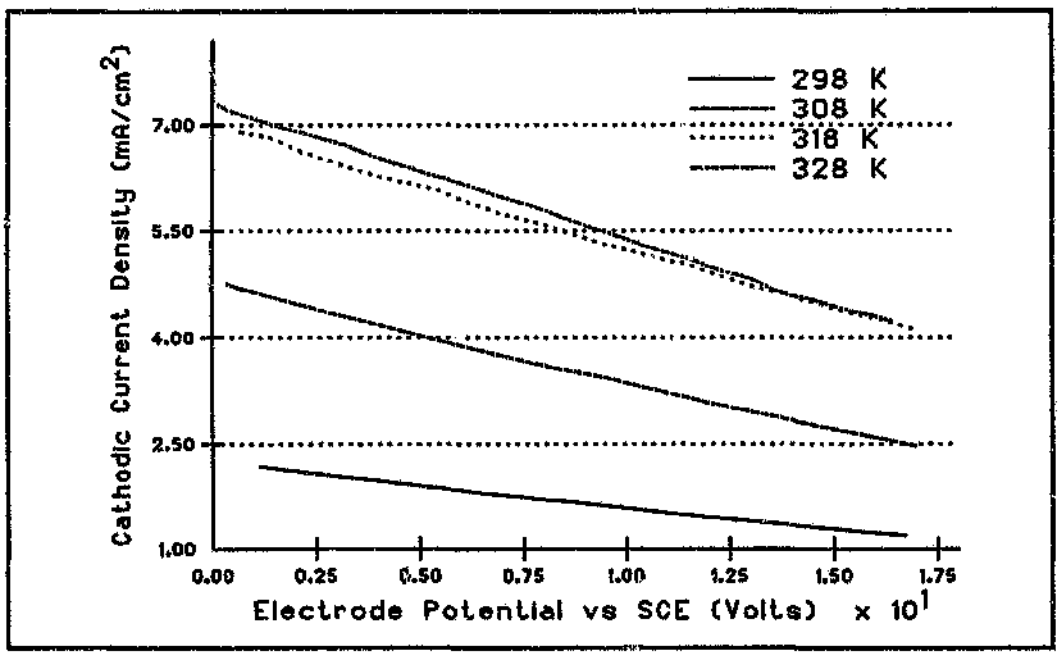


Figure 6.3 The effect of temperature on ferric reduction rate at low electrode potentials. Conditions : 0.2M Fe^{3+}, 0.5M H^{+}, 2003rpm, scan rate 1mV/s.

The activation energies calculated from the data given in Figure 6.4 confirm this observation. At higher temperatures the reaction control mechanism appears to change owing to the variation in activation energy. At lower temperatures the apparent activation of 46 $kJ.mol^{-1}$ suggests the reaction is chemically controlled whereas the apparent activation energy of 3.8 $kJ.mol^{-1}$ at elevated temperatures suggests the reaction is mass transfer controlled. Further experimental work is necessary to confirm this observation.

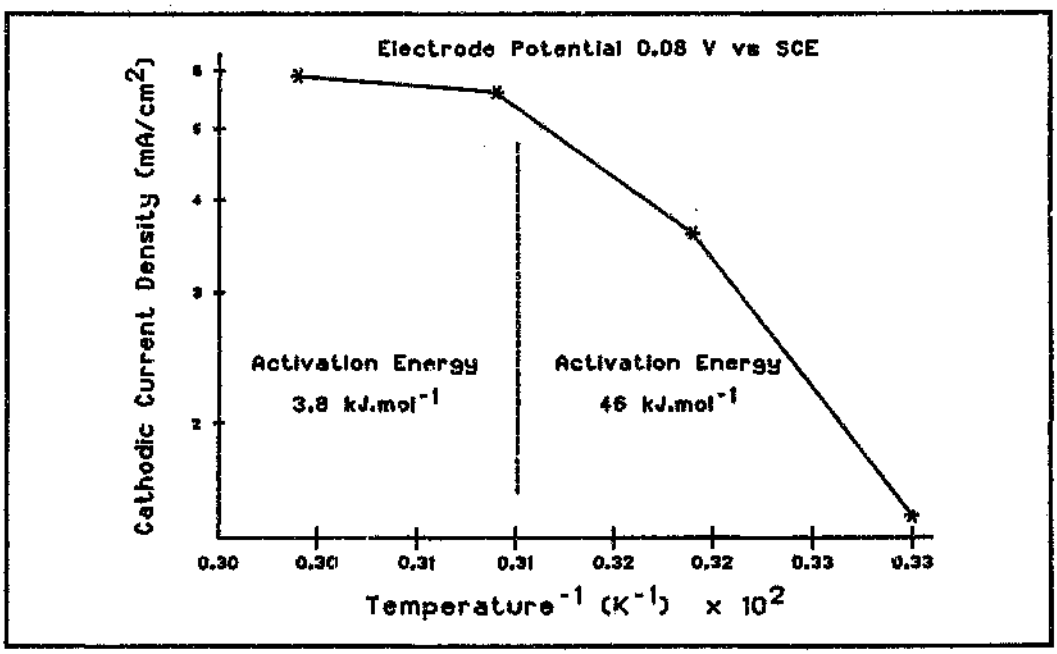


Figure 6.4 Determination of the activation energy for ferric reduction on pyrite. Conditions : 0.2M Fe^{3+}, 0.5M H^{+}, 2003rpm.

6.2 Electrochemical Characterisation Of The Galvanic Couple Formed Between Copper And Pyrite.

Increasing ferric concentration increases the galvanic current between the copper-pyrite couple. This is illustrated in Figure 6.5. Increases in ferric concentration result in an increase in the galvanic potential of the copper-pyrite couple. A linear relationship exists between the galvanic potential and the concentration of ferric ions in the solution. This is illustrated in Figure 6.6.

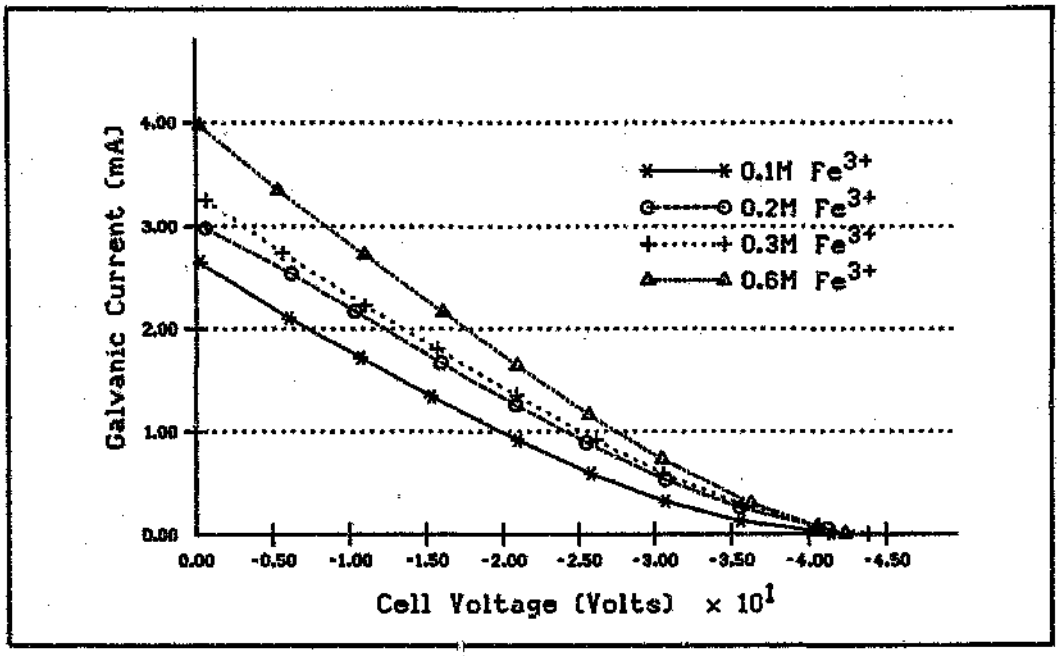


Figure 6.5 The effect of ferric concentration on galvanic current in a copper-pyrite couple. Conditions : 0.5M H^+, 2003rpm, 298K.

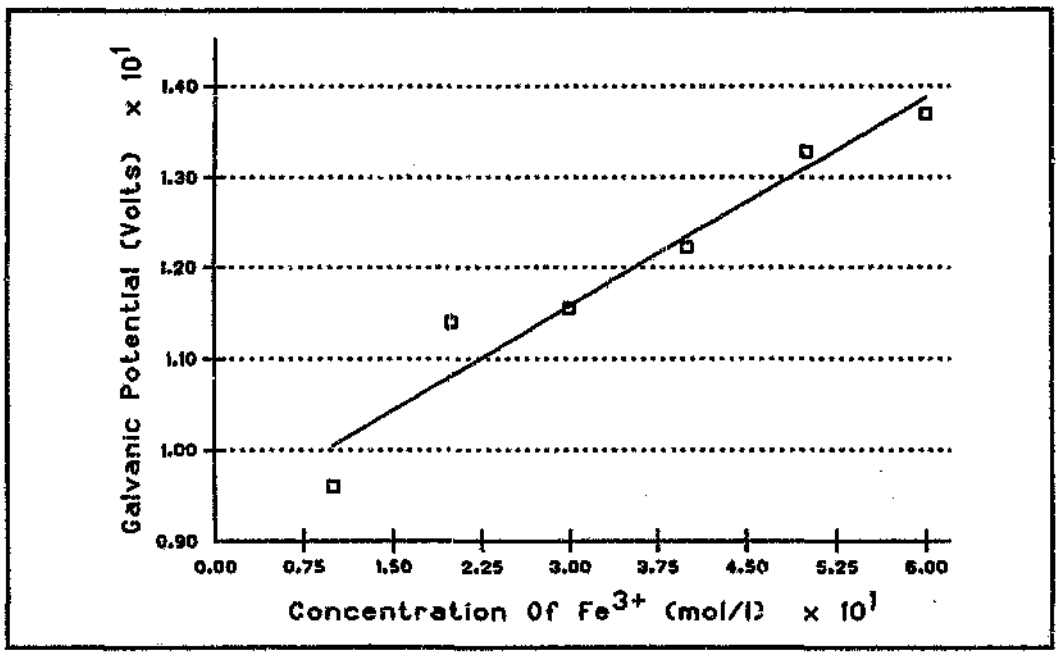


Figure 6.6 The dependence of galvanic potential on ferric concentration. Conditions : 0.5M H^+, 2003rpm, 298K.

Two factors contribute to the increase in galvanic potential with increasing ferric concentration. The first of these is the variations in the anodic and cathodic rest potentials associated with increases in ferric concentration. This is illustrated in Figure 6.7. The rest potentials of the anode and cathode become more positive with increasing ferric concentration and hence the galvanic potential will shift accordingly to more positive values.

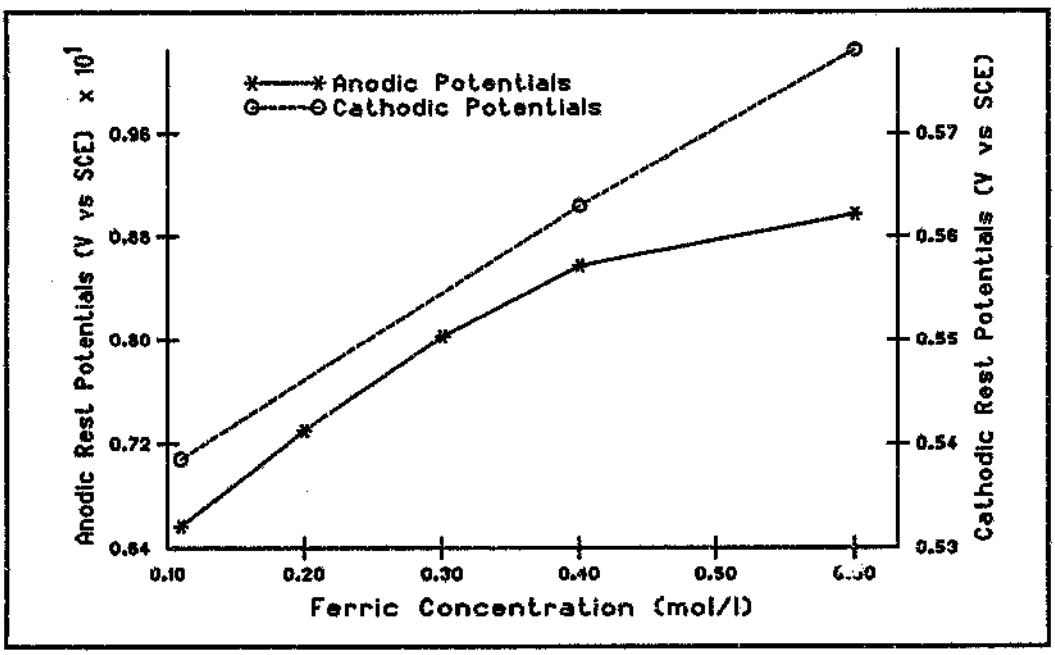


Figure 6.7 The dependence of rest potentials on ferric concentration.
Conditions : 0.5M H^+, 2003rpm, 298K.

The second contributing factor to the increase in galvanic potential is the variation in the shapes of the polarisation curves associated with increases in ferric concentration. This is illustrated in Figure 6.8. Increases in ferric concentration decrease the dissolution rate of copper and increase the ferric reduction rate on pyrite, see Sections 5.1.2 and 6.1.1 respectively. The galvanic potential occurs where the anodic and cathodic currents are equivalent. Hence for the galvanic potential to shift in a positive direction, from E_{g1} to E_{g2}, the increases in ferric concentration must have more of a pronounced effect on the rate of ferric reduction than the rate of copper dissolution.

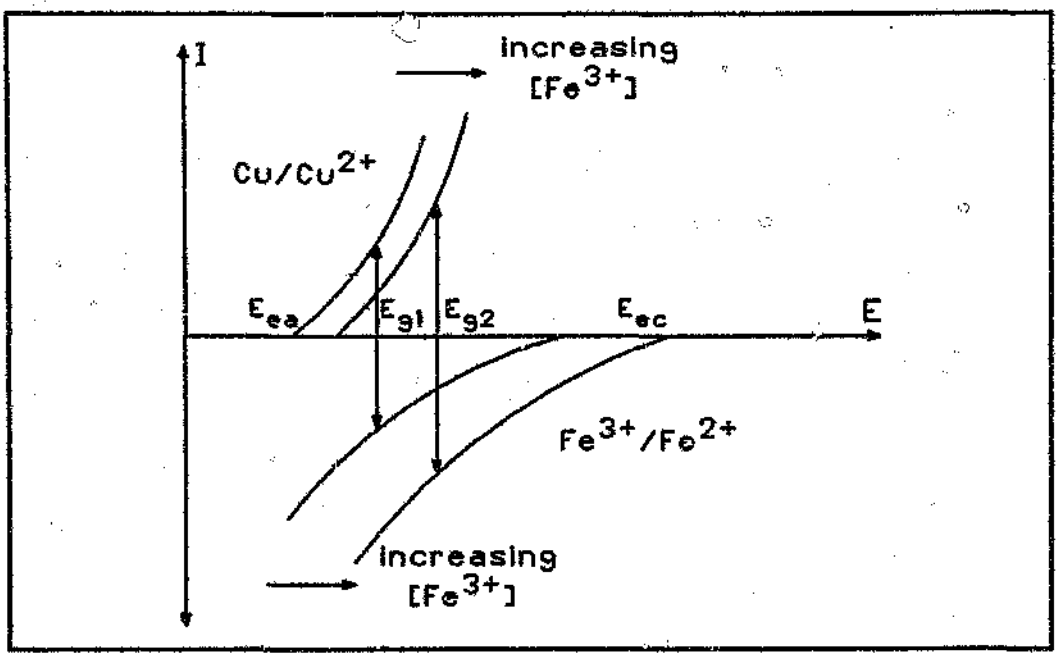


Figure 6.8 The hypothetical dependence of galvanic potential on polarisation curve shape.

The effect of increasing temperature on galvanic current is illustrated in Figure 6.9. The variation in activation energy observed in the electrochemical characterisation of pyrite, Section 6.1.3, is not observed in the galvanic couple. This is due to the strong increase in copper dissolution associated with increasing temperature.

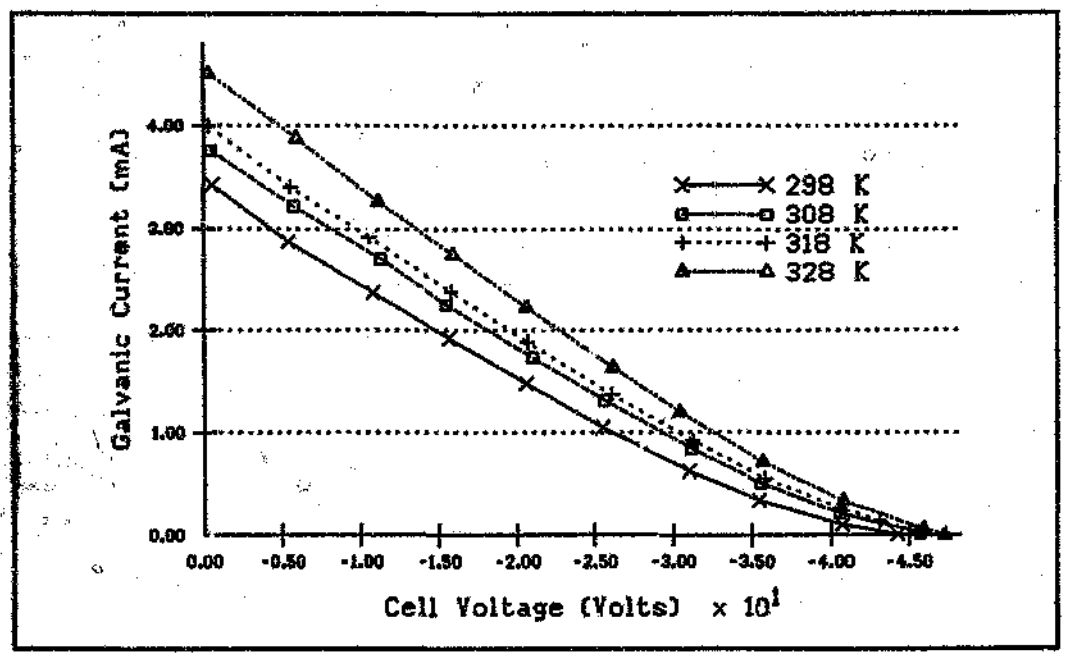


Figure 6.9 The effect of temperature on galvanic current in a copper-pyrite couple. Conditions : 0.2M Fe^{3+}, 0.5M H^{+}, 2003rpm.

6.3 Mathematical Modelling Of The Copper-Pyrite Galvanic Couple.

The parameters used in the galvanic model, Equation 3.13, to obtain the predicted galvanic currents shown in Figure 6.10, are listed in Table 6.1. The charge transfer coefficient for the reduction of ferric ions on pyrite is observed to be smaller than the charge-transfer coefficient for the reduction of ferric ions on platinum.

Table 6.1 Kinetic parameters used in the galvanic model equation for the copper-pyrite cell. Conditions : 0.2M Fe^{3+}, 0.5M H^+, 2003 rpm, 318 K.

Parameters	Anodic	Cathodic
E_o (V)	0.073	0.54
i_o ($A.m^{-2}$)	104	13
α	0.94	0.13
i_L ($A.m^{-2}$)	-	128

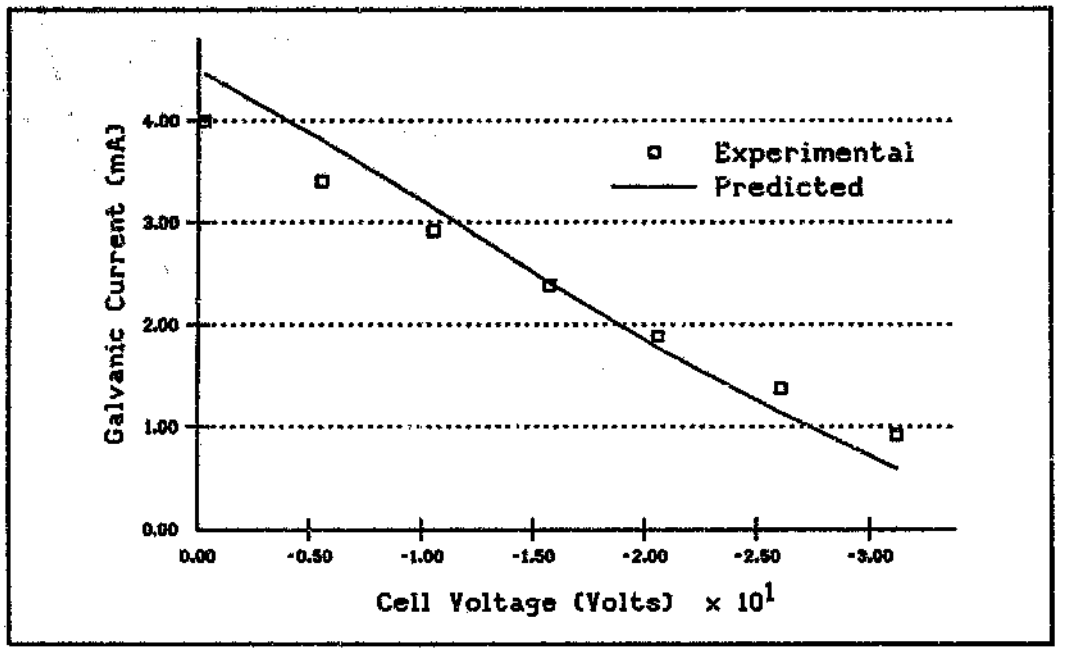


Figure 6.10 Model prediction of galvanic current in the copper-pyrite couple. Conditions : 0.2M Fe^{3+}, 0.5M H^+, 2003rpm, 318K.

There exists a favourable correspondence between the experimentally measured galvanic currents and those predicted by the galvanic model equation. This is illustrated in Figure 6.10. The differences that are present can probably be attributed to surface effects inherent in the polycrystalline pyrite electrode. These surface

effects lead to variations in the kinetic parameters. In addition to this, due to the geometry of the rotating ring disc electrode, the ferric concentration at the pyrite sc may be slighily different than the ferric concentration at the copper ring.

7. GALVANIC INTERACTION BETWEEN GALENA AND PYRITE IN ACIDIC FERRIC NITRATE SOLUTIONS.

This chapter consists of the analysis and modelling of a galvanic couple made up of two minerals. In the initial sections of the chapter the kinetics of galena dissolution and ferric reduction on pyrite are analyzed. In the latter sections of the chapter factors which effect the magnitude of the galvanic interaction between galena and pyrite are discussed. The chapter culminates in the mathematical modelling of the mineral galvanic cell.

7.1 Electrochemical Characterisation Of The Anodic Dissolution Of Galena.

The anodic dissolution of galena was characterised in sodium nitrate and ferric nitrate solutions. The reason being that the difference between the two polarisation curves yielded the rate of ferric reduction on the galena anode. In addition to this the characterisation in sodium nitrate facilitated a comparison of the kinetic parameters obtained in this research with the kinetic parameters obtained by other researchers.

7.1.1 The dependence of galena dissolution rate on sodium nitrate concentration.

No variation in the rate of galena dissolution occurs as the concentration of sodium nitrate is increased. This is illustrated in Figure 7.1. The comparison of the Tafel slopes obtained in this study with those obtained by other researchers is given in Table 7.1. The Tafel slopes compare very favourably with those obtained by other researchers.

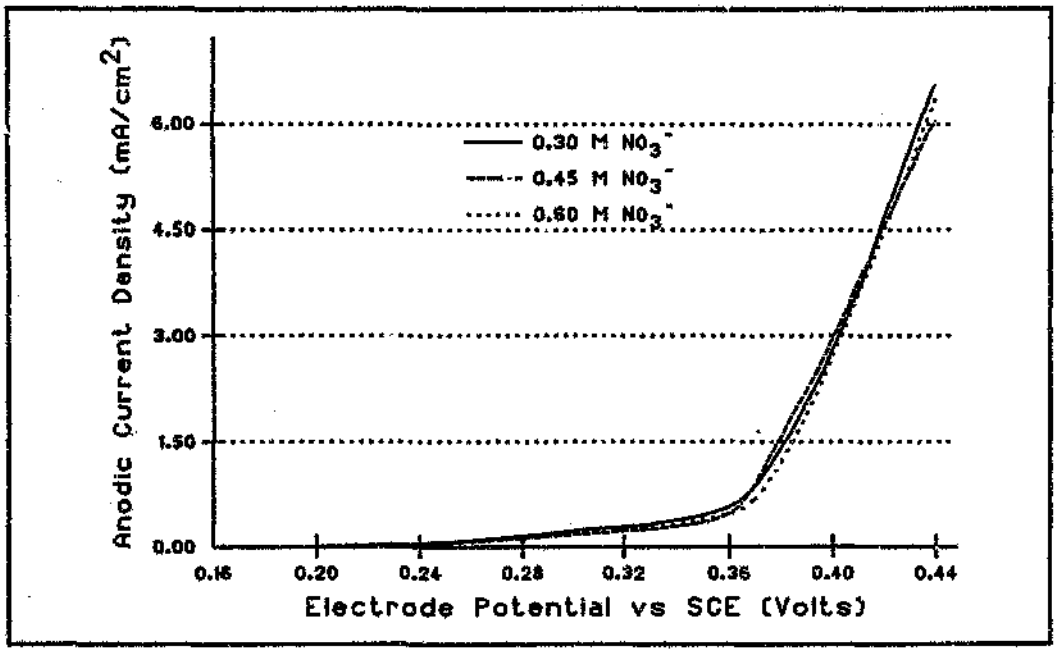


Figure 7.1 The effect of sodium nitrate concentration on the rate of galena dissolution. Conditions : 0.5M H^+, 1041rpm, 298K, scan rate 1mV/s.

Table 7.1 Comparison of kinetic parameters associated with galena dissolution.

Researchers	Tafel Constant ($mV.decade^{-1}$)
Paul *et al.* (1977)	46-113
Johnson *et al.* (1978)	60-120
Paramguru *et al.* (1979)	120
This Research	75-130

Paul *et al.* (1977) observed that at electrode potentials between 0.25 and 0.35 V vs SCE the Tafel slopes varied between 46 $mV.decade^{-1}$ and 84 $mV.decade^{-1}$. Furthermore Tafel slopes of 88 $mV.decade^{-1}$ to 113 $mV.decade^{-1}$ were observed at electrode potentials between 0.35 and 0.45 V vs SCE. The Tafel slopes obtained in this study ranged from 75 $mV.decade^{-1}$ to 130 $mV.decade^{-1}$ between electrode

potentials of 0.25 and 0.40 V vs SCE. A comparison of the exchange current densities cannot be made due to the use of a different solution in this study.

7.1.2 The dependence of galena dissolution rate on ferric nitrate concentration.

Figure 7.2 illustrates that as the concentration of ferric ions is increased the rate of galena dissolution decreases. The polarisation curves are linear at small electrode potentials and have slopes which are proportional to the concentration of ferric ions. Owing to surface effects associated with the galena electrode the exact amount of ferric reduced on the galena anode was difficult to determine.

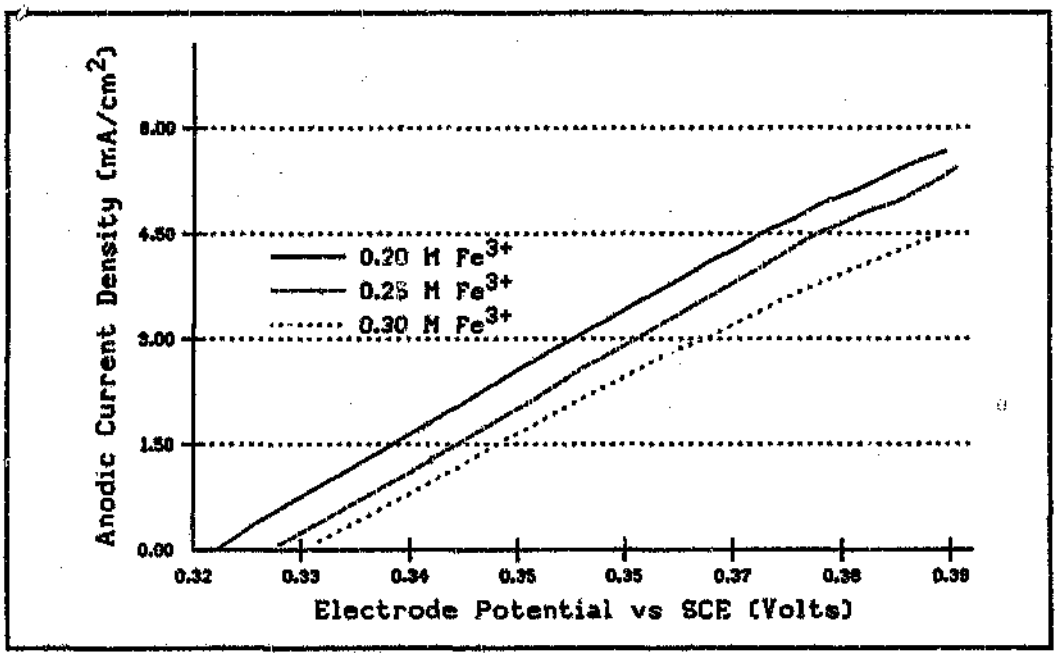


Figure 7.2 The effect of ferric concentration on the rate of galena dissolution. Conditions : 0.5M H^+, 1041rpm, 298K, scan rate 1mV/s.

7.1.3 The dependence of galena dissolution rate on electrode rotation.

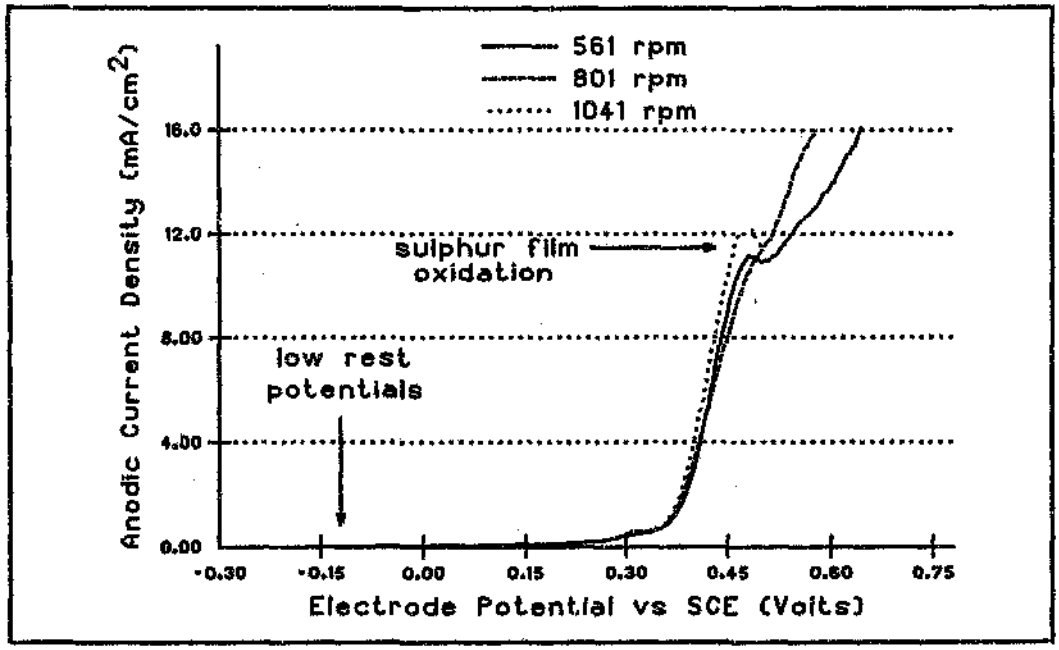


Figure 7.3 The effect of rotation on the rate of galena dissolution. Conditions : 0.6M $NaNO_3$, 0.5M H^+, 298K, scan rate 1mV/s.

The rate of galena dissolution is independent of electrode rotation in sodium nitrate solutions. This is illustrated in Figure 7.3. However, it was observed that increases in electrode rotation rate produced decreases in the dissolution rate of galena in ferric nitrate solutions. Figure 7.3 illustrates the exponential nature of the galena dissolution at electrode potentials around 0.32 V vs SCE. This confirms that the anodic dissolution of galena is an electrochemically controlled process.

Owing to similar phenomenon observed by Paul *et al.* (1977) it is believed that the peaks exhibited at approximately 0.48 V vs SCE correspond to the oxidation of the sulphur film, formed on the galena surface, to thiosulphate. This reaction is given by Equation 2.11. The galvanic potentials between galena and pyrite occurred at values of approximately 0.30 V vs SCE. Therefore the maxima and minima displayed by the sulphur film oxidation did not influence the modelling of the galena dissolution. A further maximum and sudden decline in current density was observed

at electrode potentials of 0.70 V vs SCE. This is due, it is believed, to the formation of a passive lead hydroxide film on the galena surface. Similar phenomenon were observed by Skewes (1972).

Differences in the measured anodic rest potential values were observed. The differences are apparent on comparing the rest potentials illustrated in Figure 7.3 with those of Figure 7.5. The rest in Figure 7.3 are approximately -0.20 V vs SCE, whilst those in Figure 7.5 are approximately 0.05 V vs SCE. Peters (1976) observed significant variations in the rest potentials of galena in perchloric acid solution. Figure 7.4 illustrates the sharp increase in rest potential associated with small concentrations of plumbous ions in solution. This phenomenon, however, did not effect the kinetic characterisation and modelling of the anodic dissolution of galena.

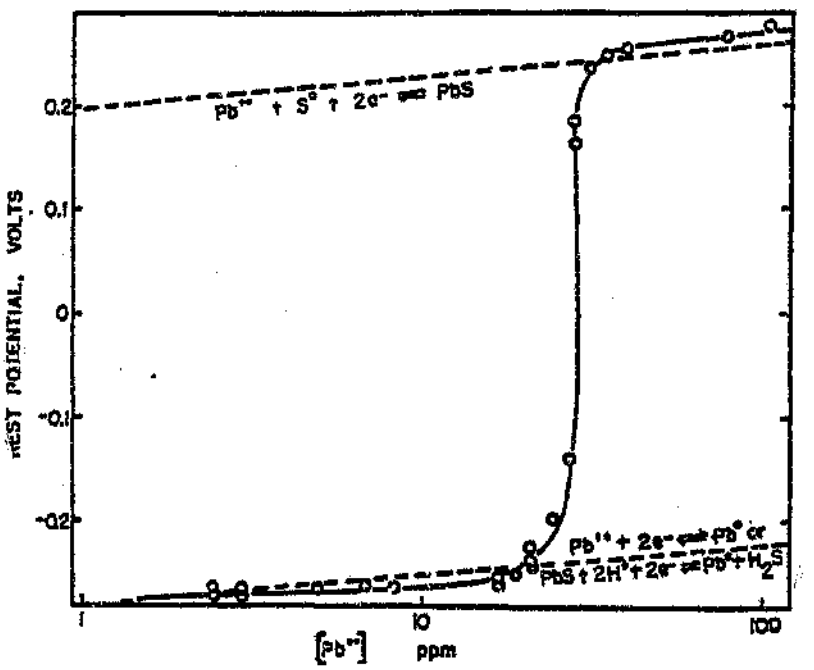


Figure 7.4 Rest potentials of PbS in $HClO_4$ solution. Peters (1976).

7.1.4 The dependence of galena dissolution rate on temperature.

Figure 7.5 illustrates the pronounced increase in the rate of galena dissolution associated with increases in temperature. The apparent activation energy for the dissolution of galena was observed to be 72 kJ.mol^{-1} at an electrode potential of 0.45 V vs SCE. This is illustrated in Figure 7.6. The magnitude of the activation energy further confirms that the dissolution of galena is an electrochemically controlled process. Johnson *et al.* (1978) observed an apparent activation energy of 52 kJ.mol^{-1} at an electrode potential of 0.38 V vs SCE.

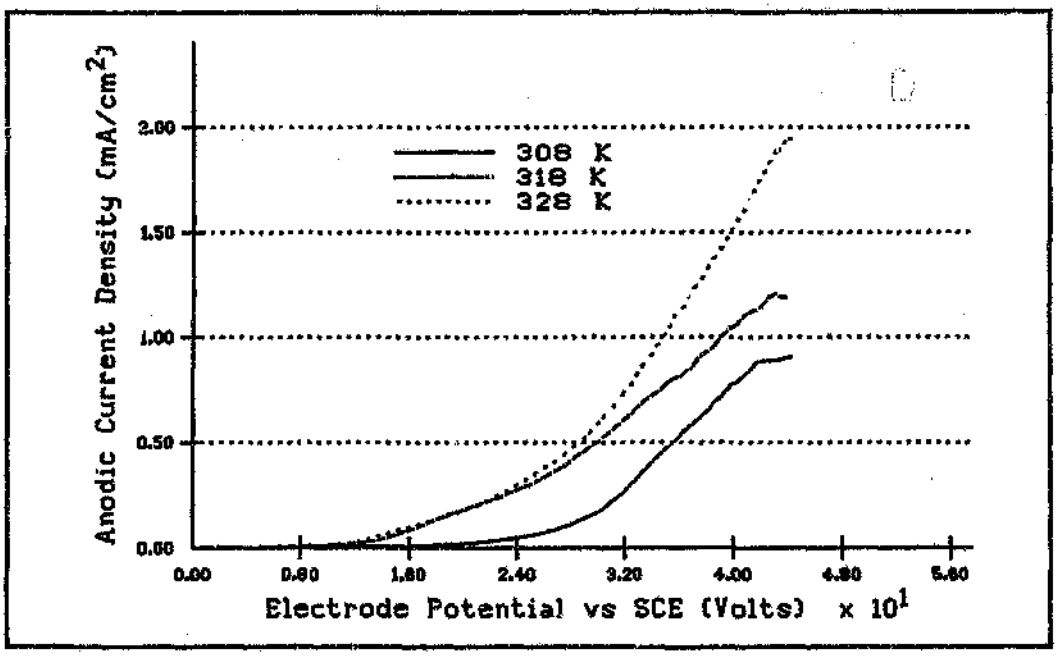


Figure 7.5 Polarisation curves illustrating the effect of temperature on galena dissolution rate. Conditions : 0.6M $NaNO_3$, 0.5M H^+, 1041rpm, scan rate 1mV/s.

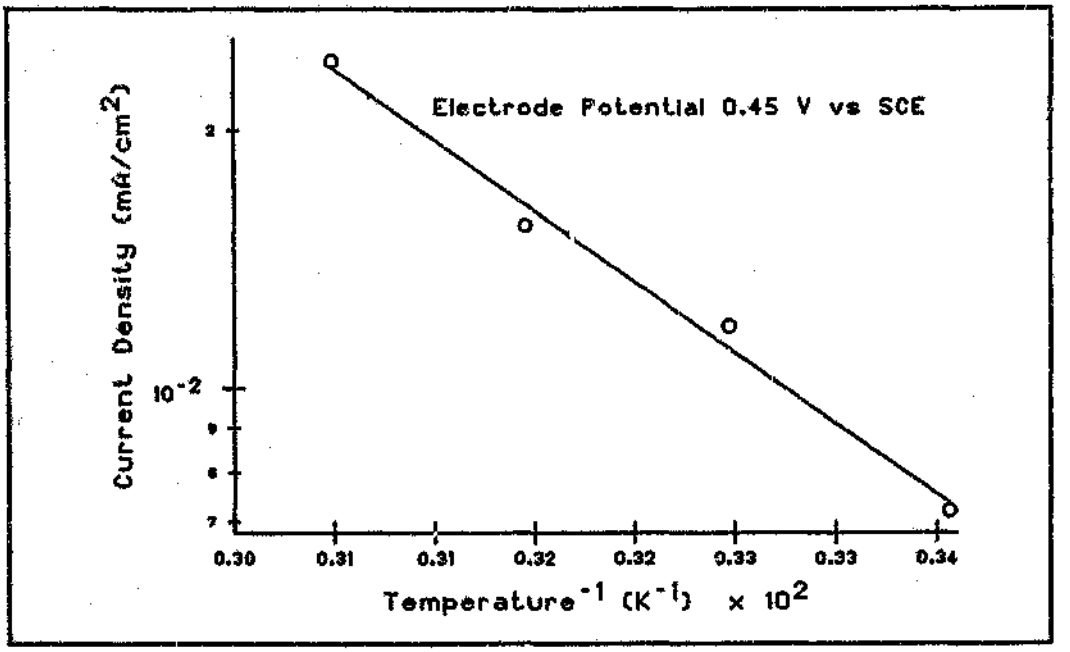


Figure 7.6 Determination of the activation energy for galena dissolution.
Conditions : 0.6M $NaNO_3$, 0.5M H^+, 1041rpm.

7.1.5 The dependence of galena dissolution rate on illumination.

Figure 7.7 illustrates the increase in galena dissolution associated with the illumination of the galena surface. The galena surface was illuminated by a UNOMAT LX500GS lightmeter. The non-illumination characterisation was achieved by covering the electrochemical cell with tin foil and hence minimising the amount of light reaching the galena electrode.

Koch (1975) observed that illumination would not be a limiting factor in the dissolution of n and p-type pyrite, n-type galena and n-type chalcopyrite. This is due to the small band gaps inherent in these minerals and a subsequent thermal transition of electrons from the valence band to conduction band is possible. The results obtained in this research contrast with the observations of Koch. This is probably due to the galena, characterised in this research, exhibiting a larger band gap. Koch (1975) observed the presence of limiting currents, under illumination, in greenockite, CdS, which has a band gap of 2.4 eV. The explanation of the effect of

illumination on galena dissolution is given in terms of the band structure theory of semiconductors. For a thorough description of semiconductor theory refer to Fraser (1977).

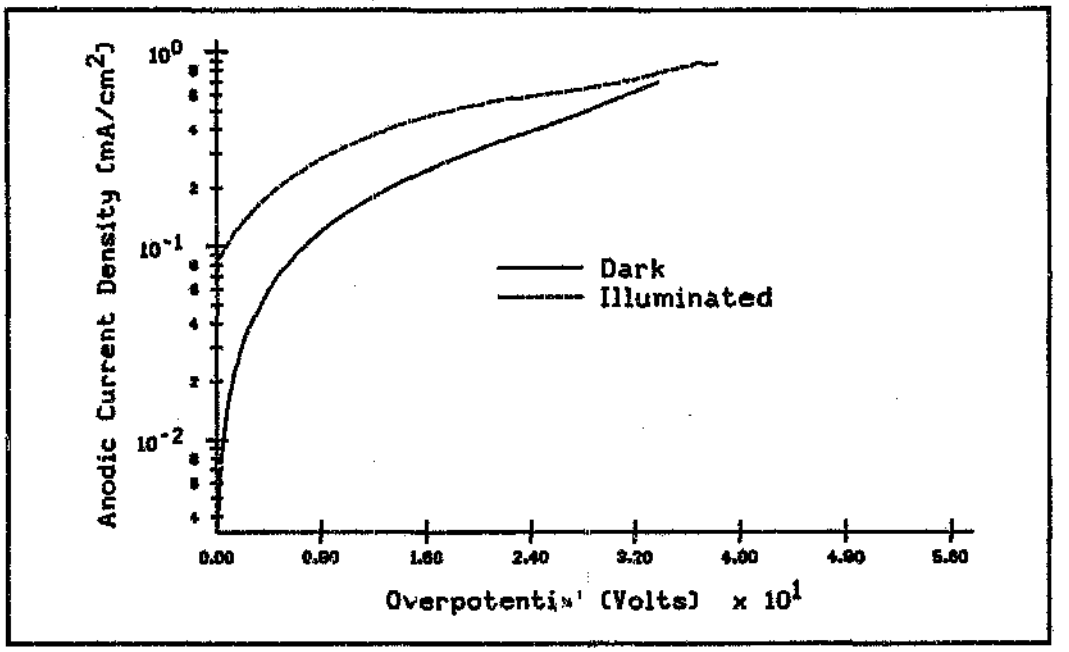


Figure 7.7 Tafel plot of the effect of illumination on the rate of galena dissolution. Conditions : 0.6M $NaNO_3$, 0.5M H^+, 1041rpm, 298K, scan rate 1mV/s.

Figure 7.8 illustrates the action of illumination on the dissolution of galena. Initially the electronic structure of the galena electrode consists of the valence band being associated with S^{2-} anions and the conduction band being associated with Pb^{2+} cations, Figure 7.8a. The conduction and valence bands are separated by a region known as the forbidden region or band gap in which no ionic species exist. The magnitude of the band gap determines whether a material is a conductor, semiconductor or insulator.

As the surface of galena is illuminated, by light of greater energy than the band gap, two electrons are excited from the valence band into the conduction band where they move into the external circuit, Figure 7.8b.

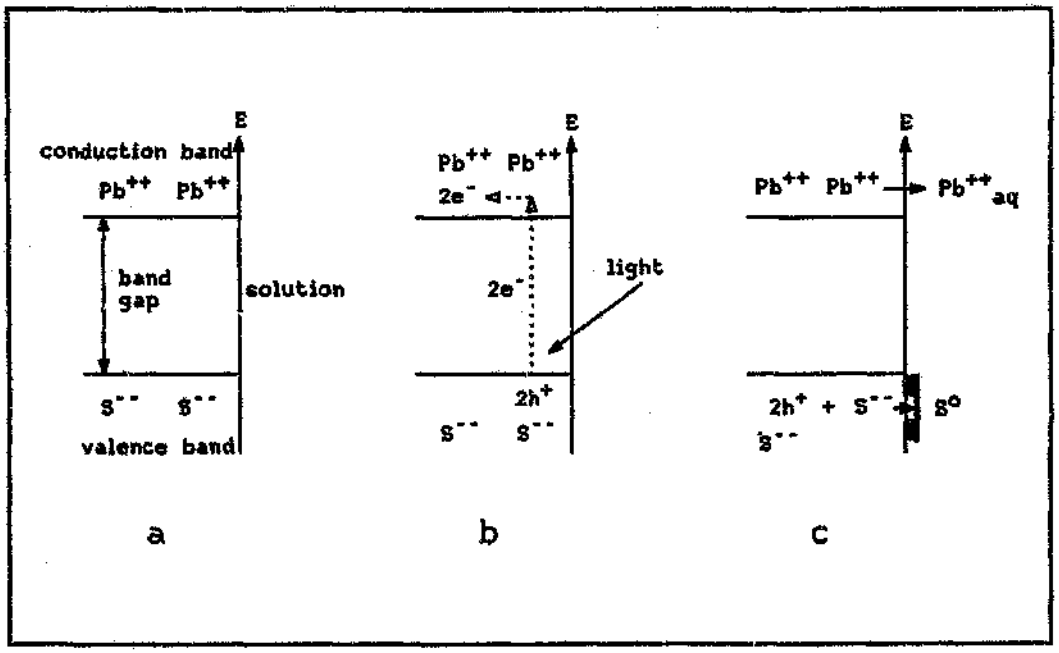


Figure 7.8 Stages in the dissolution of galena under illumination.

The two positive holes left in the valence band react with a sulphur anion to form sulphur on the surface of the electrode, Figure 7.8c.

$$S^{2-} + 2h^{+} \rightarrow S^{\circ} \qquad 7.1$$

At the same time a lead ion moves from the lattice structure into the solution.

$$Pb^{2+}_{lattice} \rightarrow Pb^{2+}_{aqueous} \qquad 7.2$$

7.2 Electrochemical Characterisation Of Ferric Reduction On Pyrite.

Similar effects as those observed for the reduction of ferric at a platinum electrode, Section 5.2, and a pyrite electrode, Section 6.1, were observed in this characterisation. The reaction rates are greater in this observation than those in Section 6.1 owing to the use of a different pyrite crystal.

7.2.1 Dependence of ferric reduction rate on concentration.

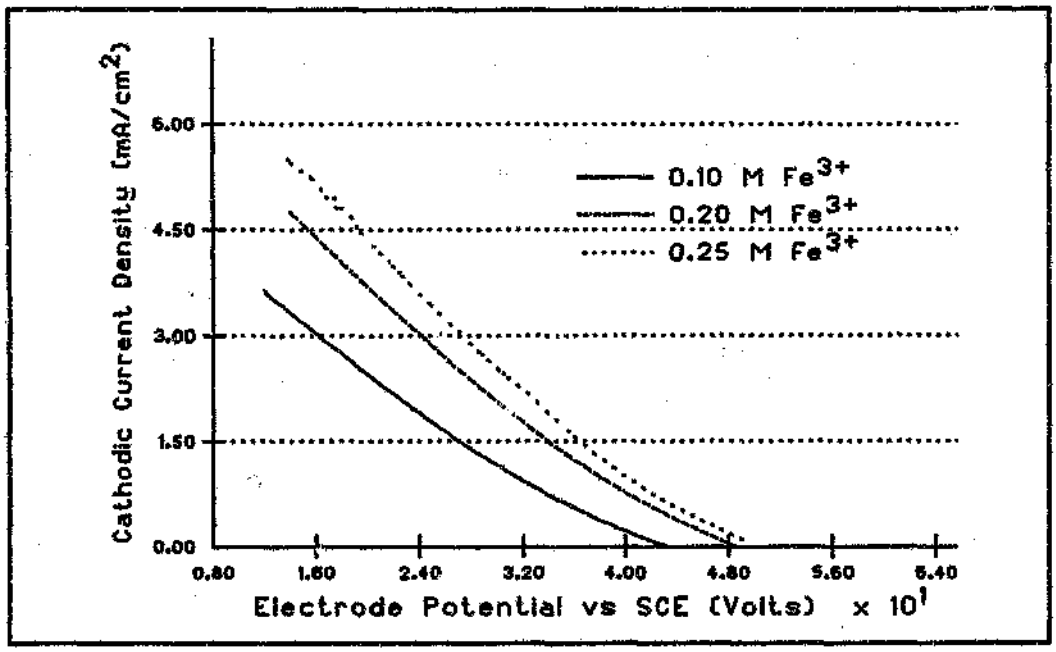


Figure 7.9 The effect of ferric concentration on the rate of ferric reduction on pyrite. Conditions : 0.5M H^+, 1041rpm, 298K, scan rate 1mV/s.

It was observed that the rate of ferric reduction increased as the concentration of ferric was increased. This is illustrated in Figure 7.9. Figure 7.10 illustrates the decrease in the diffusion coefficient, for ferric reduction on pyrite, associated with increases in ferric concentration. The Levich expression and Equation 1.16 were used to determine the diffusion coefficient for ferric reduction on pyrite. A diffusion film thickness of $1x10^{-4}$ m and a kinematic viscosity of $1.24x10^{-6}$ $m^2.s^{-1}$ yields a diffusion coefficient of $5.18x10^{-6}$ $cm^2.s^{-1}$. The diffusion coefficient corresponds well with the diffusion coefficient for the reduction of ferric ions on a platinum electrode.

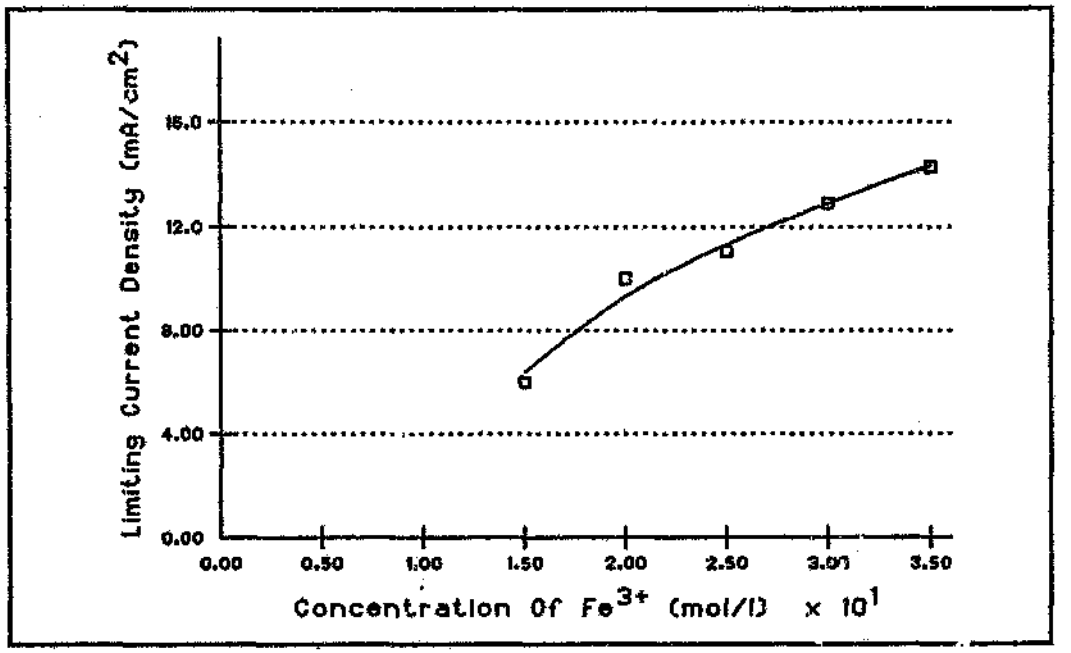


Figure 7.10 Determination of the diffusion coefficient for ferric reduction on pyrite. Conditions : 0.5M H^+, 1041rpm, 298K.

7.2.2 Dependence of ferric reduction rate on electrode rotation.

As the electrode rotation rate is increased the rate of ferric reduction on pyrite, at low electrode potentials, is increased. At high electrode potentials, near the rest potential of the ferric reduction reaction, the rotation rate has no effect on reaction rate since the reaction is electrochemically controlled. At lower electrode potentials, around 0.20 V vs SCE, the effect of rotation becomes more apparent. This is illustrated in Figure 7.11.

7.2.3 Dependence of ferric reduction rate on temperature.

The effect of temperature on the rate of ferric reduction is illustrated in Figure 7.12. The ferric reduction rate increases as the temperature is increased. In addition Figure 7.12 illustrates the increase in rest potential which is associated with increases in temperature. The effect of temperature on the rate of ferric reduction on pyrite observed in Section 6.1.3 was not observed with this pyrite sample.

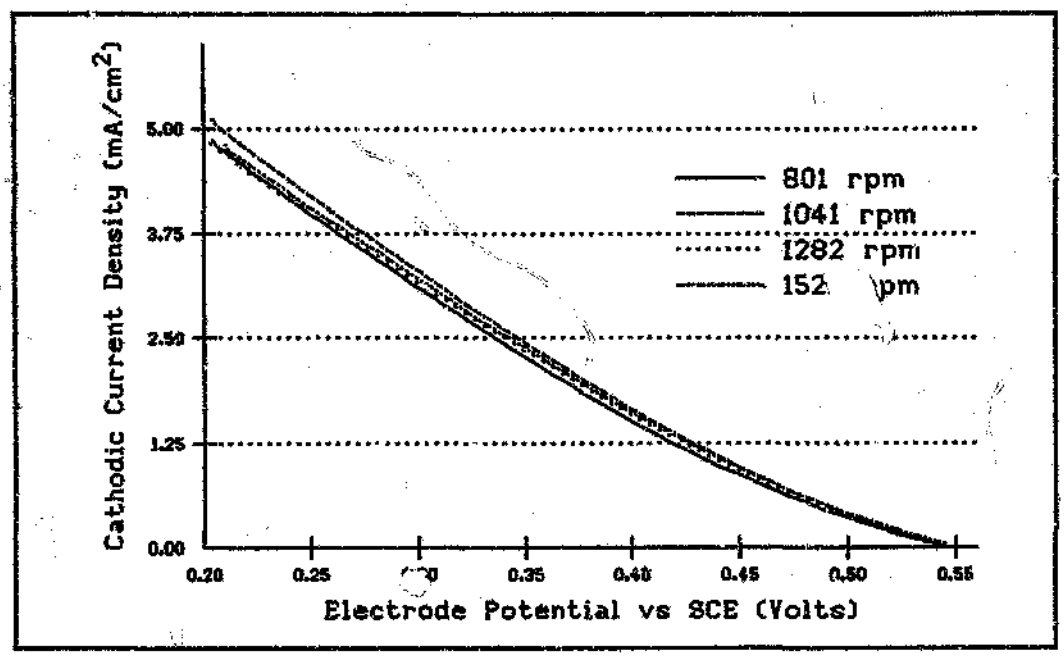


Figure 7.11 The effect of rotation on the rate of ferric reduction on pyrite.
Conditions : 0.2M Fe^{3+}, 0.5M H^+, 298K, scan rate 1mV/s.

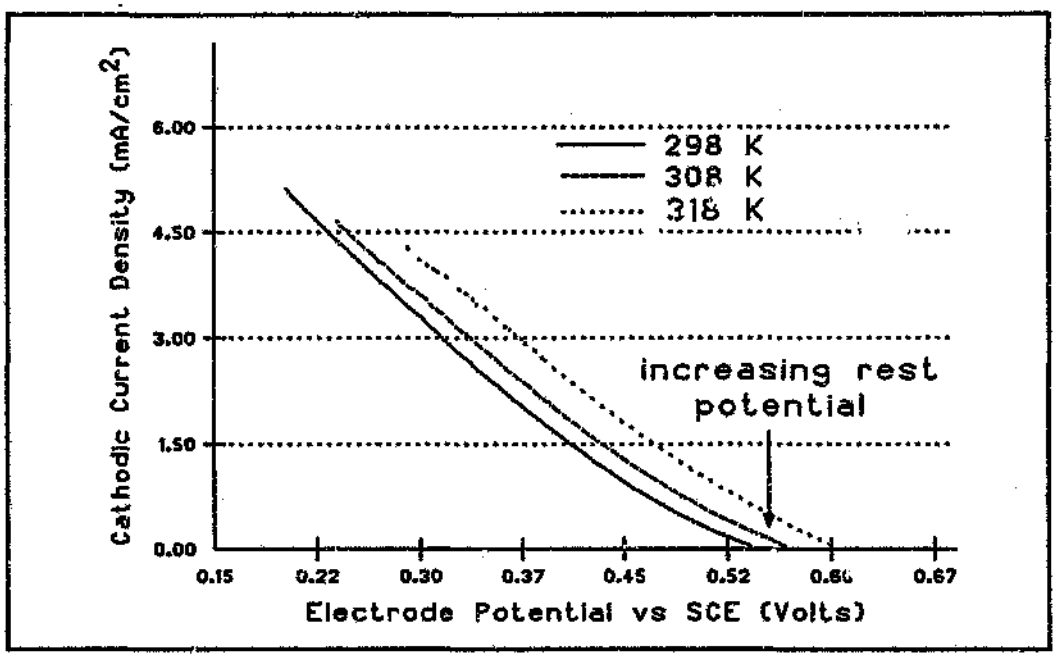


Figure 7.12 The effect of temperature on the rate of ferric reduction on pyrite.
Conditions : 0.2M Fe^{3+}, 0.5M H^+, 1041rpm, scan rate 1mV/s.

7.3 Electrochemical Characterisation Of The Galvanic Couple Formed Between Galena And Pyrite.

The galvanic potential occurs at ele . potentials of 0.30 V vs SCE. The only significant reactions in the couple are therefore the anodic dissolution of galena and the reduction of ferric ions on galena and pyrite. If a larger pyrite electrode or a more noble cathode is used the oxidation of the sulphur film and the passivation of the galena surface may become important reactions in the action of the galvanic couple.

7.3.1 Dependence of galvanic interaction on ferric concentration.

The values listed in Table 7.2 indicate that the galvanic current flowing through the galena-pyrite couple increases with increases in ferric concentration at various cell voltages.

Table 7.2 The effect of ferric concentration on the galvanic interaction between galena and pyrite. Conditions : 0.5 M H^+, 1041 rpm, 298 K, current in mA.

$[Fe^{3+}]$	0.00V	- 0.05V	- 0.10V	- 0.15V	- 0.20V
0.20M	2.41	2.07	1.76	1.30	0.74
0.25M	2.73	2.40	1.92	1.43	0.88
0.35M	3.27	2.71	2.17	1.67	1.19

The increase in galvanic current due to increases in ferric concentrations are mainly due to the associated increase in the ferric reduction rate on pyrite. An increase in ferric concentration from 0.2 M to 0.35 M increases the galvanic current by a factor of 1.35.

7.3.2 Dependence of galvanic interaction on rotation rate.

Figure 7.13 illustrates the effect of rotation rate on galvanic current. At low cell voltages, which correspond to high cathodic overpotentials, the galvanic current is increased by a factor of 1.34 as the rotation rate is increased from 1282 rpm to 1763 rpm.

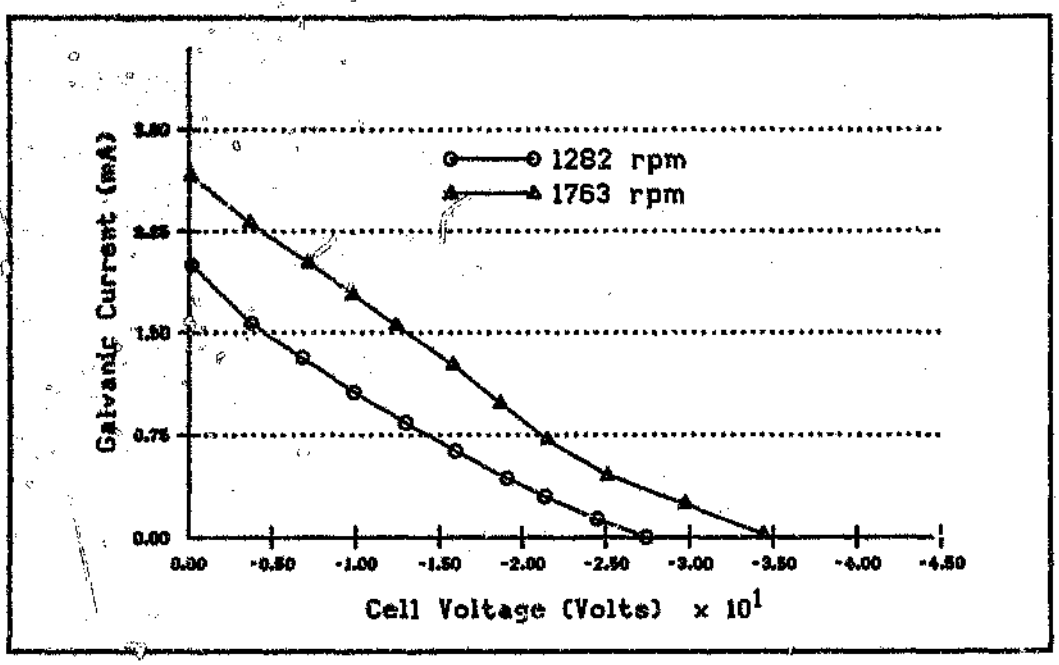


Figure 7.13 The effect of rotation on galvanic current in the galena-pyrite cell. Conditions : 0.2M Fe^{3+}, 0.5M H^+, 298K.

At high cell voltages, which correspond to electrode potentials near the rest potential, the effect of rotation becomes less pronounced. However, one would expect this effect to disappear at high cell voltages since the reactions occurring in the galvanic couple are both electrochemically controlled.

7.3.3 Dependence of galvanic interaction on temperature.

The values given in Table 7.3 indicate that the galvanic current doubles, at zero cell voltage, for an increase in temperature of 30 K. At a cell voltage of -0.05 V the galvanic current increases by a factor of 1.5. The temperature effect is so pronounced in the galvanic couple because both the anodic and cathodic half reaction rates are strongly influenced by temperature increases.

Table 7.3 The effect of temperature on the magnitude of galvanic interaction in the galena-pyrite cell. Conditions : 0.2M Fe^{3+}, 0.5M H^{+}, 1041 rpm, current in mA.

Temperature	0.00 V	- 0.05 V
298 K	2.41	2.07
318 K	3.63	2.57
328 K	4.74	3.13

7.3.4 Dependence of galvanic interaction on illumination.

Illuminating the galena pyrite couple increases the galvanic current flowing through the couple as illustrated in Figure 7.14. The illumination effect is known to effect the dissolution rate of galena, refer to Section 7.1.5. Mishra and Osseo-Asare (1987) note that illumination increases the anodic dissolution rate of n-type pyrite. Due to the semiconducting characteristics of pyrite it may be possible that illumination influences the rate at which ferric ions are reduced on pyrite.

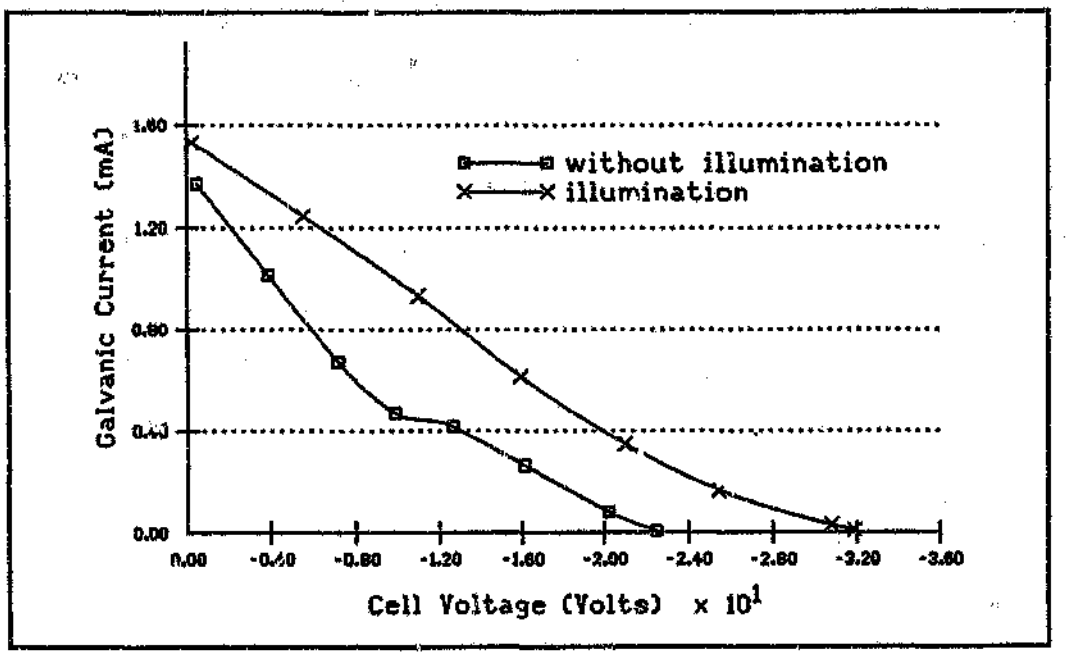


Figure 7.14 The effect of illumination on the galvanic interaction between galena and pyrite. Conditions : 0.2M Fe^{3+}, 0.5M H^{+}, 1041rpm, 298K.

7.4 Mathematical Modelling Of The Galena-Pyrite Couple.

Table 7.4 contains the parameters which were used in the model equation. The kinetic parameters for the anodic dissolution of galena and reduction of ferric ions on pyrite were determined using Equations 3.4 and 3.10 respectively.

Table 7.4 Kinetic parameters used in the galvanic model equation for the galena-pyrite cell. Conditions : 0.2 M Fe^{3+}, 0.5 M H^{+}, 1041 rpm, 308 K.

Parameters	Anodic	Cathodic
E_o (V)	0.25	0.57
i_o ($A.m^{-2}$)	2.0	16
α	0.81	0.17
i_l ($A.m^{-2}$)	-	97

It was observed that the accuracy of the galvanic model prediction is strongly dependent on the accurate experimental measurement of the anodic and cathodic rest potentials as well as the accurate determination of the anodic and cathodic kinetic parameters. The measured and model galvanic currents are illustrated in Figure 7.15. A very good correspondence exists between the experimentally measured galvanic currents and those predicted by the galvanic model equation.

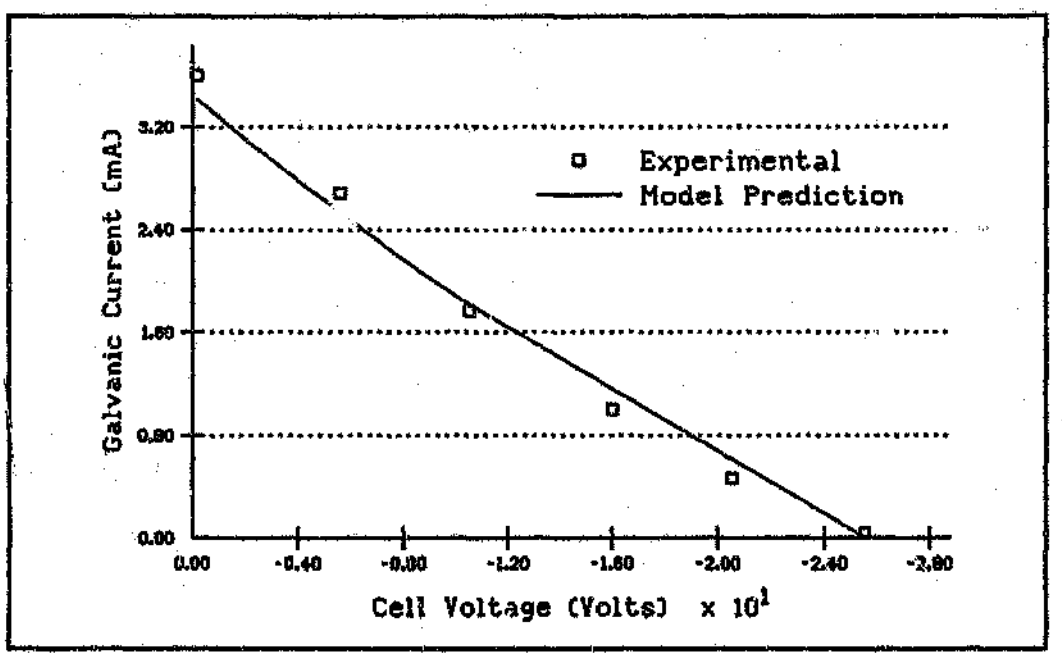


Figure 7.15 Model prediction of galvanic current in the galena-pyrite couple. Conditions : 0.2M Fe^{3+}, 0.5M H^{+}, 1041rpm, 308K.

8. DYNAMIC ASPECTS OF GALVANIC INTERACTION.

Various model equations, which account for dynamic behaviour in galvanic couples due to variations in electrode area and solution composition, are presented in this section. The results presented in Figure 8.1 verify the existence of dynamic behaviour.

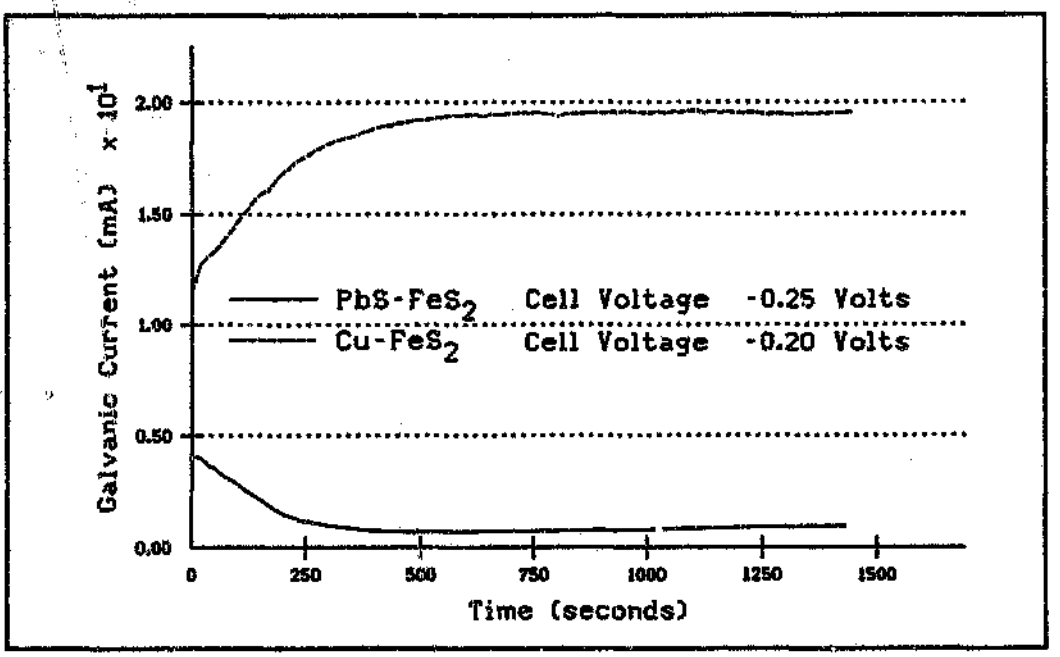


Figure 8.1 Dynamic behaviour of the copper-pyrite and galena-pyrite couples. Conditions : 0.2M Fe^{3+}, 0.5M H^{+}, 1041rpm, 298K.

It is evident that galvanic current may increase or decrease over time. The galvanic model used through Chapters 5 to 7 is a steady-state model. However certain parameters contained within the galvanic model can be expressed as dynamic functions and these are discussed in Sections 8.1 and 8.2. It is assumed that charging and discharging of the electrical double layer occurs instantaneously and therefore exerts no dynamic influence on galvanic current. The expressions presented in this chapter are derived in full in Appendix C.

8.1 Dependence Of Galvanic Interaction On Electrode Area.

The use of rotating ring disc electrodes in this research ensured that anodic and cathodic areas remained constant during electrochemical characterisation. The amount of galvanic current, and therefore reaction rate, is dependent on available surface area. Electrode surface areas may decrease due to dissolution or increase due to solid film formation.

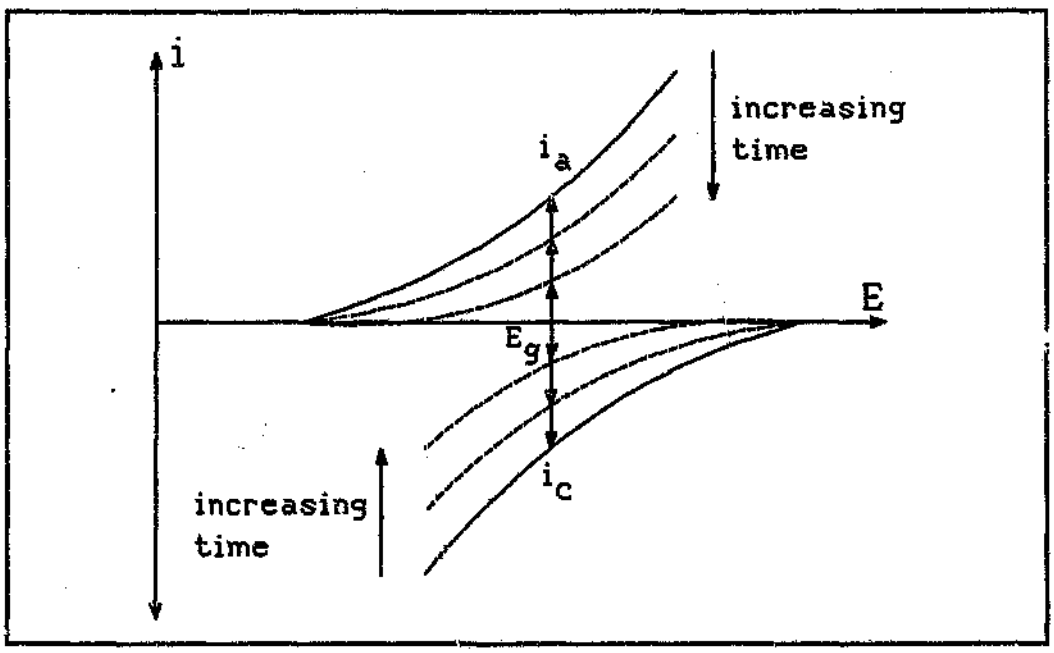


Figure 8.2 The effect of electrode areas on galvanic interaction.

Figure 8.2 illustrates the decrease in galvanic current, at the galvanic potential, due to decreases in the anodic and cathodic surface areas. Decreases in the anode and cathode surfaces areas may arise during dissolution of the anode and cathode. As the areas of the anode and cathode decrease the amount of galvanic current which can pass through the electrodes decreases accordingly.

It has been established that there are two contributors to dynamic behaviour in galvanic couples, namely variations in electrode areas and variations in solution

composition, see Section 8.2. The ionic species formed during dissolution result in variations in solution composition. To determine the sole effect of electrode area on dynamic behaviour the galvanic couple should be characterised in a large vessel where solution composition variations, due to dissolution processes, will be minimised.

The magnitude of the variation in electrode area is dependent on the rate controlling process of the galvanic couple. Three general mechanisms which are known to control dissolution rates in sulphide mineral systems are considered. The galvanic couple is assumed to consist of an anodic cone encapsulated by a large cathodic sphere. Shrinking particle theory, comprehensively covered by Levenspiel (1972), is used to describe the radius of the anodic cone over time.

Case 1 : The anodic and cathodic reactions are electrochemically controlled in the vicinity of the galvanic potential. It is assumed that the shrinking anode results in no appreciable increase in cathodic surface area. Only anodic processes occur on the anode and cathodic processes on the cathode. The relationship between the radius of the anodic cone and time is given by Equation 8.1.

$$r = R_o\left[1 - \frac{bkC^{a'}t}{H_o}\right] \qquad 8.1$$

The hypothetical decay in galvanic current in the galena-pyrite couple is illustrated in Figure 8.3. Equation 8.1 is substituted into the galvanic model and the galvanic current determined at certain time intervals. The kinetic parameters and rest potentials, determined in Chapter 7, for the dissolution of galena and ferric reduction on pyrite were substituted into the galvanic model. Under these assumed conditions the galvanic current decays slowly over time.

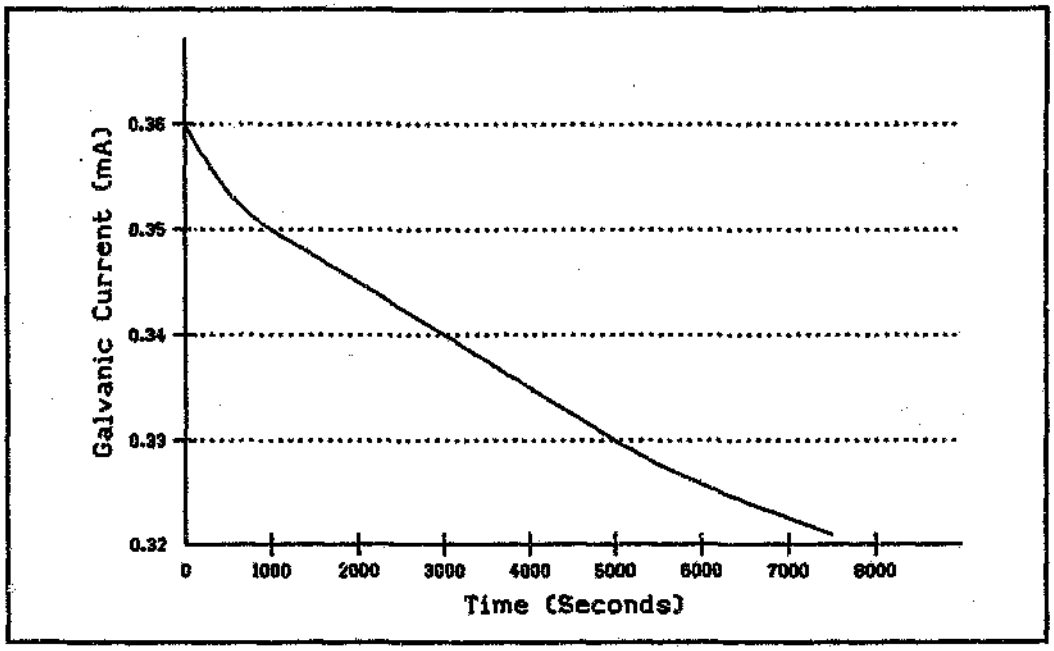


Figure 8.3 Galvanic current decay due to shrinking galena anode. Conditions : R_o = 1mm, H_o = 5mm, k = $1x10^{-6}$, b = 1, 0.2M Fe^{3+}.

Case 2 : Diffusion through a sulphur or oxide film on the anode controls the reaction rate. During sulphide mineral dissolution a film of sulphur may grow on the electrode surface or a passive oxide film may form on the electrode surface as a result of the hydrolysis of ionic species. The films may become large enough to cause the diffusion of metal ions, from the mineral dissolution, through the films to become the rate controlling process. It is assumed that only anodic processes occur on the anode and cathodic processes occur on the cathode. It is further assumed that film growth occurs at a rate which results in no variation in the original cone dimensions. The variation in cone radius with time is given by Equation 8.2.

$$\frac{3r^2}{R_0^2} - \frac{2r^3}{R_0^3} = 1 + \frac{6M_{MeS}D_{Me^{2+}}C^a_{Me^{2+}}t}{b\rho_{MeS}H_0R_0} \qquad 8.2$$

The resulting equation is nonlinear and the roots can be determined by a cubic determinant.

Case 3 : In many mineral systems the reduction of oxygen on cathodic sites controls the rate of dissolution. This is due to the slow rate of diffusion, of dissolved oxygen, to electrode surfaces. It is assumed that only anodic processes occur on the anode and cathodic processes occur on the cathode. It is further assumed that the concentration of oxygen in the bulk phase is constant. The relationship between the cone radius and time is given by Equation 8.3

$$r = \left[R_0^3 + \frac{M_{MeS} R_0 A_c D C_{b,O_2} t}{\rho_{MeS} H_0 \pi \delta} \right] \qquad 8.3$$

8.2 Dependence Of Galvanic Interaction On Solution Composition.

Solution composition is an important factor in determining the magnitude of galvanic interaction. Firstly it determines the magnitudes of the anodic and cathodic equilibrium or rest potentials. Secondly the kinetics of the anodic and cathodic reactions are influenced by solution composition.

The model, Equation 8.4, is based on the decay of the galvanic current due to the decrease in the cathodic equilibrium potential. The model was derived due to the observation of the decay in solution potential over time which was measured by using an independent platinum electrode. The decay in solution potential is illustrated in Figure 8.4.

Figure 8.4 illustrates that a decrease in solution potential is associated with the copper-platinum and copper-pyrite couples studied whilst the solution potential remains relatively constant in the galena-pyrite couple. The value of the solution potential, 0.62 V, in the galena-pyrite couple is greater than the solution potentials of the copper-platinum and copper-pyrite couples. This can probably be attributed to the galena-pyrite couple being characterised in nitrate solutions as opposed to sulphate solutions. The stronger decay in the copper-platinum and copper-pyrite couples can be attributed to the position of the galvanic potential. In these two

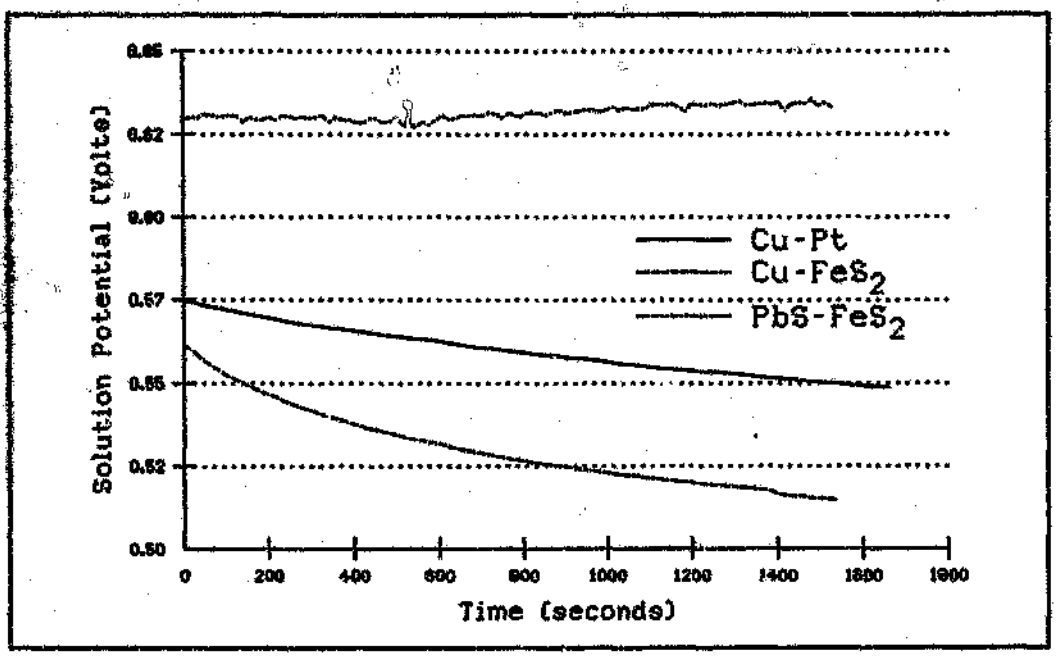


Figure 8.4 Variation in solution potential with time. Conditions : 0.2M Fe^{3+}, 0.5M H^{+}, 1041rpm, 298K.

couples the galvanic potential occurs at high cathodic overpotentials and subsequently high rates of ferric reduction occur. The variation in the ferric-ferrous ratio results in a decrease in solution potential and hence galvanic current.

For this reason a model was developed which accounts for the decay in cathodic equilibrium potential over time. Figure 8.5 graphically depicts the decay in galvanic current, through points 1 to 3, due to variations in the ferric-ferrous ratio which causes a decrease in cathodic equilibrium potential.

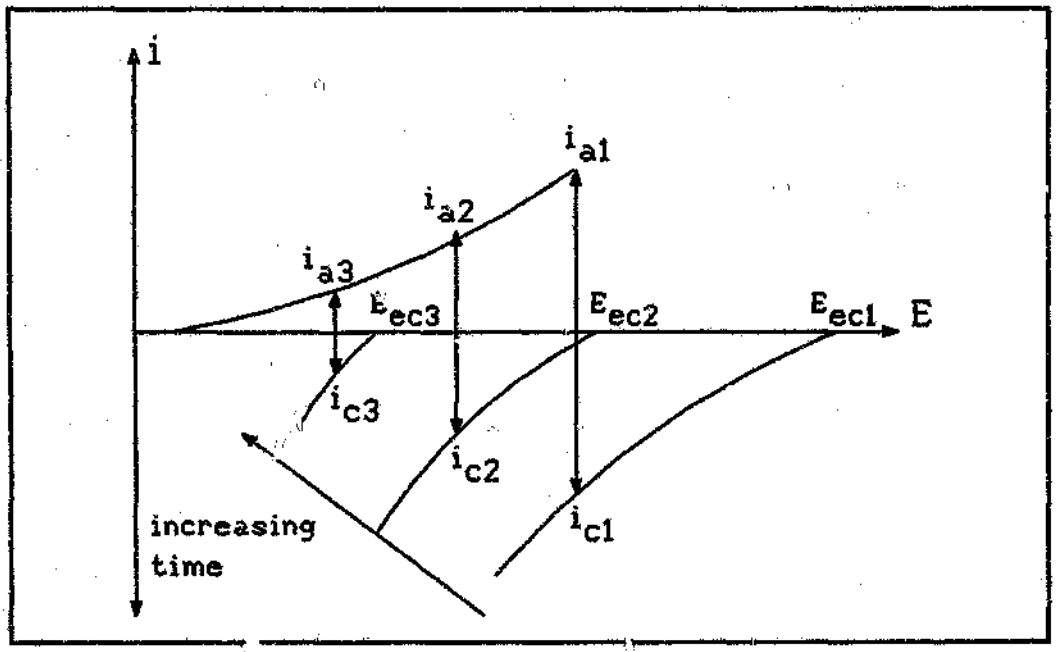


Figure 8.5 Decay in galvanic current due to decay in cathodic equilibrium potential.

The model, Equation 8.4, is based on the assumptions that no variations in the anodic equilibrium potential occur, no variations in kinetic parameters occur and no voltage drop exists across the electrodes.

$$\frac{dE_{e,c}}{dt} = Z\left[\frac{\left[A_c i_{l,c}\left(1-\exp\left(y_1(E-E_{e,c})\right)\right)\left(1+\exp\left(y_2(E_{e,c}-E^{\circ}_{e,c})\right)\right)^2\right]}{\exp\left(y_2(E_{e,c}-E^{\circ}_{e,c})\right)\left[1+\frac{i_{l,c}}{i_{o,c}}\exp\left(y_1(E-E_{e,c})\right)\right]}\right] \qquad 8.4$$

where:

$$Z = \frac{RT}{VF^2 C_{Fe^{3+}}} \qquad 8.5$$

$$Y_1 = \frac{\alpha_a F}{RT} \qquad 8.6$$

$$Y_2 = \frac{F}{RT} \qquad 8.7$$

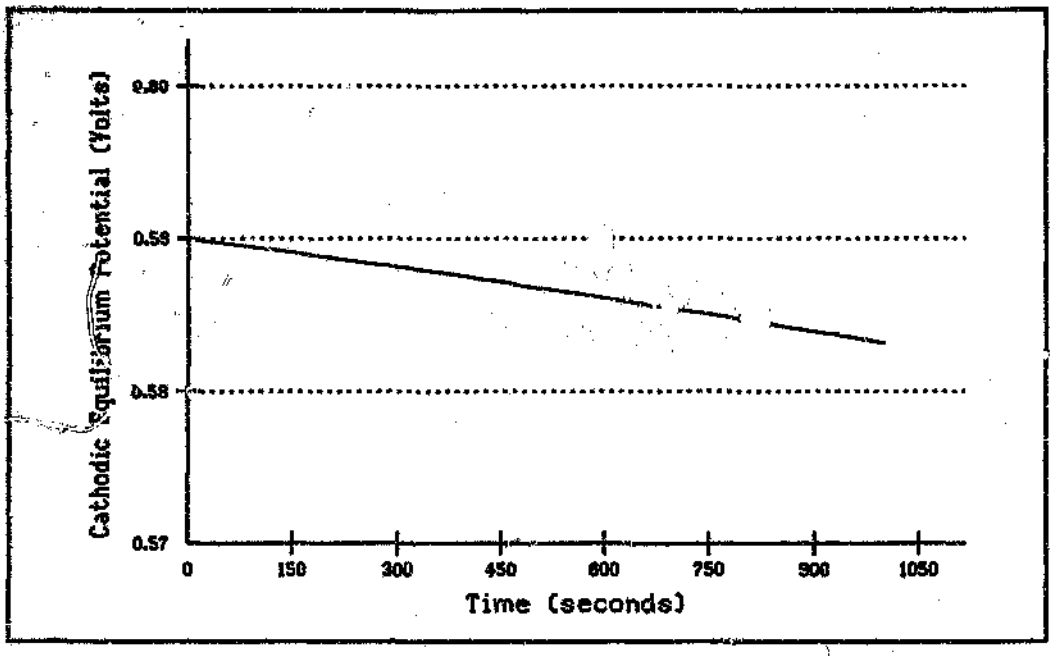


Figure 8.6 Model prediction of the cathodic equilibrium potential decay in the copper-platinum cell. Conditions : 0.2M Fe^{3+}, 0.5M H^+, 1041rpm, 298K.

Model Equation 8.4 is solved using a fourth order Runge Kutta technique, ref. Appendix B. The model solution for the copper-platinum couple is illustrated in Figure 8.6. The model predicts a small decay in cathodic equilibrium potential over time which suggests that the ferric-ferrous ratio does not contribute greatly to the solution potential decay. The model therefore requires further development to account for variations in the anodic equilibrium potential and kinetic parameters.

9. CONCLUSIONS AND RECOMMENDATIONS.

A review of the literature revealed that galvanic interactions between sulphide minerals are generally described qualitatively. The magnitude of the galvanic interaction is generally related to the difference between the cathodic and anodic equilibrium potentials (refer to Chapter 1). This is an approximation since the kinetic parameters of the anodic and cathodic reactions are an important criterion in determining magnitudes of galvanic interaction. Descriptions of galvanic interaction which have included kinetic parameters are specific to a certain couple and/or have not been experimentally verified. The aims of this research were therefore to provide a general mathematical basis for describing galvanic interaction based on thermodynamic and kinetic parameters. In addition experimental verification of the validity of the mathematical model was required.

A voltage balance over a galvanic couple provides an excellent basis for describing galvanic interaction quantitatively. (Refer to Section 3.1). The voltage balance accounts for the cell emf, kinetic aspects of the anodic and cathodic half reactions, voltage characteristics of the electrode-electrode contact and the voltage across the solution. The cell emf can be determined by experimentally measuring the anodic and cathodic equilibrium potentials. The kinetic characteristics of the anodic and cathodic half reactions were determined by utilising the three-electrode cell, Section 4.2.2, and pseudo-steady-state potentiostatic measurements. The kinetic parameters associated with each half reaction were determined by regressing the polarisation data with the Butler-Volmer equation or the combined Butler-Volmer and diffusion equation. The use of a potentiostat, during the studies of the galvanic couples, allowed a ready study of the effect of mineral-mineral contact on galvanic interaction. The overall galvanic model equation was readily solved using a Regula-Falsi iteration technique.

Three galvanic couples, constructed as rotating ring disc electrodes (refer to Section 4.2.1), were characterised in acidic ferric sulphate or ferric nitrate solutions. The copper-platinum couple, whose chemistry is simpler than that of sulphide minerals,

was studied initially to determine the validity of the model. The copper dissolution reaction is found to be an electrochemically controlled reaction whilst the reduction of ferric ions on a platinum cathode is found to be controlled by electrochemical and mass transfer processes. The kinetic parameters obtained for both reactions are in excellent agreement with those of other researchers. The model prediction of galvanic current correlates well with the experimentally measured galvanic currents. (Refer to Chapter 5).

The copper-pyrite couple consisted of a metallic conductor, copper, and a n-type conductor, pyrite. The reduction of ferric ions on the pyrite cathode was observed to be controlled by electrochemical and mass transfer processes. At temperatures less than 318 K the reduction reaction appears to be controlled by electrochemical mechanisms, as suggested by the activation energy of 46 $kJ.mol^{-1}$, whilst at higher temperatures, at the same electrode potential, the activation energy of 3.8 $kJ.mol^{-1}$ suggests the reaction is controlled by a mass transfer mechanism. (Refer to Section 6.1.3). Further verification of this observation is recommended. The model and experimental galvanic currents are in good correspondence. The strength of this correspondence is strongly dependent on the accurate measurement of anodic and cathodic rest potentials and kinetic parameters.

The galena-pyrite couple consisted of two n-type conductors. The kinetic parameters obtained during the study of the anodic dissolution of galena are in excellent agreement with those obtained by other researchers. Illumination of the galena-pyrite electrode surface resulted in an increase in galvanic current. (Refer to Section 7.1.5). The effect is due to the excitation of electrons from the valence band to the conduction band in n-type galena. From this observation it is concluded that the semiconducting characteristics of sulphide minerals strongly influence the magnitude of galvanic interaction. There is a very good correspondence between the experimentally measured galvanic currents and those predicted by the galvanic model equation. (Refer to Section 7.4).

Galvanic interaction is observed to exhibit dynamic behaviour. (Refer to Chapter 8). A solid basis has been developed for the mathematical description of dynamic behaviour due to variations in electrode area and solution composition. The proposed dynamic models can be readily incorporated into the galvanic model equation. Further development and experimental verification of the dynamic expressions is recommended.

10. REFERENCES.

Angell, D.H., and Dickinson, T. (1972) '*The kinetics of the ferrous/ferric and ferro/ferricyanide reactions at platinum and gold electrodes. Part I. Kinetics at bare-metal surfaces.*', J. Electroanal. Chem., 35, pp. 55-72.

Atkins, P.W. (1986) '*Physical Chemistry*', 3rd Edition, Oxford University Press.

Attia, Y.A., and El-Zeky, M. (1988) '*Extraction of precious metals from refractory complex sulphides by bioleaching : Effects of galvanic interaction of sulphides*', Precious and Rare Metal Technologies, Proceedings of a Symposium on Precious and Rare Metals, A.E. Torma and I.H. Gundiler (Ed.), pp 241-254.

Bard, A,J., and Faulkner, L.R. (1980) '*Electrochemical Methods : Fundamentals And Applications*', John Wiley and Sons.

Berry, V.K., Murr, L.E., and Hiskey, J.B. (1978) '*Galvanic interaction between chalcopyrite and pyrite during bacterial leaching of low-grade waste*', Hydrometallurgy, 3, pp. 309-326.

Bertocci, U., and Turner, D.R. (1974) '*Copper*', In: Encyclopedia of Electrochemistry of the Elements Vol II., Allen J. Bard (Ed.), Marcel Dekker INC, New York, pp. 383-497.

Bochmann, H.G., and Vielstich, W. (1988) '*On the reaction rate of the Fe^{2+}/Fe^{3+} redox couple in sulfate solution*', Electrochimica Acta, vol. 33, no. 6, pp. 805-809.

Bockris, J., and Reddy, A.K.N. (1970) '*Modern Electrochemistry*', vol. 2, John Wiley and Sons, New York.

Crundwell, F.K. (1988) '*The influence of the electronic structure of solids on the*

anodic dissolution and leaching of semiconducting sulphide minerals', Hydrometallurgy, 21, pp. 155-190.

Davis, G.O., Kolts, J., and Sridhar, N. (1968) '*Polarisation effects in galvanic corroston*', Corrosion, vol 42, no. 6, pp. 329-336.

Dutrizac, J.F., Macdonald, R.J.C., and Ingraham, T.R. (1971) '*Effect of pyrite, chalcopyrite and digenite on rate of bornite dissolution in acidic ferric sulphate solutions*', Canadian Metallurgical Quarterly, 10, pp. 3-7.

Dutrizac, J.E., and MacDonald, R.J.C. (1973) '*The effect of some impurities on the rate of chalcopyrite dissolution*', Canadian Metallurgical Quarterly, vol. 12, no. 4, pp. 409-420.

Eadington, P., and Prosser, A.P. (1969) '*Oxidation of lead sulphide in aqueous suspensions*', Trans. Instn. Min. Metall., vol. 78, pp. C74-C82.

Fangteng, S., and Charles, E. (1988) '*A theoretical approach to galvanic corrosion, allowing for cathode dissolution* ', Corrosion Science., vol. 28, no. 7, pp. 649-655.

Fraser, D.A. (1977) '*The physics of semiconductor devices*' Clarendon Press, Oxford.

Hepel, T. (1984) '*Electrochemistry of selective and competitive leaching of metals from sulphide concentrates*', Proc. Int. Symp. on Electrochem. in Min. and Metal Processing, P.E. Richardson (Ed), Electrochem. Soc., Pennington, pp 362-373.

Hepel, T., Hepel,M., and Pomianowski,A. (1984) '*Effect of galvanic local cells on the oxidative leaching of metal sulphides*', Proc. Int. Symp. on Electrochem. in Min. and Metal Processing, P.E. Richardson (Ed), Electrochem. Soc., Pennington, pp. 432-446.

Hiskey, J.B., and Wadsworth, M.E. (1975) '*Galvanic conversion of chalcopyrite*', Metallurgical Transactions B, vol 6B, pp. 183-190.

Johnson, J.W., Chang, J., Narasagoudar, R.A., and O'Keefe, T.J. (1978) '*Anodic dissolution of galena concentrate in perchloric acid*', J. App. Electrochem., vol. 8, pp. 25-32.

Jones, D.A. (1968) '*Monitoring galvanic short-circuit current*', Electrochem Technol., vol. 6, pp. 241-245.

Jones, D.A. (1984) '*Polarisation studies of brass-steel galvanic couples*', Corrosion, vol. 40, no. 4, pp. 181-185.

Koch, D.F.A. (1975) '*Electrochemistry of sulphide minerals*', In: Modern aspects of electrochemistry, J. O'M Bockris and B.E. Conway (Eds), vol. 10, Plenum Press, New York, pp. 211-237.

Levenspiel, O. (1972) '*Chemical Reaction Engineering*', 2nd Edition, John Wiley and Sons, New York.

Lee, H.P., Nobe, K., and Pearlstein, A.J. (1985) '*Film formation and current oscillations in the electrodissolution of Cu in acidic chloride media. I. Experimental studies*', J. Electrochem. Soc, vol. 132, no. 5, pp 1031-1037.

Levich, V. (1962) '*Physiochemical Hydrodynamics*', In: Int. Series on Phys. and Chem. Eng. Sciences, N. Amundson (Ed), Prentice Hall.

Li, J., Zhong, T.K., and Wadsworth, M.E. (1992) '*Application of mixed potential theory in hydrometallurgy*', In: Hydrometallurgy Theory and Practice., Proceedings of the Ernest Peters Int. Symp., W.C. Cooper and D.B. Dreisinger (Ed), Hydrometallurgy, 29, pp. 47-60.

Lorenzen, L., and van Deventer, J.S.J. (1992) '*Electrochemical interactions between gold and its associated minerals during cyanidation*', In: Hydrometallurgy Theory and Practice., Proceedings of the Ernest Peters Int. Symp., W.C. Cooper and D.B. Dreisinger (Ed), Hydrometallurgy, 30, pp. 177-194.

Madsen, B. (1981) '*Determination of ferric ion diffusion and activity coefficients from chronopotentiometric data*', Bureau Of Mines, PGH, P.A. 25801, 21pp.

Majima. H., and Peters, E. (1968) '*Electrochemistry of sulphide dissolution in hydrometallurgical systems*', Proc. Int. Min. Proc. Cong., Leningrad, 13pp.

Majima, H. (1969) '*How oxidation affects selective flotation of complex sulphide ores*',Canad. Met. Quart., vol. 8, no. 3, pp. 269-273.

Mansfield, F. (1971) '*Area relationships in galvanic corrosion*', Corrosion, vol. 27, no. 10, pp 437-442.

Mansfield, F. (1973) '*The relationship between galvanic current and dissolution rates*', Corrosion, vol. 29, no. 10, pp. 403-405.

Mansfield, F., and Parry, E.P. (1973) '*Galvanic corrosion of bare and coated Al alloys coupled to stainless steel 304 or Ti-6Al-4V*', Corrosion Science, vol. 13, pp. 605-621.

Mattsson, E., and Bockris, J. (1959) '*Galvanostatic studies of the kinetics of deposition and dissolution in the copper + copper sulphate system*', Faraday Society Trans., vol. 55, pp. 1585-1601.

Mehta, A.P., and Murr,L.E. (1983) '*Fundamental studies of the contribution of galvanic interaction to acid-bacterial leaching of mixed metal sulphides*', Hydrometallurgy, 9, pp. 235-256.

Mishra, K.K., and Osseo-Asare, K. (1987) '*Photodissolution of coal pyrite*', Fuel, vol. 66, pp. 1161-1162.

Mizoguchi, T., and Habashi,F. (1983) '*Aqueous oxidation of zinc sulphide, pyrite and their mixtures in hydrochloric acid*', Trans. Instn Min. Metall., C92, C14-C19.

Nowak, P., Krauss, E., and Pomianowski, A. 1984) '*The electrochemical characteristics of the galvanic corrosion of sulphide minerals in short-circuited model galvanic cells*', Hydrometallurgy, 12, pp. 95-110.

Paramguru, R.K., Bose, S.K., and Sircar, S.C. (1979) '*Technical note : Electrode kinetics studies on compacted lead sulphide electrodes*', Trans. Instn. Min Metall C, vol. 88, pp. C197-C202.

Paul, R.L., Nicol, M.J., Diggle, J.W., and Saunders, A.P. (1977) '*The electrochemical behaviour of galena, I. Anodic dissolution*', Electrochimica Acta, vol. 23, pp. 625-633.

Peters, E. (1976) '*The electrochemistry of sulphide minerals*', In: Trends in electrochemistry, J. O'M. Bockris, D.A.J Rand., and B.J. Welch (Eds.), Plenum Press, New York, pp. 267-290.

Pletcher, D. (1991) '*A First Course In Electrode Processes*', Alresford Press Ltd, Great Britain, 274pp.

Rao, S.R., and Finch, J.A. (1988) '*Galvanic interaction studies on sulphide minerals*', Canadian Metallurgical Quarterly, vol. 27, no. 4, pp. 253-259.

Roy Morrison, S. (1980) '*Electrochemistry at semiconductor and oxidised metal electrodes*', Plenum Press, New York.

Shuey, R.T. (1975) '*Semiconducting Ore Minerals*', Elsevier Publishing Company,

Amsterdam.

Skewes, H.R. (1972) '*Electrowinning of lead directly from galena*', Proc Australas. Inst. Min. Metall., no. 244, pp. 35-41.

Springer, G. (1970) '*Observations on the electrochemical reactivity of semiconducting minerals*', Trans. Instn. Min. Metall., vol. 79, pp. C11-C14.

Thomas, G., and Whalley, B.J.P. (1958) '*The leaching of manganese from pyrolusite by pyrite*' Canad. J. Chem. Engng., (1), pp.37-43.

APPENDIX A.

Energy Dispersive X-Ray Analysis (EDXA) of the mineral samples used in the galvanic couples.

A.1 EDXA of the pyrite disc in the copper-pyrite couple.

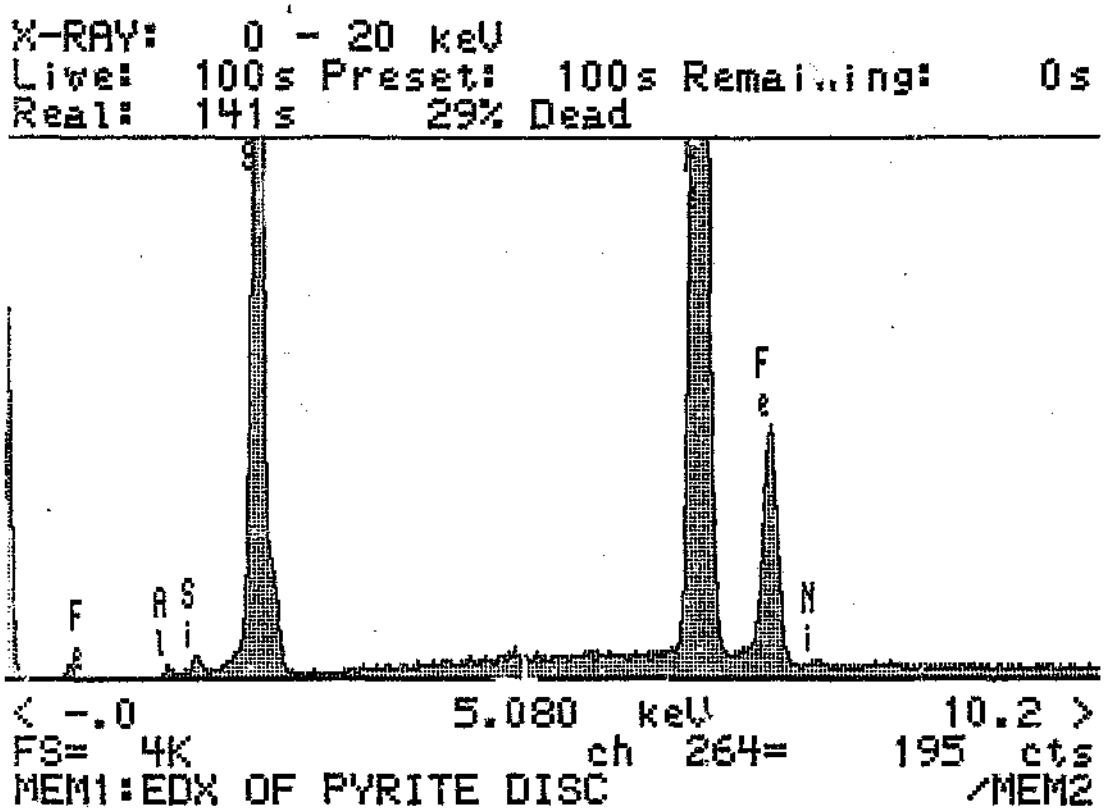


Figure A.1 EDXA peaks associated with the pyrite disc electrode.

The pyrite disc exhibits two large iron peaks and a large sulphur peak. The pyrite appears to be iron rich which implies, in a pure pyrite sample, that n-type

conduction occurs. The existence of small silicon and aluminium peaks are observed to the left of the sulphur peak. The amounts of silicon and aluminium are negligible and probably occur in the form of silica and aluminosilicate.

A.2 EDXA of the galena disc in the galena-pyrite couple.

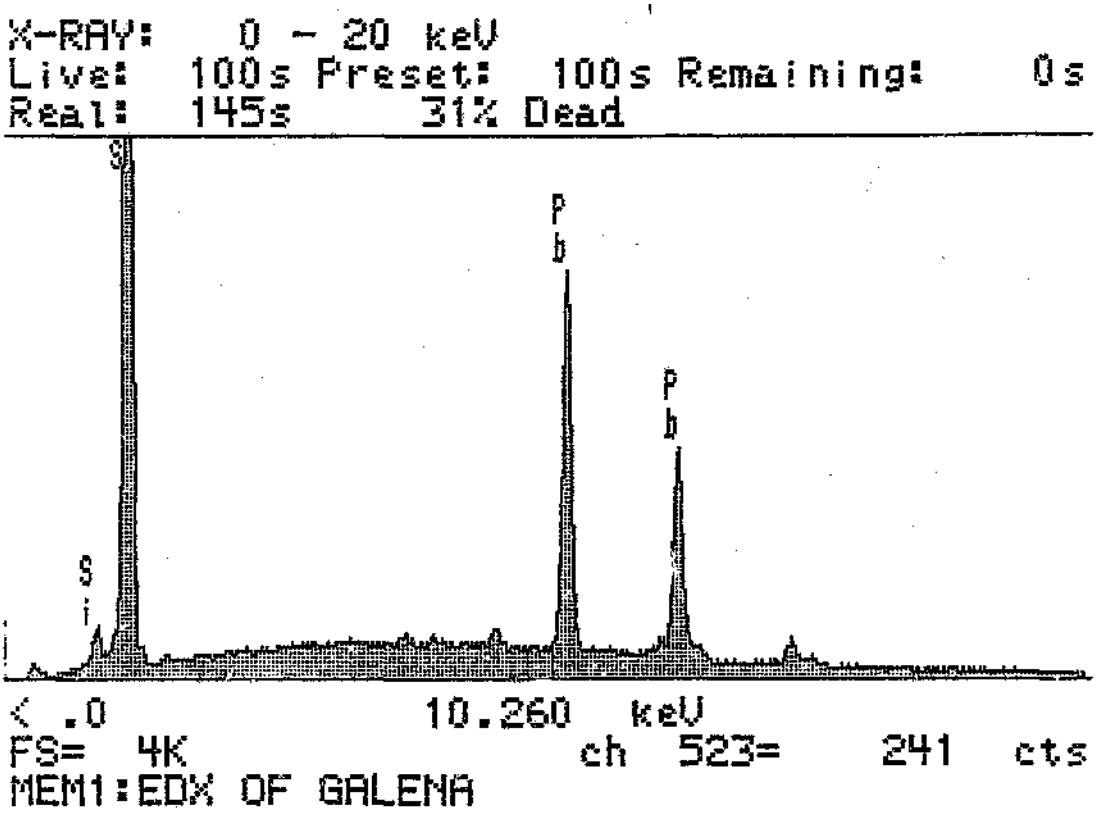


Figure A.2 EDXA peaks associated with the galena disc electrode.

The large peak on the left of Figure A.2 is a combined lead-sulphur peak. The existence of two further peaks of lead implies that the galena disc is an n-type conductor. A negligible amount of silicon, probably in the form of silica, is present in the mineral.

A.3 EDXA of the pyrite ring in the galena-pyrite couple.

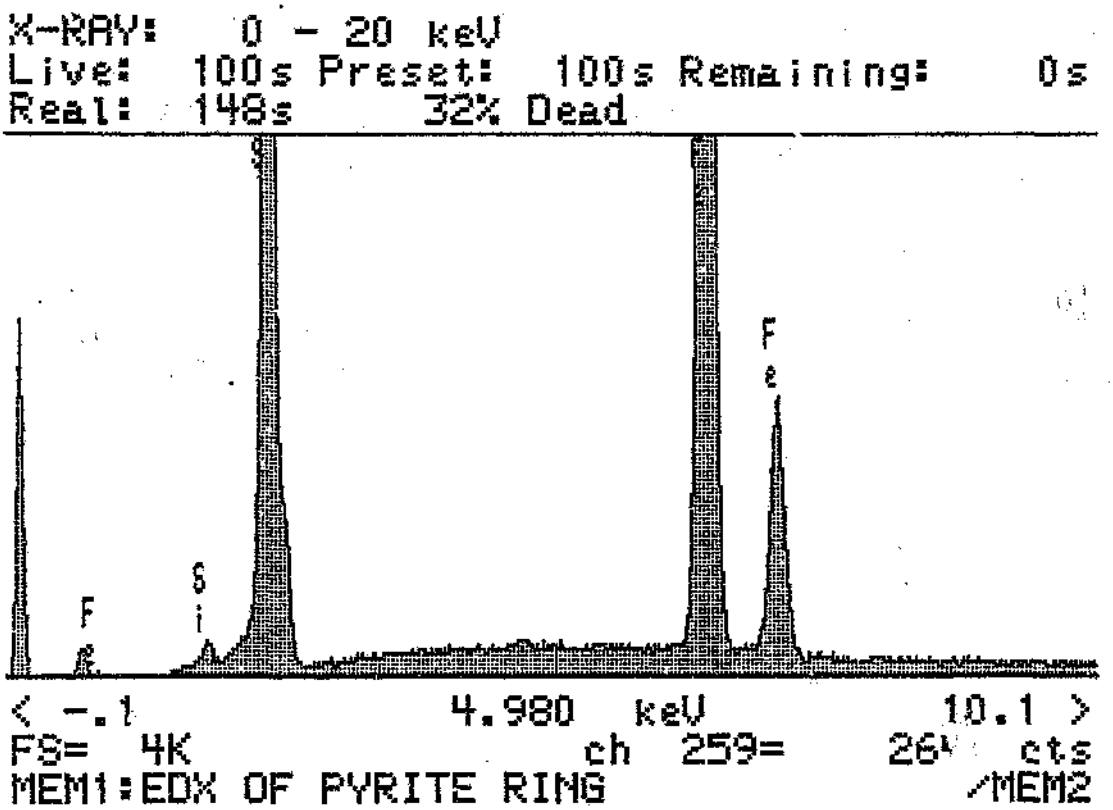


Figure A.3 EDXA peaks associated with the pyrite ring electrode.

The magnitude of the peaks imply that pyrite is iron rich and hence a n-type conductor. The negligible amount of silicon present probably occurs in the form of silica.

APPENDIX B.

Computer programs for recording experimental data and solving model equations.

B.1 Program to record voltage and current data during polarisation studies.

```
10  CLEAR 701
20  ! PRINTER IS 1
30  SET TIME TIME("00:00:00")
40  T=TIMEDATE
50  PRINT ""
60  PRINT "GALVANIC CURRENT     OGRAM"
70  MASS STORAGE IS ":HP9121,7
80  INPUT "ENTER THE FILENAME FOR DATA STORAGE :",Filename$
90  DISP "DOES ";Filename$;" EXIST (Y/N) :";
100 LINPUT Option$
110 IF Option$="Y" THEN
120   DISP "DO YOU WISH TO OVERWRITE THIS FILE (Y/N) :";
130   LINPUT Overwrite$
140   IF Overwrite$="N" THEN STOP
150 ELSE
160   CREATE ASCII Filename$&":HP9121,700,1",600
170 END IF
180 ASSIGN @File TO Filename$
190 FOR I=1 TO 300
200   OUTPUT 709;"DCV";3
201   ENTER 709;Voltage
202   Volttime=TIMEDATE
210   OUTPUT 709;"DCV";4
211   ENTER 709;Current
212   Currtime=TIMEDATE
220 OUTPUT @File;Voltage,Volttime-T,Current,
221 Currtime-T,CHR$(13),CHR$(10);
230 PRINT Voltage,Volttime-T,Current,Currtime-T;
240 PRINT CHR$(13)
250 NEXT I
260 END
```

B.2 Program to record experimental data for the dynamic galvanic couple study.

```
10  CLEAR 701
20  ! PRINTER IS 1
30  SET TIME TIME("00:00:00")
40  T=TIMEDATE
50  PRINT ""
60  PRINT "DYNAMIC GALVANIC CURRENT PROGRAM"
70  MASS STORAGE IS ":HP9121,700,1"
80  INPUT "ENTER THE FILENAME FOR DATA STORAGE :",Filename$
90  DISP "DOES ";Filename$;" EXIST (Y/N) :";
100 LINPUT Option$
110 IF Option$="Y" THEN
120   DISP "DO YOU WISH TO OVERWRITE THIS FILE (Y/N) :";
130   LINPUT Overwrite$
140   IF Overwrite$="N" THEN STOP
150 ELSE
160   CREATE ASCII Filename$&":HP9121,700,1",600
170 END IF
180 ASSIGN @File TO Filename$
190 FOR I=1 TO 100
200   OUTPUT 709;"DCV";3
201   ENTER 709;Appvoltage
202   Appvolttime=TIMEDATE
210   OUTPUT 709;"DCV";4
211   ENTER 709;Galvcurrent
212   Galvurrenttime=TIMEDATE
220   OUTPUT 709;"DCV";5
221   ENTER 709;Anodepot
222   Anodepottime=TIMEDATE
230   OUTPUT 709;"DCV";6
231   ENTER 709;Cathodepot
232   Cathodepottime=TIMEDATE
240   OUTPUT 709;"DCV";7
241   ENTER 709;Electrolytepot
242   Electrolytepottime=TIMEDATE
250 OUTPUT @File;Appvoltage,Appvolttime-T,
    Galvcurr,Galvcurrtime-T,Anodepot,Anodepottime-T,
    Cathodepot,Cathodepottime-T,Electrolytepot,
    Electrolytepot-T CHR$(13),CHR$(10);
260 PRINT Appvoltage,Appvoltime-T,Galvcurr,
    Galvcurrtime-T,Anodepot,Anodepottime-T,
    Cathodepot,Cathodepottime-T,Electrolytepot,
    Electrolytepottime-T;
270 PRINT CHR$(13)
280 FOR J=1 TO 30000
```

```
281  NEXT J
290  NEXT I
300  END
```

B.3 Program utilising a Regula-Falsi iteration technique to solve the galvanic model equation.

```
Program Regula_Falsi_Current_Iteration (Input,Output);

Var

a,b : real; {Upper and lower guesses}
ioa,Aa,alpha_a,Eea : real; {Anodic parameters}
ilc,ioc,Ac,alpha_c,Eec : real; {Cathodic parameters}
temp,Vapp : real; {General model parameters}
n : integer; {No. of iterations}
infilevar,outfilevar : text; {Data file variables}
infilename,outfilename : string[20]; {Data file names}
{-------------------------------------------}
Procedure DefineDataFile;
{Procedure to open the input and ouput data files as {well as read in the model
parameters}

Begin

 Writeln('Enter the name of file containing the parameters');
 Readln(infilename);
 Assign(infilevar,infilename);
 Reset(infilevar);
 Readln(infilevar);
 Readln(infilevar,a,b,n);
 Readln(infilevar);
 Readln(infilevar,alpha_a,ioa,Aa,Eea);
 Readln(infilevar);
 Readln(infilevar,alpha_c,ioc,Ac,ilc,Eec);
 Readln(infilevar);
 Readln(infilevar,temp,Vapp);

 Writeln('Enter the name of the output data file');
 Readln(outfilename);
 Assign(outfilevar,outfilename);
 Rewrite(outfilevar);
```

```
End;
{-----------------------------------------------}
Procedure Iterate(n:integer;
                  a,b,Eea,Eec:real);
{This procedure uses a Regula Falsi iteration technique}
{to solve for the galvanic current}

Type
Vector = array[1..200] of real;

Var
i                              : integer;
cellemf                        : real;
xa,xb,xs                       : vector;
overpotanode1,overpotanode2,
overpotcathode1,overpotcathode2 : vector;

Begin

 i:=0;
 Cellemf:=Eec-Eea;

 For i:=1 to n do

  Begin
   Overpotanode1[i]:=(8.314*Temp)/(alpha_a*96485)
                    *ln(a/(ioa*Aa));
   Overpotcathode1[i]:=(8.314*temp)/(alpha_C*96485)
                      *ln((ilc-a/Ac)/(ilc*(a/(Ac*ioc)
                      +1)));
   Overpotanode2[i]:=(8.314*Temp)/(alpha_a*96485)
                    *ln(b/(ioa*Aa));
   Overpotcathode2[i]:=(8.314*temp)/(alpha_C*96485)
                      *ln((ilc-b/Ac) ac*(b/(Ac*ioc)
                      +1)));
   xa[i]:=cellemf-(abs(Vapp)+abs(overpotanode1[i])
         +abs(overpotcathode1[i]));
   xb[i]:=cellemf-(abs(Vapp)+abs(overpotanode2[i])
         +abs(overpotcathode2[i]));
   xs[i]:=b-(((b-a)*xb[i])/(xb[i]-xa[i]));
   a:=xs[i];
   Writeln(outfilevar,i,' ',xs[i]);
  End;

End;
{-----------------------------------------------}
Begin{Main Program}
```

```
a:=0;          {variable initialisation}
b:=0;
Aa:=0;
Ac:=0;
ioa:=0;
ioc:=0;
ilc:=0;
vapp:=0;
temp:=0;
alpha_a:=0;
alpha_c:=0;

DefineDataFile;
Iterate(n,a,b,Eea,Eec);

Close(infilevar);
Close(outfilevar);

End.{Main Program}
{-------------------------------------------}
```

B.4 Program utilising a 4th order Runge Kutta technique to solve the cathodic equilibrium potential decay over time.

```
Program Dynamic_Galvanic_Current(Input,Output);

Type
Vector = Array[1..1000] of Real;

Var
infilename,outfilename : string[20];
infilevar,outfilevar : text;
i,d : integer;
a,b,h : real; {Runge kutta boundaries and steplength}
temp,conc,vol,areacath,limcurr,
alpha_c,excd,stdpot,emix : real;

{-------------------------------------------}
Procedure ReadInData;

{Procedure to read in the kinetic and thermodynamic}
{parameters for the cathodic reaction.}

Begin

  Writeln('Enter the file containing equation parameters');
```

```
  Readln(infilename);
  Assign(infilevar,infilename);
  Reset(infilevar);
  Readln(infilevar);
  Readln(infilevar,a,b,d);
  Readln(infilevar);
  Readln(infilevar,temp,conc,vol);
  Readln(infilevar);
  Readln(infilevar,areacath,limcurr,alpha_c,excd,
        stdpot,emix);

End;

{-----------------------------------------}
Procedure OutputDataFile;

{Procedure to output Runge Kutta results}

Begin

  Writeln('Enter the name of the output data file');
  Readln(outfilename);
  Assign(outfilevar,outfilename);
  Rewrite(outfilevar);

End;

{-----------------------------------------}
Procedure RungeKutta(d : integer;
                     a,b,temp,conc,vol,areacath,limcurr,
                     alpha_c,excd,stdpot,emix : real);


Type

  Vector = Array[1..1000] of Real;

Var

  v1,v2,v3,v4,v5: real; {variables in model equation}
  z : integer;
  k1,k2,k3,k4 : real; {Runge kutta parameters}
  x,y : vector;

Begin

  v1:=0; {Variable initialisation}
  v2:=0;
```

```
v3:=0;
v4:=0;
v5:=0;
z:=0;
k1:=0;
k2:=0;
k3:=0;
k4:=0;

h:=(b-a)/d;
v1:=(8.314*temp)/(vol*sqr(96485)*conc);
v2:=areacath*limcurr;
v3:=(alpha_c*96485)/(8.314*temp);
v4:=96485/(8.314*temp);
v5:=limcurr/excd;
x[1]:=0; {Setting initial time value}
y[1]:=0.6112; {Initial equilibrium potential value}

For i:=1 to d+1 do

 Begin

  k1:=h*v1*((v2*(1-exp(-v3*(emix-y[i])))
      *sqr((1+exp(v4*(y[i]-0.77)))))
      /(exp(v4*(y[i]-0.77))*
      (1+v5*exp(-v3*(emix-y[i])))));
  k2:=h*v1*((v2*(1-exp(-v3*(emix-(y[i]+k1/2))))
      *sqr((1+exp(v4*((y[i]+k1/2)-0.77)))))/(exp(v4*
      ((y[i]+k1/2)-0.77))*(1+v5*exp(-v3*(emix-(y[i]+
      k1/2)))));
  k3:=h*v1*((v2*(1-exp(-v3*(emix-(y[i]+k2/2))))
      *sqr((1+exp(v4*((y[i]+k2/2)-0.77)))))/(exp(v4*
      ((y[i]+k2/2)-0.77))*(1+v5*exp(-v3*(emix-(y[i]+
      k2/2)))));
  k4:=h*v1*((v2*(1-exp(-v3*(emix-(y[i]+k3))))
      *sqr((1+exp(v4*((y[i]+k3)-0.77)))))/(exp(v4*
      ((y[i]+k3)-0.77))*(1+v5*exp(-v3*(emix-(y[i]+
      k3)))));
  y[i+1]:=y[i]+1/6*(k1+2*k2+2*k3+k4);
  x[i+1]:=x[i]+h;
  Writeln(outfilevar,x[i+1],' ',y[i+1]);

  End;

End;

{-----------------------------------------}
Begin {Main program}
```

```
  i:=0; d:=0; a:=0; b:=0; h:=0;
  temp:=0; conc:=0; vol:=0;areacath:=0;
  limcurr:=0; alpha_c:=0; excd:=0; stdpot:=0;
  emix:=0; {variable initialisation}

  ReadInData;
  OutputDataFile;
  RungeKutta(d,a,b,temp,conc,vol,areacath,limcurr,alpha_c,
          excd,stdpot,emix);
  Close(infilevar);
  Close(outfilevar);

End. {Main program}
```

APPENDIX C.

Derivation of dynamic expressions for galvanic current.

C.1 Relationship between cone radius and time for a galvanic couple in which the anodic and cathodic reactions are electrochemically controlled.

It is assumed that anodic processes on the cathode and cathodic processes on the anode are negligible. The model is derived for a small anodic cone encapsulated in a spherical cathode in such a manner that only the circular base of the cone is exposed to solution, refer to Figure C.1. It is assumed that the shrinking anode, due to its small size, results in no appreciable increase in cathodic surface area.

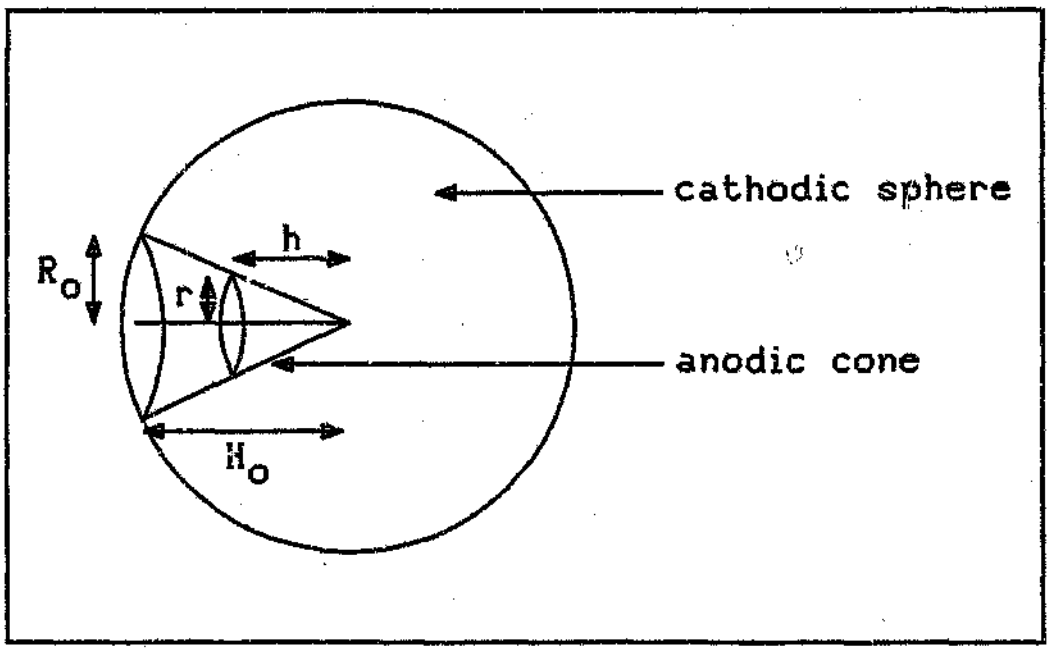


Figure C.1 Galvanic couple consisting of an anodic cone and cathodic sphere.

Figure 8.2 illustrates the polarisation curves for anodic and cathodic reactions which are electrochemically controlled. The model is derived for the case where a mineral anodically dissolves and ferric ions are reduced at the cathode. It is assumed that the anode shrinks i.e. the sulphur film on the surface is either oxidised or grows at a slower rate in comparison with the shrinking rate of the mineral. At the galvanic potential, E_g, the anodic and cathodic currents are equal:

$$i_g = i_a = -i_c \qquad \text{C.1}$$

where:

$$k_{red}[MeS]\exp\left(\frac{\alpha_a nF}{RT}(E_g - E_{e,a})\right) = k_{ox}[Fe^{3+}]\exp\left(\frac{-\alpha_c nF}{RT}(E_g - E_{e,c})\right) \qquad \text{C.2}$$

If the anodic and cathodic charge-transfer coefficients are equivalent the galvanic potential can be expressed as:

$$E_g = E_{e,c} - E_{e,a} + \frac{RT}{\alpha nF}\ln\left(\frac{k_{red}}{k_{ox}[Fe^{3+}]}\right) \qquad \text{C.3}$$

Substituting this expression into the Butler-Volmer expression for the anodic current, i_a, one obtains the following:

$$\text{Rate} = I_a = A_a nFk^1[Fe^{3+}]^{-0.5} \qquad \text{C.4}$$

where:

$$k^1 = \frac{k_{red}^2}{k_{ox}} \qquad \text{C.5}$$

A dynamic mass balance over the shrinking anodic cone results in:

$$mols_{MeS}|_t = mols_{MeS}|_{t+\Delta t} + A_{MeS}.rate.\Delta t \qquad C.6$$

substituting Equation C.4 into Equation C.6 and using the relationship of similar triangles on the cone, refer to Figure C.1,

$$h = \frac{rH_o}{R_o} \qquad C.7$$

one obtains:

$$-\frac{\rho_{MeS}}{M_{MeS}} \frac{d\left(\frac{\pi r^3 H_o}{3R_o}\right)}{dt} = bk^1[Fe^{3+}]^{-0.5} \qquad C.8$$

This resolves to:

$$\int_{R_o}^{r} dr = -\frac{R_o bk^1[Fe^{3+}]^{-0.5}}{H_o}\int_0^t dt \qquad C.9$$

Integrating Equation C.9 one obtains the final expression relating the radius of the cone to time:

$$r = R_o\left(1 - \frac{bk^1[Fe^{3+}]^{-0.5}t}{H_o}\right) \qquad C.10$$

C.2 Diffusion through a sulphur or oxide film on the anodic surface controls the rate of reaction.

It is assumed in this derivation that the film grows at a rate which results in no variation in the original cone dimensions. It is assumed the diffusion of metal ions

from the reaction surface through the film controls the reaction rate.

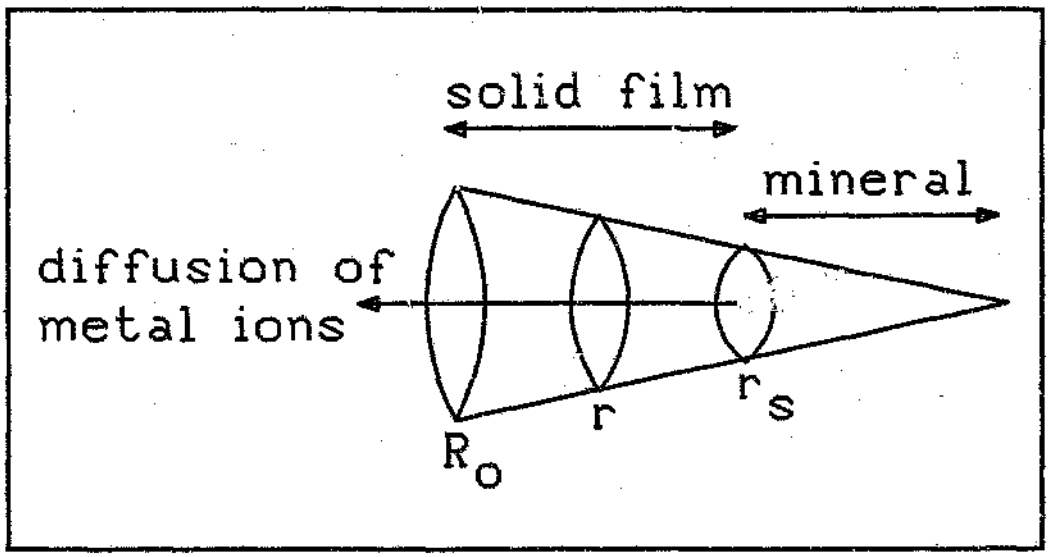


Figure C.2 Diffusion of metal ions through the anodic cone.

In the initial stage of the derivation it is assumed that the metal ions diffuse more quickly through the film than the sulphide mineral shrinks. This allows one to assume that the metal sulphide is stationary. The rate of the metal sulphide, MeS, reaction at any instant is given by its rate of diffusion from the reaction surface.

$$-\frac{dn_{Me^{2+}}}{dt} = \pi r_s^2 J_{r_s} = \pi R^2 J_{R_o} = \pi r^2 J_r = \text{constant} \qquad \text{C.11}$$

The concentration profile of Me^{2+} within the solid film is expressed by Fick's law for equimolar counter diffusion.

$$J_r = D_{Me^{2+}(S^0)} \frac{dC_{Me^{2+}}}{dr} \qquad \text{C.12}$$

Substituting Equation C.12 into C.11 one obtains the following expression:

$$-\frac{dn_{Me^{2+}}}{dt}\int_{r_s}^{R_o}\frac{1}{r^2}dr = \pi D_{Me^{2+}g^o}\int_{C_s}^{C_{R_o}=0} dC_{Me^{2+}} \qquad \text{C.13}$$

Integrating Equation C.13 one obtains the expression:

$$-\frac{dn_{Me^{2+}}}{dt}\left(\frac{-1}{R_o}+\frac{1}{r_s}\right) = -\pi D_{Me^{2+}g^o}C_s \qquad \text{C.14}$$

Equation C.14 represents the conditions of a reacting particle at any time. For a specific cone size the rate of reaction of the cone remains constant. However as the reaction progresses the sulphur layer gets thicker and the concentration profile of metal ions across the profile thins. This results in a decrease in the diffusion rate of metal ions.

The number of moles of metal ions can be expressed as:

$$n_{Me^{2+}} = \frac{\rho_{Me^{2+}}\pi r_s^3 H_o}{3R_o M_{Me^{2+}}} \qquad \text{C.15}$$

and

$$n_{Me^{2+}} = \frac{1}{b}n_{MeS} \qquad \text{C.16}$$

Using Equations C.14, C.15 and C.16 one obtains the following:

$$\int_{R_o}^{r_s}\left(r_s - \frac{r_s^2}{R_o}\right)dr_s = \frac{R_o M_{MeS} D_{Me^{2+}} C_{Me^{2+}g^o}}{b\rho_{MeS}H_o}\int_0^t dt \qquad \text{C.17}$$

Integrating Equation C.17 one obtains:

$$\frac{3r_s^2}{R_o^2} - \frac{2r_s^3}{R_o^3} = 1 + \frac{6M_{MeS}D_{Me^{2+}}C_{Me^{2+}s}t}{b\rho_{MeS}H_oR_o} \qquad C.18$$

C.3 Reduction of dissolved oxygen on cathodic sites controls the rate of reaction.

In many instances the reduction of oxygen on the surface of a cathode is the rate limiting process. The dynamic balance over the anodic cone is dependent on the surface area of the cathode. It is assumed that no variations in cathodic area occurs. The dynamic balance over the anodic cone is therefore:

$$mols_{MeS}|_t = mols_{MeS}|_{t+\Delta t} + A_c.rate.\Delta t \qquad C.19$$

If the concentration of dissolved oxygen in the bulk solution is constant and the concentration at the surface is zero the rate of diffusion is given by:

$$Rate = \left(\frac{I}{A_cnF}\right) = \frac{DC_{b,o_2}}{\delta} \qquad C.20$$

Substituting C.20 into C.19 one obtains the following:

$$-\frac{dn_{MeS}}{dt} = \frac{A_cDC_{b,o_2}}{\delta} \qquad C.21$$

Expressing moles of metal sulphide in terms of cone radius and height, refer to Equation C.15, one obtains the following integral expression:

$$\int_{R_o}^{r} r^2 dr = \frac{M_{MeS}R_oA_cDC_{b,o_2}}{\rho_{MeS}\pi H_o\delta}\int_0^t dt \qquad C.22$$

Integrating and rearranging Equation C.22 one obtains the following expression for

the radius of the anodic cone in terms of time:

$$r = \left(R_o^3 + \frac{M_{MeS} R_o A_c D C_{b,O_2} t}{\rho_{MeS} \pi H_o \delta} \right)^{\frac{1}{3}} \qquad \text{C.23}$$

C.4 Galvanic current decay due to decay in cathodic equilibrium potential.

Solution composition variations cause variations in the kinetic parameters and equilibrium potentials of the half reactions in a galvanic couple. The model derived accounts for variation in galvanic current due to a decrease in the cathodic equilibrium potential only, the reasons for this are outlined in Section 8.2. It is assumed that the only cathodic reaction is the reduction of ferric to ferrous ions.

The shift in the cathodic equilibrium potential due to composition changes can be accounted for by the Nernst equation. For the ferric reduction to ferrous reaction the following relationship is valid:

$$E_{e,c} = E^{\circ}_{e,c} + \frac{RT}{nF} \ln\left(\frac{[Fe^{3+}]}{[Fe^{2+}]} \right) \qquad \text{C.24}$$

By mass balance, assuming the solution volume remains constant, the $[Fe^{2+}]$ at any time can be expressed in terms of $[Fe^{3+}]$ i.e:

$$[Fe^{2+}]_t = [Fe^{3+}]_{t=0} - [Fe^{3+}]_t \qquad \text{C.25}$$

Substituting Equation C.25 into C.24 and rearranging one obtains the expression:

$$[Fe^{3+}]_t = \frac{[Fe^{3+}]_{t=0} \exp\left(\frac{F}{RT} (E_{e,c} - E^{\circ}_{e,c}) \right)}{\left(1 + \exp\left(\frac{F}{RT} (E_{e,c} - E^{\circ}_{e,c}) \right) \right)} \qquad \text{C.26}$$

The current generated in a reaction can be equated to the rate of a reaction through Faraday's Law.

$$\text{Rate} = \frac{vd[Fe^{3+}]_t}{dt} = \frac{I(E_{e,c})}{nF} \qquad \text{C.27}$$

In this study there is a reduction of ferric ions on the anode as well and therefore the rate expression is theoretically be given by:

$$\text{Rate} = \frac{vd[Fe^{3+}]}{dt} = \frac{I(E_{e,c})}{nF} + \frac{\beta I(E_{e,c})}{nF} \qquad \text{C.28}$$

where β is given by:

$$\beta = \frac{\text{amount of current for reaction on anode}}{\text{net galvanic current}} \qquad \text{C.29}$$

The amount of ferric reduced on the anode is neglected in this analysis. Substituting C.26 into C.27 one obtains a differential equation which equates the differential of the cathodic equilibrium potential over time to the rate of reaction:

$$d\frac{[Fe^{3+}]_{t=0}\exp\left(\frac{F}{RT}(E_{e,c} - E^{\circ}_{e,c})\right)}{\left(1 + \exp\left(\frac{F}{RT}(E_{e,c} - E^{\circ}_{e,c})\right)\right)} = \frac{I(E_{e,c})}{nF} \qquad \text{C.30}$$

The reduction of ferric to ferrous ions is a mass transfer and electrochemically controlled process. The cathodic current in terms of the cathodic equilibrium potential is therefore given by:

$$I(E_{e,c}) = \frac{A_c i_{1,c}\left(1 - \exp\left(\frac{\alpha_c F}{RT}(E - E_{e,c})\right)\right)}{1 + \frac{i_{1,c}}{i_{o,c}}\exp\left(\frac{\alpha_c F}{RT}(E - E_{e,c})\right)} \qquad \text{C.31}$$

Substituting Equation C.31 into C.30 and using the chain rule one obtains the following model equation:

$$\frac{dE_{e,c}}{dt} = Z\left(\frac{\left(A_c i_{1,c}(1-\exp(y_1(E-E_{e,c}))\right)\left(1+\exp(y_2(E_{e,c}-E^{\circ}_{e,c}))\right)^2}{\exp(y_2(E_{e,c}-E^{\circ}_{e,c}))\left(1+\frac{i_1}{i_o}\exp(y_1(E-E_{e,c}))\right)}\right) \qquad \text{C.32}$$

where:

$$Z = \frac{RT}{\nu F^2 C_{Fe^{3+}}} \qquad \text{C.33}$$

$$y_1 = \frac{\alpha_c F}{RT} \qquad \text{C.34}$$

$$y_2 = \frac{F}{RT} \qquad \text{C.35}$$

Author: Holmes Paul Richard.

Name of thesis: Galvanic interactions between minerals during dissolution.

PUBLISHER:

University of the Witwatersrand, Johannesburg
©2015

LEGALNOTICES:

Copyright Notice: All materials on the University of the Witwatersrand, Johannesburg Library website are protected by South African copyright law and may not be distributed, transmitted, displayed or otherwise published in any format, without the prior written permission of the copyright owner.

Disclaimer and Terms of Use: Provided that you maintain all copyright and other notices contained therein, you may download material (one machine readable copy and one print copy per page)for your personal and/or educational non-commercial use only.

The University of the Witwatersrand, Johannesburg, is not responsible for any errors or omissions and excludes any and all liability for any errors in or omissions from the information on the Library website.